Impacts of rapid land use change on the meandering dynamics of the Kinabatangan River, Borneo

Alexander J. Horton

2017

Thesis submitted for the degree of

Doctorate of Philosophy

Summary

Agricultural expansion is driving tropical deforestation and the conversion of fertile floodplains along large meandering rivers. Yet despite a wealth of research showing the importance of riparian vegetation to the processes of riverbank retreat, little is known of the geomorphic response of large rivers to the rapid removal of natural riparian cover. The Kinabatangan River in Northern Borneo offers an important opportunity to study the morphological change induced by extensive land conversion, as palm oil plantations have replaced much of the floodplain forest in recent decades.

Using LANDSAT imagery from 1989 – 2014 I examine the impact of widespread land use change on the meandering dynamics of the Kinabatangan River, and quantify the provision of an ecosystem service by riparian reserves to adjacent oil palm plantations.

Rates of channel migration following deforestation increase by >23%, and the correlation between planform curvature and rates of riverbank retreat only became strongly positive and significant after the removal of natural riparian cover, suggesting an important role of forests in the evolution of meandering rivers, even when riverbank heights exceed the depth of root penetration.

By means of a numerical model of channel migration that explicitly represents the role of a dense root network in controlling the residency time of slump blocks, I then demonstrate that riparian vegetation can affect rates and patterns of channel migration by altering the composition and fate of failed bank material armouring the bank toe.

Furthermore, I estimate the value of the geomorphic ecosystem service that riparian reserves provide by protecting adjacent oil palm plantations from bank erosion over long-term economic horizons.

Acknowledgements

I would like to express my profound gratitude to the many people who have contributed in all sorts of ways to the work presented in this thesis.

I have been fortunate enough to have three wonderful supervisors who have always been on hand to offer advice and support. My heartfelt thanks goes out to each of them in turn: To Dr José Constantine for being so enthusiastic, for always offering up the big picture idea, and for generally KIR. To Dr Eli Lazarus for the craft of research, for the sage advice, and for the little man coffee jam sessions. And to Dr TC Hales for always taking the time, for making me think about something other than rivers, for making me work for it, but mostly for being a mentor.

Special mention goes to my co-supervisor Dr Benoît Goossens for getting me out into the field, and for sharing his passion for conservation (though not durian). I'd also like to thank Dr Mike Bruford for all his advice, contributions, and for helping to make this work better.

Thank you to everyone who made my time at the Danau Girang Field Centre in Borneo such an amazing experience, especially the field staff and Ollie Francis who helped me clear so much Elephant grass and dig so many holes.

To my colleagues at Cardiff University who made the everyday drudge of completing my PhD a fun reality – thank you so much, especially those in the Geomorph lab, Huw Mithan and Rhodri Thomas. I need to say a big thank you to Dr Rob Parker for dragging me along to every conceivable outdoor activity irrespective of the Welsh weather, and to Josh Ahmed for keeping me laughing all the way to the finish, and for Vegas road trips.

I'd like to say thank you to my sponsors, this work would not have been possible if it wasn't for the funding I received from both the Natural Environment Research Council and the British Society of Geomorphology.

Finally, but most emphatically, I would like to say thank you to my whole family, especially my Mum, my Dad, and my Sisters. Your love and support have always made me believe that I can achieve anything, thank you so much for everything you've done for me. And lastly to Bethan, for all your encouragement, for your patience, for being a distraction, for making me laugh, and for making everything better – thank you.

Contents

List of figures

List of tables

Chapter 1:

Thesis Introduction

1.1 Motivation

Meandering rivers are features of the Earth's surface found across every biome, from temperate forests of the northern latitudes to arid deserts of the subtropics, water collecting from across a landscape forms a single sinuous channel that migrates through its floodplain. As meanders grow and develop over time they constantly remobilise sediment, reshaping the landscape to construct new surfaces for riparian vegetation to colonise. Channel migration is the result of bank retreat coupled with bar formation, where material eroded from land bordering an upper portion of river is deposited downstream to form new land along the inside of a meandering bend. The process of meandering in alluvial rivers is governed by the complex interactions of a three dimensional flow structure, channel planform, sediment transport, and the geotechnical properties riverbanks [*Nardi et al.*, 2013; *Konsoer et al.*, 2016a]. Floodplain vegetation plays a crucial role in determining the characteristics of a fluvial system [*Hadley*, 1961; *Zimmerman et al*., 1967; *Gran and Paola*, 2001; *Allmendinger et al*., 2005], altering the geotechnical properties of riverbanks [*Abernethy and Rutherfurd*, 2000; *Simon and Collison*, 2002; *Pollen and Simon*, 2005], the near bank flow structure [*Daniels and Rhoads*, 2003], and the long-term channel planform [*Camporeale et al.*, 2005; *Perucca et al.*, 2006; *Camporeale and Perucca*, 2013] – thereby directly affecting the components controlling river meandering. As human development continues to colonise the Earth's surface, it becomes increasingly important to understand how land-use change can alter the feedbacks between biological and physical processes [*Murray et al.*, 2009].

Each year sees the conversion and degradation of an estimated 5.5 M ha of tropical forests worldwide as agricultural expansion drives land use change [*Baccini et al.,* 2012;

Houghton, 2012]. In Southeast Asia, which hosts some of the highest rates of tropical deforestation in the world [Keenan *et al.*, 2015], rapid agricultural expansion is dominated by the palm-oil industry [Boucher *et al.*, 2011; Stibig *et al.*, 2014]. The ideal conditions for the cultivation of oil palm are found in the narrow band of latitudes roughly 10˚ either side of the equator [*Basiron et al.*, 2007]. As the demand for palm oil and its derivatives is expected to increase with the continued economic growth of the two largest markets, India and China [Murphy, 2014], the scarcity of suitable land is likely to expand production beyond the confines of Southeast Asia driving further forest conversion in tropical regions worldwide such as Colombia and Brazil [*Pirker et al.*, 2016].

Tropical deforestation is often centred along large meandering rivers [*Obidzinski et al.*, 2007; *Latrubesse et al.*, 2009], which provide both access to fertile floodplains and a ready-made transportation network [*Armenteras et al.*, 2006; *Renó et al.*, 2011]. The conversion of floodplain forests has the potential to effect geomorphic change [*Boucher et al.*, 2011]. Yet despite a wealth of research showing the importance of riparian vegetation to the processes of riverbank retreat [*Hickin*, 1984; *Hupp and Osterkamp*, 1996; *Langendoen and Simon*, 2008; *Docker and Hubble*, 2009; *Gurnell*, 2014], little is known of the geomorphic response resulting from the rapid removal of floodplain forest along large rivers [*Latrubesse et al.*, 2009]. Alterations to the meandering dynamics of river systems may lead to accelerated loss of agricultural land [*Amiri-tokaldany et al.*, 2004], damage to infrastructure [*Piegay et al.*, 1997], and increased sediment loading that would propagate consequences downstream [*Downs and Simon*, 2001; *Constantine et al.*, 2014]. Effectively mitigating these negative consequences in future land conversion along large river boundaries requires the quantification of historic geomorphic response to better understand the reach scale effects of forest removal on bank retreat processes, and to inform predictive models.

The Kinabatangan River in Sabah, Malaysia, offers an important opportunity to study the morphological change induced by rapid land conversion along tropical river boundaries. Widespread deforestation has transformed much of the Kinabatangan's lowland floodplain as oil palm plantations have replaced tropical forest, leading to the complete removal of natural riparian cover along many reaches, which has been clearly recorded in Landsat imagery. This provides an opportunity to quantify the geomorphic response of the Kinabatangan River to the conversion of its floodplain forest, and to examine in detail the relationship between riparian vegetation and the mechanisms that drive riverbank retreat.

Ecosystem functions and services constitute flows of materials, energy, and information from natural capital stocks to the benefit of human welfare [*Costanza et al.*, 1997]. Any quantifiable geomorphic response resulting from the removal of natural riparian cover may be viewed as the consequence of a shift in ecosystem functions. Where this shift is to the detriment of adjacent plantations, the retention of natural forest cover may provide a beneficial ecosystem service. In assessing the potential economic benefit of forest retention to agricultural plantations in close proximity to the Kinabatangan River, I hope to provide a case study that might be used to define a geomorphic ecosystem function within a formal ecosystem approach policy framework.

In measuring the historic response of the Kinabatangan River to the total removal of riparian forest, attempting to identify the shift in mechanisms driving geomorphic change, and assessing the potential benefit to adjacent oil palm plantations derived from an associated geomorphic ecosystem function, this investigation seeks to better understand the role of floodplain forest in the meandering dynamics of a large tropical river in ways that might practically inform the management of future forest conversion.

1.2 Main aim and research questions

The principal aim of this research is to assess the role of tropical floodplain forest as a control on the meandering dynamics of a large river by quantifying the morphological impact of its removal at the reach scale, defining 'large river' to be a river where bank heights far exceed the depth of root penetration. To address this aim I pose the following research questions:

1. How do rates of channel migration differ between sections of river banked by riparian forest, and sections cleared of riparian cover?
2. Does the removal of riparian forest alter the relationship between riverbank retreat and curvature induced forcing of river flows?
3. Does riparian forest preform a geomorphic function, and could this be used as an ecosystem service to adjacent agricultural land?
4. By what process(es) can riparian forest exert a control on rates of channel migration when riverbank heights far exceed rooting depths?

By examining these questions I hope to better understand the dominant mechanisms that drive meander migration along large rivers, and explore the potential for riparian forest as a first order control on rates of channel migration along the Kinabatangan River.

1.3 Thesis structure

Chapter 2 provides a general introduction to the subject of riverbank retreat, outlining the governing processes, and the current understanding of how riparian vegetation interacts with these processes. Chapters 3, 4, and 5 are then presented as a series of journal manuscripts, each with a distinct research question, but later chapters build on the work presented in the former. In Chapter 3, I compare rates of channel migration along the Kinabatangan River for sections cleared of riparian vegetation with those that maintain

forest cover for the period 1989 - 2014, and examine the role velocity perturbations play in controlling riverbank retreat. In Chapter 4 I provide estimates for mean area of land lost per unit length of river under different scenarios of future land conversion along sections of river flowing through unprotected forest, and quantify the economic worth of retaining riparian buffers to protect oil palm plantations adjacent to the Kinabatangan River. In Chapter 5 I then demonstrate how riparian vegetation might plausibly affect the processes of riverbank retreat where riverbank heights exceed rooting depths, by modifying an existing model framework to explicitly represent a dense root network within slump block armament. Finally, chapter 6 offers a broader discussion, with general conclusions and suggestions for further research.

1.4 The Lower Kinabatangan

Draining 16,800 km^2 of northern Borneo, the Kinabatangan River (**Figure 1**) flows for 560 km from the interior mountains of the Maliau Basin to the Sulu Sea.

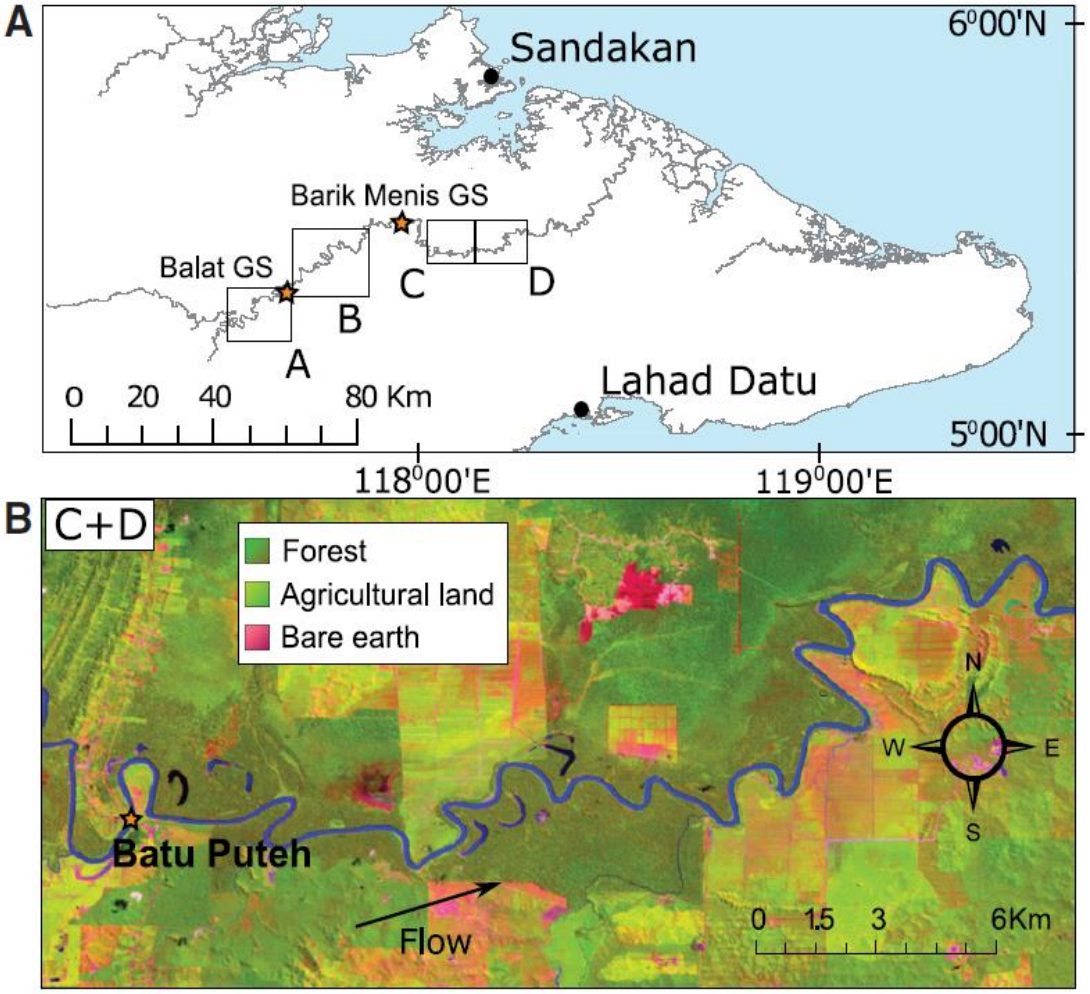

Figure 1: Locations of study reaches (A–D) and Barik Menis and Balat gauging stations (GS), Kinabatangan River, Malaysia. B: False-colour composite of Landsat satellite bands 3, 4, and 5 taken in October 2009, showing extent of reach C and D and location of Batu Puteh village (orange star), with legend defining associated land-cover types.

The climate is typical of a humid tropical environment, with mean annual rainfall exceeding 2500 mm (**Figure 2**) and consistent mean temperatures of around 30 °C, making it ideal for oil palm cultivation [*Pirker et al.*, 2016]. In recent decades, over half of the natural floodplain cover has been converted to agricultural plantations, and much of the remaining forest has been heavily impacted by commercial timber exploitation [*Abram et al.*, 2014]. Yet despite high levels of habitat degradation and fragmentation, the lower floodplains of

the Kinabatangan (5°20′− 5°45′ N, 117°40′− 118°30′ E) are one of the most important Malaysian wetlands for bio-diversity harbouring 129 species of mammal, 314 species of birds, 101 species of reptiles, and 33 species of amphibians [*Lackman-Ancrenaz and Manokaran,* 2008; *Bruford et al.*, 2010]. Many of these species are threatened IUCN (International Union for Conservation of Nature) Red List species such as the Bornean elephant, Bornean orangutan, and proboscis monkey [*Goossens et al.*, 2005; *Estes et al.*, 2012]. In an effort to safeguard this important ecological resource, the Lower Kinabatangan Wildlife Sanctuary (LKWS) was gazetted in 2005, comprising a total of 27,000 ha covering a patchwork of habitat types: riverine forest, seasonally flooded forest, swamp forest, dry dipterocarp forest, and mangroves. However, significant areas of unprotected forest remain outside the protected areas, and despite conservation initiatives to secure these unprotected forests, they remain threatened with future conversion to oil palm [*Abram et al.*, 2014].

1.4.1 Study Reaches

I selected each of my four study reaches to provide examples of riverbanks with varying degrees of land-cover alterations, and to ensure observations of river meandering were unhindered by geological (e.g., bedrock outcrop) or engineering (e.g., riverbank revetment) controls (**Figure 1A**). Within these study reaches the river has an average bankfull river width of 112.7 m (1σ = 1.4 m) (**Table A1 in the Appendix**), measured as the average distance between vegetated banks. The majority of the forest cover along the riverbanks is seasonally inundated primary forest that has been degraded by selective logging, though there are small sections classified as virgin reserves. Within each of the four reaches there are sections of riverbank entirely cleared of riparian forest, most of which have been

colonised by tall grass species (*Phragmites australis* and *Pennisetum purpureum*). Riverbanks are >8 m in height, whilst the rooting depth of large trees penetrate roughly 2 m, and the grasses along cleared sections penetrate 0.5–1.0 m. Coordinates of the upstream and downstream extremities, streamwise length, sinuosity, and number of cleared sections for each study reach are listed in **Table 1**.

Table 1: List of reach characteristics

	Reach A	Reach B	Reach C	Reach D
Streamwise length [m]	54500	43603	29415	21088
Sinuosity	2.73	2.41	1.46	2.64
Upstream Coordinates [^{0}lat, ^{0}lon]	5.2217, 117.4982	5.3595, 117.6655	5.4123, 117.9394	5.4106, 118.0789
Downstream Coordinates [^{0}lat, ^{0}lon]	5.3595, 117.6655	5.4729, 117.7989	5.4106, 118.0789	5.4600, 118.1573
No. cleared river sections	7	6	4	5

1.4.2 Rainfall Data

Rainfall data was recorded at Balat Gauging station from 1985 – 2013 (**Figure 2**), and was provided by the Department of Irrigation and Drainage in Kota Kinabalu, Sabah, Malaysia.

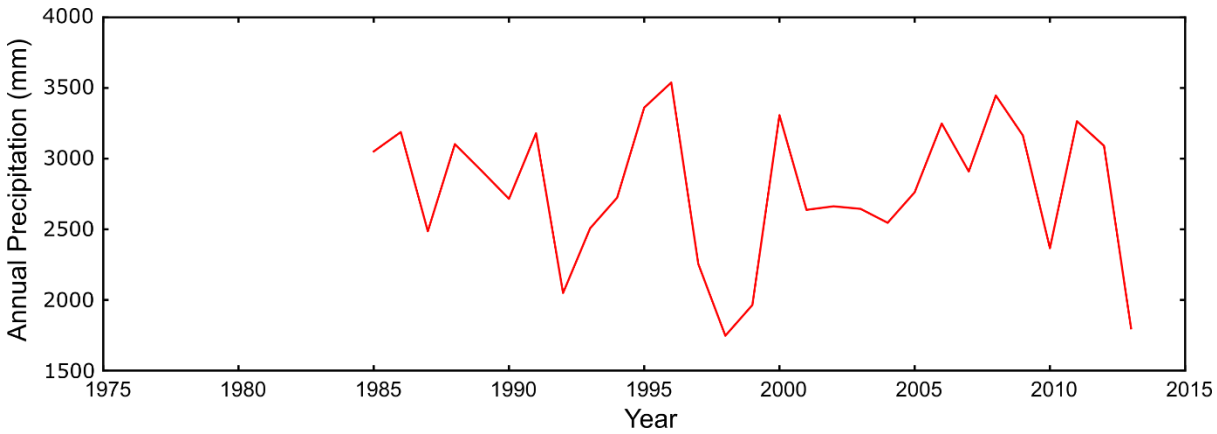

Figure 2: Annual Rainfall data collected from Balat station (1985 – 2013). Mean of 2780 mm across all years.

1.4.3 River Discharge

Discharge data was recorded at Balat Guaging station from 1978 – 2013**,** and Barik Menis Guaging station from 2000 – 2013 (**Figure 3**)**.** Both sets of data were provided by the Department of Irrigation and Drainage in Kota Kinabalu, Sabah, Malaysia.

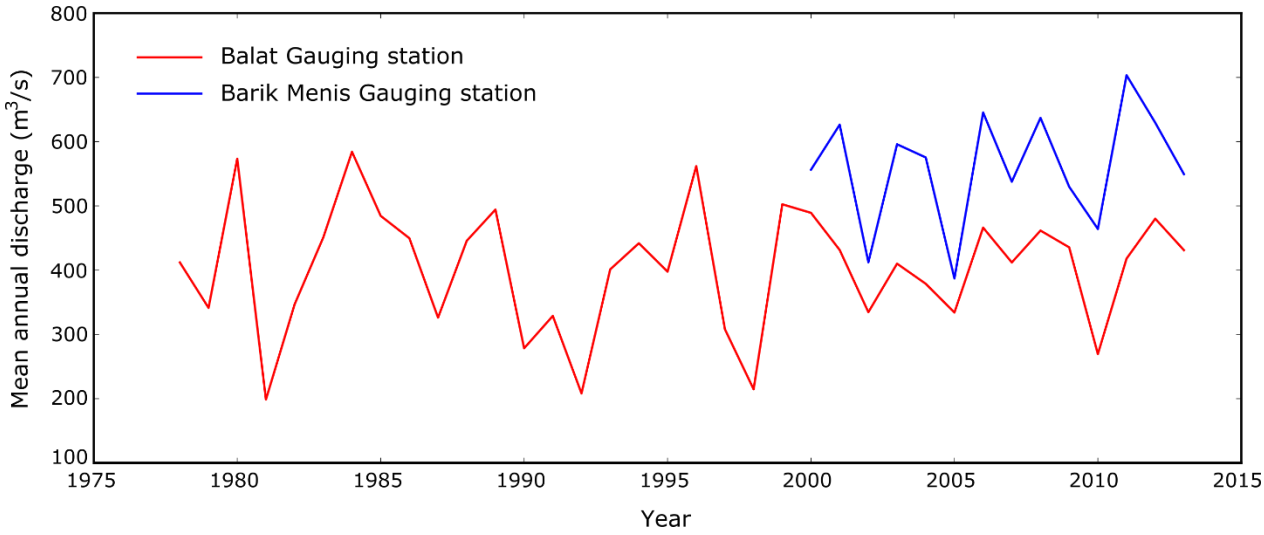

Figure 3: Mean annual discharge data collected from Balat gauging station (1978 – 2013), and Barik Menis (2000 – 2013).

Chapter 2:

Meandering rivers

Early investigations into the relationship between river hydrology and sediment transport sought to develop general relationships describing the transportation capacity of a fluvial system, and its potential for geomorphic change [*Gilbert*, 1877; *Shields*, 1936; *Einstein*, 1950; *Partheniades*, 1965; *Bagnold*, 1966]. Whilst the origins of modern fluvial geomorphology can be found in seminal works attempting to understand the ubiquitous forms of river meanders [*Leopold and Wolman*, 1957, 1960; *Schumm*, 1960]. Developing relations of large scale patterns to describe generic features, such as the relation between meander wavelength and river discharge, the emphasis was on longer timeframes assuming that meander formation tends towards a state of dynamic equilibrium, with investigations into the processes that govern riverbank retreat conducted at the reach scale [*Lane*, 1955; *Wolman*, 1959]. In the 1970 - 1980's the emphasis shifted to quantitative research at a smaller scale, looking at the short-term processes that govern meander development, seeking to identify and describe the underlying physical principles behind observed empirical relationships [*Hickin*, 1974; *Brice*, 1977; *Hooke*, 1980; *Thorne et al.*, 1981; *Nanson and Hickin*, 1986; *Odgaard*, 1986, 1987; *Osman and Thorne*, 1988].

2.1 Riverbank retreat

In examining the processes that drive meander development at the scale of individual bends, riverbank retreat was understood to be the driver of morphodynamic change, and a consequence of two distinct events: the delivery of failed riverbank material to the channel margins by abrupt riverbank collapse (mass failure), and the removal of sediment from the bank face by fluvial scour (fluvial entrainment) [*Lawler et al.*, 1997]. It is the balance of these two events that governs the development of meandering forms, as the relative dominance

of either one controls the adjustment of riverbanks, and rates of channel migration [*Thorne,* 1991].

2.1.1 Fluvial entrainment

Fluvial entrainment is the removal of riverbank and riverbed material by lift and drag forces applied by the channel flow [*Thorne et al.*, 1981]. In the case where river bed and bank material is made of non-cohesive soil particles, rates of erosion are dependent upon the balance of effective shear stresses exerted by the water and the critical shear stress of the particulate matter. *Shields* [1936] conducted a study of the forces necessary to initiate bed load movement in a river made of uniform non-cohesive material. He demonstrated that the critical shear stress of non-cohesive soil is a function of grain shape, density, and size, with the latter being the dominant consideration. Unlike non-cohesive materials, cohesive sediment does not erode by discrete particle entrainment, but rather as an aggregate [*Thorne*, 1991], being made of very fine particles that have a large specific surface area relative to their mass, which provides a net negative electrical-surface charge on the particle [*Simon and Collison*, 2001], which is responsible for the electro-chemical bonds that bind particles and form aggregates. It is the formation of aggregates, and their response to environmental factors that makes predicting the erodibility of cohesive sediment difficult. The shear stress required to erode cohesive sediment is not only dependent upon the grain size distribution of the sediment, grain density, and grain shape; but also the microscopic and macroscopic clay properties, the temperature and pH of the flowing water, the thixotropy of the sediment, soil moisture content, and the topography of the riverbank - for these will all determine the size of entrained aggregates [*Kamphuis and Hall*, 1983]. *Clark & Wynn* [2007] present a detailed review of the various means by which critical shear stress of cohesive soils can be approximated - comparing the extended Shields diagram [*Vanoni*,

1977], an empirical derived expression for τ_c as a function of clay percentage [*Julian and Torres*, 2006], and several expressions for τ_c as a function of plasticity index, dispersion ratio, mean particle size, and percent clay [*Smerdon and Beasley*, 1961].

Rates of fluvial entrainment are commonly predicted using the excess shear model, either in the form suggested by *Arulanandan et al.* [1980]

$$\varepsilon = k_d(\tau_a - \tau_c)^a$$

or *Kandiah*, [1974]

$$\varepsilon = k_d\left(\frac{\tau_a}{\tau_c} - 1\right)^a$$

where ε is the erosion rate [m/s], k_d is an empirically derived erodibility coefficient, τ_a is applied shear stress on the soil boundary [Pa], τ_c is the critical shear stress of the material [Pa], and a is a fitted exponent usually assumed to be 1.

Measurements, or model approximations, of the flow field around a meander bend are required to estimate rates of fluvial entrainment, as they are dependent upon the boundary shear stress acting on the bank face. Rates of riverbank retreat are then dependent upon the balance between the volume of sediment delivered to the bank toe by mass failure, and its subsequent removal by fluvial entrainment [*Thorne,* 1991].

2.1.2 Mass Failure Mechanisms

Where the rate of fluvial entrainment exceeds the rate of sediment deposition at the bank toe, the angle and/or the height of the river bank will increase [*Osman and Thorne*, 1988; *Thorne*, 1991]. This steepening of the bank face may lead to instability and mass failure when shear stresses imposed by the weight of bank material exceed the shear strength of the soil on the most critical potential failure surface [*Lawler*, 1992, 1995]. In non-cohesive soils, mass failure is mainly in the form of avalanching, where individual particles that make

up the bank face cascade to the base when the slope angle is higher than that of repose [*ASCE Task Committee*, 1998]. Where river banks are comprised of cohesive and non-cohesive layers, either cantilever, planar, or rotational failure occur. The predominant mechanism of failure is determined by the composite geotechnical properties of the bank, and the prevalence of fluvial entrainment at the lower layers. Where a cohesive layer sits atop a non-cohesive base layer, fluvial scour of the lower layer can lead to undercutting, and the cohesive top layer then wastes by cantilever failure [*Thorne et al.*, 1981]. *Pizzuto* [1984] proposed a five-part model to describe cantilever failure, where preferential scouring of the lower (non-cohesive) bank leaves an overhanging portion of the upper layer, which is subject to large tensile stresses (**Figure 4**).

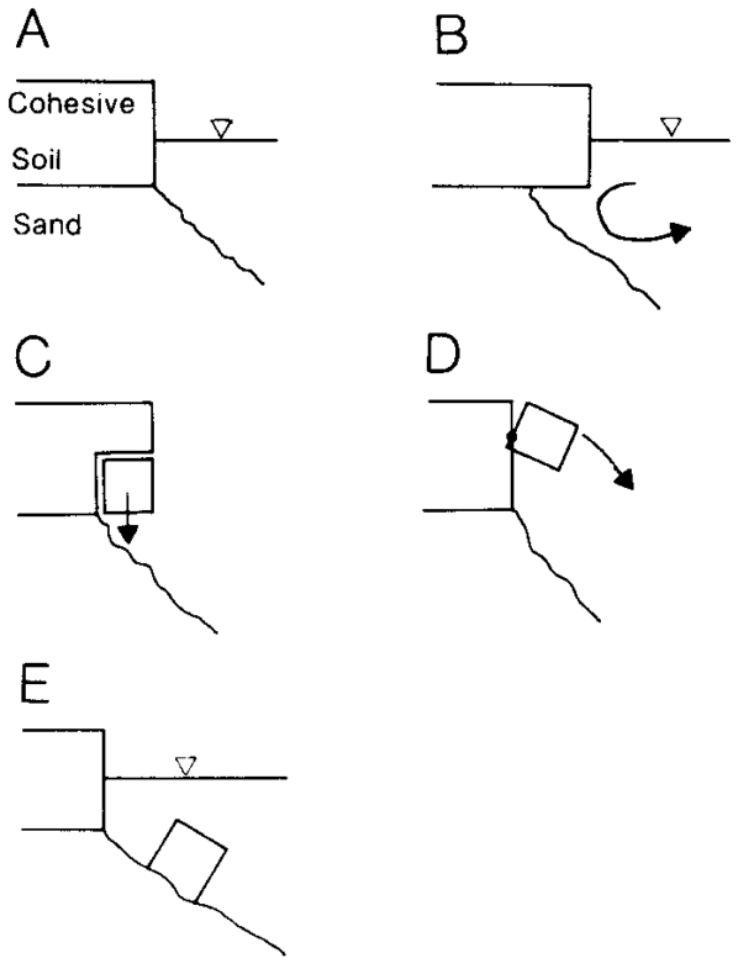

Figure 4: Five-part model of cantilever failure. 1C is tensile failure, and 1D is a beam failure. [Pizzuto, 1984]

If horizontal planes of weakness exist within the cohesive layer, tensile failures may cause the lower portion of the overhanging block to fail (**Figure 4C**). When gravitational forces cause shear stresses that exceed the resistive shear strength, the overhanging block fails either along a vertical plane, or where disruptive moments acting about an internal axis exceed the restoring moments, the block rotates into the river channel (**Figure 4D**).

For cantilever failure to occur, the composite shear strength of bank material needs to be sufficient to allow overhanging of the upper layers to develop. Where the internal cohesion of riverbank sediments is insufficient to support overhanging bank geometries, mass wasting occurs by planar failures either along a potential planar surface, or about a rotational moment. In channels where bank slope is relatively shallow (<60°), the dominant failure mechanism is rotational slip [*ASCE Task Committee*, 1998], which has been extensively studied in the field of hill slope stability analysis, and established methods exist for predicting the factor of safety for a riverbank in terms of the ratio of restoring to disturbing moments about the centre of a failure circle [*Bishop*, 1955; *Varnes*, 1978] (**Figure 5A**).

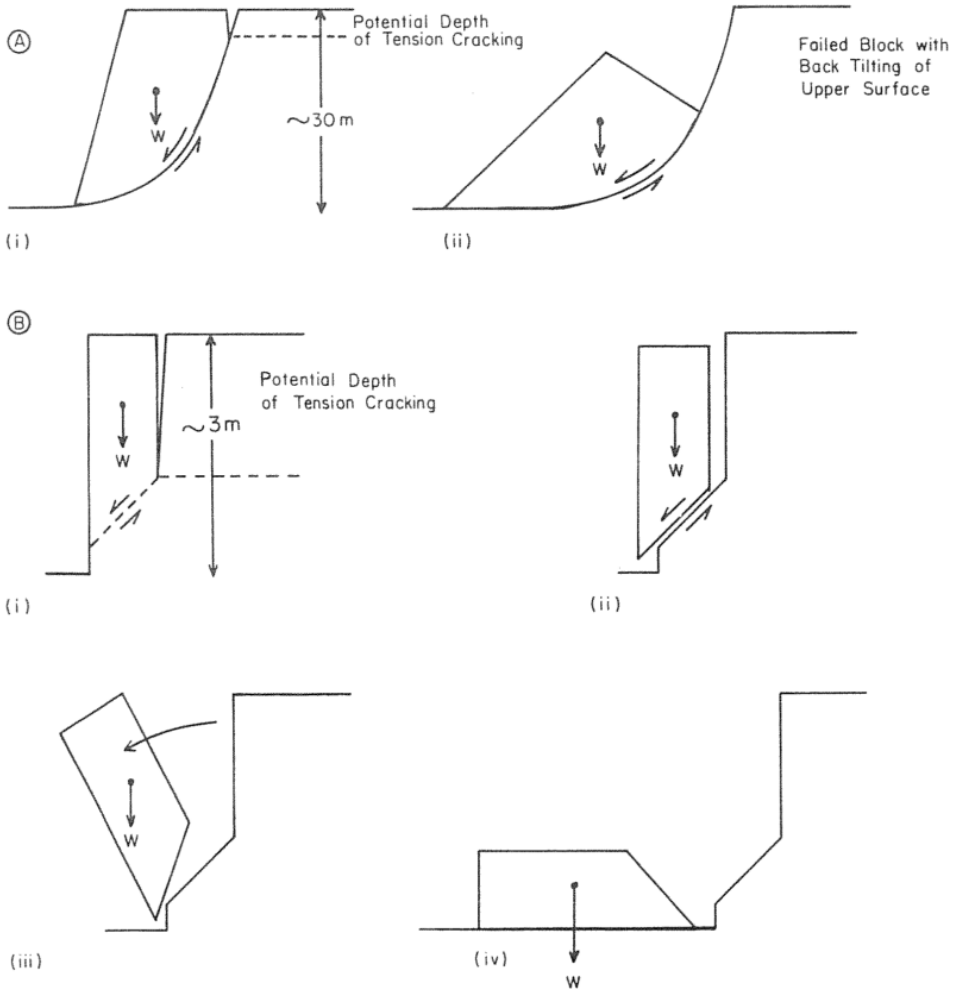

Figure 5: (a) Rotational slip in cohesive river bank: (b) Planar failure in cohesive river bank. Taken from Thorne et al. [1981]

Rotational slips are the least common failure mechanisms as they require the formation of high banks at a relatively shallow gradients [*Simon*, 1989]. **Figure 5B** shows a planar failure, which is the predominant form of mass wasting in the absence of undercutting [*ASCE Task Committee*, 1998]. A number of slope-stability models have been developed for the prediction of bank retreat by failure events in a cohesive riverbank, most taking the form of a limit equilibrium model that evaluates a factor of safety along potential slide surfaces [*Darby and Thorne*, 1996]. The factor of safety expression for planar shearing is the ratio between resisting stresses and driving stresses. For the simple case of a planar

failure of unit width and length, the resistive stress (shear strength) can be described by the standard Mohr – Coulomb equation [*Simon et al.*, 2000]:

$$S_r = c' + (\sigma - \mu)tan\phi' \qquad (1)$$

where S_r is shear strength, c' is effective cohesion (kPa), σ is the normal stress (kPa), μ is pore-water pressure (kPa), and ϕ' is the effective friction angle (°).

The normal stress is given by:

$$\sigma = Wcos\beta \qquad (2)$$

where W is the weight of the failure block (N) and β is the angle of the failure plane.

Driving stresses (S_d) are the shear stresses of the failure block acting parallel to the failure plane:

$$S_d = Wsin\beta \qquad (3)$$

Fluvial entrainment of material from the lower layers of riverbanks steepens the angle of repose, which increases the size and so weight of failure blocks along potential slip planes until the driving stresses outweigh the resistive stresses, inducing bank collapse. Though in nature, steep river banks will often fail before the predicted height or slope angle has been attained due to tension cracks that form in the bank, weakening the material and truncating the potential failure surface [*ASCE Task Committee*, 1998]. Tension cracks may isolate large blocks of river bank material which then fail by shearing along a plane (**Figure 5B**).

The frequency, magnitude, and type of mass failure along riverbanks is strongly affected by the antecedent conditions of riverbank materials, and the hydrological regime within the bank structure. In this regard, climatically driven processes that act on the riverbank to weaken and weather the material can play an important role in governing rates of riverbank retreat [*Lawler*, 1992, 1995]. Early studies conducted by *Wolman* [1959] and

Knighton [1973] illustrated the propensity for streams to erode with frequent small events under wet conditions predominantly during winter. These observations have directed many subsequent studies to quantify the effect of wetting and drying of riverbank material, pore water pressures, and temperature fluctuations on riverbank erosion rates. These subaerial processes are dominant controls on rates of riverbank retreat in headwater reaches, where boundary shear stresses are insufficient to generate significant fluvial entrainment without the bank material having first been loosened or displaced [*Abernethy and Rutherfurd*, 1998]. Despite assertions that subaerial processes are merely preparatory processes of secondary importance, observations of matric suction on the stability of riverbanks suggest otherwise [*Casagli et al.*, 1999; *Rinaldi and Casagli*, 1999; *Simon et al.*, 2000; *Simon and Collison*, 2001]. During low and moderate river stage, the water table is usually deep in comparison to the bank height of an incised river channel, meaning that a large portion of the riverbank is unsaturated and experiences negative pore-water pressures exerted by capillary action [*Simon et al.*, 2000; *Schiller and Wynne*, 2009]. Negative pore-water pressures act as apparent cohesion, binding the soil and significantly increasing the critical shear strength of the riverbank. To incorporate this effect, the standard Mohr – Coulomb equation is modified as in *Fredlund and Rahardjo* [1993]

$$S_r = c' + (\sigma - \mu_a)tan\phi' + (\mu_a - \mu_w)tan\phi^b \qquad (4)$$

where μ_a is air pressure, μ_w is pore-water pressure and ϕ^b is the increase in shear strength (°) due to matric suction, which is generally 10° – 20°, but attains a maximum of ϕ' under saturated conditions where pore water pressures are positive, recovering the standard Mohr – Coulomb equation. Although subaerial climatic processes play a role in the regulation of pore-water pressures within the riverbank, studies by *Simon and Collison* [2001] and *Rinaldi et al.* [2004] demonstrate that the generation of positive pore-water

pressures is largely driven by the rise and subsequent fall of river stage. On the rising limb of a river hydrograph, the bank saturates and pore-water pressures switch from negative to positive due to lateral seepage from the channel to the bank. This reduces the resisting stresses of the bank material, and destabilises the riverbank. As the high flow event then recedes, the removal of hydrostatic confining pressures induces mass failures, suggesting that a river bank is at its most susceptible to erosion when thoroughly wetted by a series of peak flow events [*Casagli et al.*, 1999; *Rinaldi et al.*, 2004]. In addition to increasing pore-water pressures within the bank structure, large fluctuations in river stage can cause undercutting from lateral seepage, whereby particles are entrained by ground water flowing from a saturated bank to the channel margin [*Fox and Wilson*, 2006; *Wilson and Periketi*, 2007; *Cancienne et al.*, 2008]. More commonly, seepage erosion occurs where a river bank crosses the boundary between materials of differing hydraulic conductivities, or where high infiltration rates cause a perched water table to develop above water-restricting horizons [*Wilson et al*., 1991; *Jones*, 1997]. For any model of riverbank stability to provide quantitative estimates of bank retreat, there needs to be a sub-model describing the process of fluvial entrainment that accounts for the removal of material at the bank toe.

2.1.3 Modelling Riverbank Retreat

Some of the earliest models of riverbank retreat were stochastic in nature, expressing bank erosion as a function of the flow field around a meander bend in an open channel [*Ikeda et al.*, 1981; *Johannesson and Parker*, 1989]. Based on an analytic solution of the St Venant equations of shallow water flow in a sinuous channel [*Engelund*, 1974], they treat meander development as a spatial convolution, where local bend migration is a mathematically weighted aggregate of up-stream curvature and bed topography. Rather than explicitly represent the changing geometry of river banks by processes at the local scale, these

investigations recognised the interdependency of meanders, and sought to understand the complex patterns observed across floodplains by replicating their formation and development over longer timeframes. Reductionist in form, the models linearly relate the erosion of riverbanks to the velocity perturbation along the outer bank (the difference between depth-averaged velocity at the outer bank and cross-sectional mean velocity) byway of an empirically calibrated erodibility coefficient [*Hasegawa*, 1977; *Ikeda et al.*, 1981; *Johannesson and Parker*, 1989] – a stochastic amalgamation of properties governing the relative erodibility of a riverbank: material composition, vegetation density, and hydrological conditions. In representing the asymmetric flow field around a meander bend that results from an acceleration of river flows induced by curvature and bed topography, and the secondary convective currents driven by a transverse super-elevation of the water surface, linear theories of meander migration are able to replicate observed patterns; such as the down-stream skew of maximum migration, and the preferential development of larger bends [*Hasegawa*, 1989; *Pizzuto and Meckelnburg*, 1989; *Furbish*, 1991]. Although higher order solutions to the Navier-Stokes equations have been developed [*Zolezzi and Seminara*, 2001; *Camporeale et al.*, 2007; *Abad et al.*, 2013], due to their complexity, and the relative success of the *Ikeda et al.* [1981] and *Johannesson and Parker* [1989] models in predicting observed evolution, the first order numerical approximation suggested by *Sun et al.* [1996] is still commonly employed to estimate near-bank velocities and associated riverbank retreat [*Micheli et al.*, 2004; *Constantine et al.*, 2009].

2.1.4 Coupled Mechanistic and Stochastic Models

Models that link rates of riverbank erosion to the near-bank flow velocity via an empirically calibrated erodibility co-efficient assume an idealised floodplain homogeneity, and fail to relate bank retreat to the physical characteristics of the sedimentary environment [*Darby et*

al., 2002]. Recent years have seen the development of coupled models that account for both the flow field around a meander bend and the mechanistic processes driven by bank geometry and stratigraphy. *Darby et al.* [2002, 2007] couple a hydraulic erosion model with a finite element seepage and limit equilibrium stability analysis to assess the relative importance of profile deformation and variations in bank hydrology in triggering mass wasting, highlighting the importance of representing process interaction. Both the studies of *Langendoen and Simon* [2008] and *Motta et al.* [2012] couple a first order solution to the flow field around a meander bend [*Ikeda et al.*, 1981; *Johannesson and Parker*, 1989] with the physically-based streambank erosion algorithms of the CONCEPTS (CONservational Channel Evolution and Pollutant Transport System) channel evolution model, finding that a mechanistic representation of bank failures improves the long-term reproduction of observed forms compared to stochastic bank erodibility. The application of coupled models thus far have dealt with vertical heterogeneity of bank material by mechanistically representing bank stratigraphy, however, representing the spatial heterogeneity across floodplain materials may be more important for the accurate reproduction of the planform dynamics of large meandering rivers [*Konsoer et al.*, 2016a].

In 2011, *Parker et al.* presented 'A new framework for modelling the migration of meandering rivers' that highlighted the importance of representing the armouring effect of failed material. Based on the continuity of sediment transport, it describes the co-evolution of outer and inner banks as they adjust to changes in planform geometry tending towards a state of equilibrium. This marks a break from previous modelling frameworks in its representation of independent banks connected by the morphodynamic flow field in the shared bed region. Several studies have adapted this model framework, incorporating slump-block armament as a proxy for the effect of cohesion on retarding bank retreat, and

allowing dynamic width adjustment as the channel moves through the floodplain [*Asahi et al.*, 2013; *Motta et al.*, 2014]. By way of a globally imposed formative Shield's number *Eke et al.* [2014] directly link the processes of bank erosion and bar deposition, effectively closing the system. The representation of vegetated slump-block armouring prevents runaway erosion of unprotected banks that is characteristic of purely non-cohesive channels [*Gran and Paola*, 2001; *Tal and Paola*, 2010]. However, none of the coupled simulations of meander migration explicitly represent the influence of riparian vegetation in controlling rates of riverbank retreat.

2.2 Effects of Vegetation on Riverbank Retreat

Many studies have demonstrated the importance of riparian vegetation on determining channel geometry [*Hadley,* 1961; *Zimmerman et al.,* 1967; *Allmendinger et al.*, 2005]. Vegetation may even be a necessary requirement to maintain a meandering planform in environments where cohesion in sparse – with some investigations finding that rivers shift between braided and single-thread systems as the type and density of vegetation across the floodplains change [*Mackin,* 1956; *Brice,* 1964; *Gran and Paola*, 2001; *Tal and Paola*, 2010].

Smith [1976] conducted a study of the stabilising properties of root networks on the banks of the Saskatchewan River in Banff, Canada, concluding that, for cool environments with heavily vegetated banks, erosion rates were 20,000 times less than non-vegetated banks. Though this marks an extremity in early attempts to quantify the effects of vegetation, further studies found significant reductions in the rates of channel migration along vegetated riverbanks [*Hickin*, 1984; *Odgaard*, 1987; *Pizzuto and Meckelnburg*, 1989; *Beeson and Doyle*, 1995]. *Micheli et al.* [2004] compared erodibility coefficients of sections of the Sacramento River flowing through stands of both riparian forest and agricultural

vegetation, finding that erodibility coefficients along banks with riparian coverage were reduced 90 – 150%. Subsequent studies have tended to focus on process representation, identifying the mechanisms by which vegetation alters the structural properties of riverbanks, or reduces rates of fluvial entrainment.

2.2.1 Fluvial Entrainment

Vegetation affects fluvial entrainment by altering the balance of boundary shear stress to resistive forces. The addition of roughness along channel margins due to vegetation reduces near bank velocities, and can deflect flows towards the channel centre [*Thorne and Furbish*, 1995a; *Nepf and Vivoni*, 2000; *Bennett et al.*, 2002; *Hopkinson and Wynn*, 2009]. However, reductions in boundary shear stresses may be offset by the induction of turbulence effects that promote localized scouring along the bank face [*Czarnomski and Tullos*, 2012]. The overall contribution of vegetation to rates of fluvial scour are difficult to quantify and are highly site specific, as any alteration to the direction and intensity of the near bank flow field varies with vegetation density, type, rigidity, and location [*Kouwen and Li*, 1980; *Righetti*, 2008].

In addition to affecting the shear stresses within the channel by altering the flow field, vegetation alters the structure and composition of the bank material itself, thereby affecting the erodibility of riverbanks. In binding the soil together, root structures reduce the propensity of soils to erode by fluvial scour [*Dunaway et al.*, 1994; *Mamo and Bubenzer*, 2001; *Gyssels et al.*, 2005; *De Baets et al.*, 2006; *De Baets and Poesen*, 2010; *Vannoppen et al.*, 2015]. Although the presence of a root network has been shown to reduce streambank erodibility [*Smith*, 1976; *Wynn and Mostaghimi*, 2006; *Langendoen et al.*, 2009; *Pollen-Bankhead and Simon*, 2010], the effect of vegetation on the critical shear stress of materials is less well defined [*Mamo and Bubenzer*, 2001]. Root exudates of plants may also influence

the chemical composition of soils, altering the internal cohesion and so resistance to erosion [*Pojasok and Kay*, 1990; *Wynn and Mostaghimi*, 2006].

2.2.2 Hydrological Effects

Riparian vegetation alters the hydrology of riverbanks in a variety of ways, some promote stability, whist others reduce stability [*Pollen et al.*, 2004]. The main destabilising contribution of vegetation is in altering infiltration pathways and the hydraulic conductivity of riverbank materials. In creating macropores, channels carved by roots that are conduits for flow, rates of precipitation infiltration are higher and can more extensively penetrate bank materials [*Simon and Collison*, 2002]. Rainfall that penetrates through the riparian canopy may also be concentrated around the stem and trunk of vegetation, creating localised areas of high pore-water pressures [*Durocher*, 1990]. These both contribute to the saturation of the riverbank, and so reduce the frictional shear strength of the soils, which promote instability and can lead to mass failure.

With the exception of intense rainfall periods during winter months (not in growing season), destabilising alterations to riverbank hydrology as a result of riparian vegetation are counteracted primarily by the functions of canopy interception, evaporation, and transpiration, which is the extraction of soil moisture by the absorption of plant roots followed by stomatal evaporation. The combined effect of reducing precipitation through-fall, and directly drawing water out from the soil column, is to greatly increase the matric suction within the soil matrix, and by extension, the apparent cohesion of the riverbank material [*Simon and Collison*, 2002; *Pollen et al.*, 2004; *Fatahi et al.*, 2006; *Pollen-Bankhead and Simon*, 2010].

2.2.3 Mass Failures

Soil is generally strong in compression, but weak in tension. Plant roots are weak in compression, but strong in tension [*Thorne*, 1990]. Root-permeated soil, therefore, makes up a composite material that has enhanced strength. Roots that anchor themselves into the soil in order to support the above ground vegetation provide reinforcement to the soil matrix by transferring shear stress in the soil to tensile stress in the roots [*Coppin et al.*, 1990]. The study of soil reinforcement by roots has long been of interest to researchers in the field of slope stability. *Waldron* [1977] was amongst the first to quantify root reinforcement by comparing in situ shear box measurements of soils with root networks, followed by numerous investigations into the effect of fibre reinforcement on hill slope stability for application in civil engineering [*Wu et al.*, 1979; *Endo*, 1980; *Waldron and Dakessian*, 1981; *Gray and Ohashi*, 1983; *Coppin et al.*, 1990]. Application to the stability of riverbanks came later [*Thorne*, 1990; *Abernethy and Rutherfurd*, 1998, 2000], where root reinforcement was evaluated using simple perpendicular root models such as that proposed by *Wu et al.* [1979]

$$c_r = T_r \frac{A_r}{A} (cos\theta tan\phi + sin\theta) \qquad (5)$$

where c_r is the increase in soil strength [kPa], T_r is the tensile strength of roots [kPa], A_r is the area of shear surface occupied by roots [m^2], A is the area of shear surface [m^2], θ is the shear distortion from vertical [degrees], and ϕ is the friction angle of soil [degrees]. **Figure 6** illustrates the *Wu et al.* [1979] model, where a root initially perpendicular to the shear plane deforms as the soil undergoes shear. As the root deforms to an angle of θ, tensile stresses accumulate in the root counteracted by the frictional shear strength of the soil-root interface, which is assumed to be larger than the tensile limit of the root, simulating root

breakage rather than pull-out. The value of: (cos θ tan ϕ + sinθ) is relatively insensitive to variations of θ and ϕ within the range of expected values (40 – 90° and 25 - 40° respectively), and so an empirically derived approximation of 1.2 is usually adopted [*Wu et al.,* 1979] . The Mohr-Coulomb equation can be further modified to incorporate additional shear stress (c_r) to estimate the overall shear strength of the soil-root composite within a riverbank.

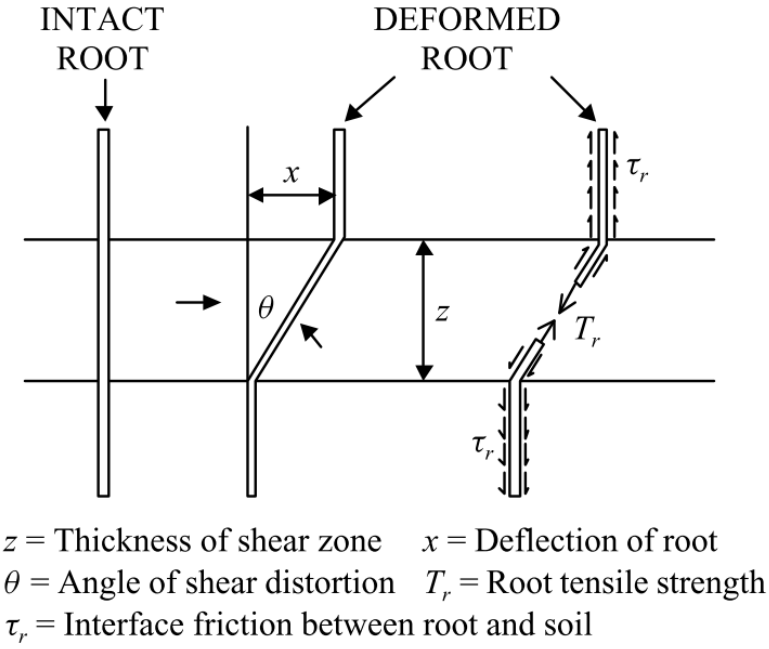

Figure 6: Root-reinforcement model with a flexible elastic root aligned perpendicularly to the shear zone at start. Taken from Abernethy and Rutherfurd [2001].

The *Wu et al.* [1979] model assumes that all roots fail by rupture not pull-out, so that fibres utilise their full tensile strengths before failure. A more significant simplification is the assumption that all roots utilise their maximum tensile strengths before failing simultaneously. In reality a soil-root matrix contains a distribution of root sizes and tensile maximums - roots with lower tensile maximums or relative elasticity fail first, and the weight redistribution of the of the soil matrix triggers a progressive cascade failure [*Pollen and Simon*, 2005]. In not representing the redistribution of weight and progressive root

failure, static models effectively sum the tensile strengths of all roots [*Waldron*, 1977; *Wu et al.*, 1979], overestimating the root reinforcement of soils.

Accounting for cascade failure, fibre bundle models (FBMs) estimate the additional shear strength added to a material by a network of fibres as less than the sum strength of the individual fibres. An early example of a FBM was proposed by *Daniels* [1945], which has been modified to take one of two general forms: global load sharing (GLS), or local load sharing (LLS). Both GLS and LLS FBMs initially distribute an imposed weight evenly across a bundle of *n* fibres, gradually increasing the load until the first fibre breaks, when the global load is then redistributed amongst the remaining *(n-1)* fibres. Should this redistribution cause additional fibres to rupture, the load is once again redistributed until it causes no further ruptures. The applied load is then increased and the process of redistribution following ruptures is repeated until all fibres have failed [*Pollen and Simon*, 2005]. GLS and LLS FBMs differ in the way they redistribute the global load after rupture. In the GLS models, the load is distributed evenly amongst the remaining fibres, where as in an LLS model, the load is redistributed to the fibres in close proximity to the failed fibre. The application of fibre bundle models have more accurately approximated the additional shear strength added to riverbanks by a riparian root network, which is both significant and highly variable [*Kun and Raischel*, 2006; *Loades et al.*, 2010; *Schwarz et al.*, 2010].

2.2.4 Model representation

To evaluate the relative impact of different vegetation effects on meandering dynamics at multiple scales, *Van de Wiel and Darby* [2004] adapted an existing mechanistic model of riverbank retreat to account for additional bank roughness on the flow field along the outer bank, and fibre reinforcement of riverbanks. Although riparian vegetation has the potential to increase localised bank retreat by altering flow patterns around individual meander

bends, at the reach scale vegetation is a stabilising influence that reduces floodplain loss, and has considerable impact on channel planform evolution. *Langendoen et al*. [2009] expanded upon this work by coupling the mechanistic model of riverbank retreat (incorporating a simple approximation of root reinforcement) with a Riparian Ecosystem Management Model (REMM) to account for the effect of vegetation on the internal hydrological composition of the riverbank. Comparing observations and modelled simulations from a riparian tree stand, grass buffer, and unvegetated riverbank, they conclude that both riparian buffers reduced riverbank retreat, but that the magnitude of the reduction in the case of a grass buffer was only slight. By contrast, the coarse root network greatly enhanced riverbank stability, suggesting that hydrological implications of vegetation on bank retreat are less dominant than mechanical when averaged over an annual cycle. This conclusion is refuted by the work of *Van der Wiel and Darby* [2009] that isolates the mechanical contribution of vegetation to bank stability as it effects the progressive failure of a variety of modelled banks. By representing root position across a potential failure plane, and the consequential impact on the factor of safety for a range of morphological and sedimentological conditions, they conclude that the magnitude of mechanical reinforcement is small, typically inducing changes less than 5%.

These detailed mechanistic evaluations of riparian vegetation's influence on rates of channel migration require extensive parameterisation, and so take place on the scale of individual meanders or small reaches over short timeframes. Therefore, models that stochastically amalgamate the multiple influences of vegetation on riverbank retreat have been developed to assess the role of vegetation dynamics in controlling long-term meander formation at the floodplain scale [*Perucca et al.*, 2007; *Camporeale and Perucca*, 2013]. By proportionately altering the erodibility coefficient used in a linear model of channel

migration [*Zolezzi and Seminara*, 2001] relative to the biomass of vegetation present along riverbanks, and running a sub-model that simulates the growth of vegetation (and so biomass) as a function of river proximity, complex linear and non-linear interactions give rise to a wide variety of meander formations highlighting the importance of vegetation dynamics on the morphological evolution of river systems.

Despite significant progress in our understanding of the role of trees in riverbank stability and retreat, there have been few attempts to quantify the geomorphic response of a large river catchment to extensive deforestation [*Latrubesse et al.*, 2009]. This is of acute importance in tropical regions, where vast tracks of riparian floodplain forests are being converted to agricultural lands [*Boucher et al.*, 2011].

Chapter 3:

Modification of River Meandering by Tropical Deforestation

Author Contributions

Much of the text presented here is a reproduction of a collaborative paper that was drafted by Dr José Antonito Constantine and myself, whilst the data processing, analysis, and model development are solely my own work.

3.1 Introduction

Tropical forests are the only forest biome to have experienced increased rates of forest loss during the past decade because of global demands for food and biofuels. The implications of such extensive forest clearing on the dynamics of tropical river systems remain relatively unknown, despite extensive study into the role of riparian vegetation in controlling channel migration. It is unclear the extent to which floodplain forest effects riverbank stability where rooting depths are only a fraction of riverbank heights, such as along many large meandering rivers [*Constantine et al.*, 2009; *Langendoen et al.*, 2009]. Even so, sustained erosion could be prevented by the supply of trees and rooted sediment to the base of riverbanks from the eroded riparian corridor [*Thorne and Furbish*, 1995a; *Parker et al.*, 2011], which may also act to buttress and stabilize the riverbank profile. The transient nature of these eroded and failed materials inside the river channel has made it unclear whether trees are important to the long-term meandering dynamics of large rivers [*Motta et al.*, 2014], preventing insight into the morphodynamic impacts of intensive deforestation taking place across tropical river systems worldwide.

Using the Kinabatangan River as a natural laboratory, I assess the role of trees in controlling rates and patterns of riverbank erosion along a large meandering river, by comparing rates of channel migration between forested river sections, and sections of the river cleared of riparian cover. I conclude by proposing hypotheses to explain an observed change in the relationship between rates of riverbank erosion and modelled estimates of the curvature-driven forcing of river flow following deforestation.

3.2 Methods

3.2.1 Channel migration

Using sequences of Landsat images (6 TM/Landsat-5, 1 ETM/Landsat 7, 1 OLI/Landsat 8 scenes; identification numbers listed in **Table 2**), I calculated average annual rates of riverbank erosion (M_R) for the time period 1989–2014.

Table 2: Landsat image identification

Year	Path	Row	ID
1989	117	056	LT51170561989264BKT00
1996	117	056	LT51170561996220CLT00
2001	117	056	LE71170562001177EDC00
2005	117	056	LT51170562005260BKT00
2009	117	056	LT51170562009223BKT00
2014	117	056	LC81170562014365LGN00

For each of the images, I corrected for atmospheric reflectance using the Dark Image Subtraction method [*Chavez*, 1996] before deriving the normalized difference vegetation index (NDVI). To automate the process of consistent riverbank identification, I defined the riverbank as the location where the NDVI transitioned into values ranging from 0.39 to 0.49, values that separated densely vegetated surfaces (NDVI≥0.6) from sparsely vegetated or bare earth surfaces. Having defined the riverbanks, I then derived channel centerlines by interpolating through digitized points located halfway between channel margins at 100 m intervals. Values of M_R were then calculated after *Constantine et al.* [2009] and *Micheli et al.* [2004], in which superposed centerlines from successive Landsat images created polygons that represented the total area of eroded bank material. Mean erosion rates for river sections spanning individual meanders were then defined as the sum of the polygon areas within each section divided by the average streamwise length of the section.

Analysing 67 river sections, I documented river position every 5–7 years, which provided a total of 330 M_R estimates. To distinguish between forested river sections, and those cleared of forest, I developed a land classification scheme using the software eCognition, which uses a set of training data to identify spectral signatures and shape parameters [*Baatz et al.*, 2000] from the 2009 Landsat 5 set of bandwidths that correspond to forested land, agricultural land, and bare earth. The set of training data were constrained to areas that were clearly visible in a high-resolution image (Google Earth™), and to areas that I observed in the field. To verify this classification scheme, I applied it to the remainder of the 2009 Landsat image and confirmed its application using Google Earth™. I then applied this classification to each Landsat image prior to 2009 denoting undisturbed banks as *forested sections* and deforested banks as *cleared sections*. Forested river sections in the 2014 Landsat 8 image were identified using several high resolution images from Google Earth™. All estimates of M_R were then categorized based on the land use classification for the eroding bank. Forested sections contributed 255 estimates of M_R and cleared sections contributed 75 estimates (from 22 distinct river sections).

3.2.2 Linear theory of meander migration

Although there are higher-order models describing river meandering by curvature-driven forcing of river flows (e.g., [*Pittaluga and Seminara*, 2011]), the linear theory of meander migration [*Ikeda et al.*, 1981] provides a simple and effective approach for assessing the role of trees in the meandering dynamics of large rivers [*Perucca et al.*, 2007]. Accordingly, M_R at any location along a meander can be stated as the product of a dimensionless coefficient (ε) and a term reflecting the near-bank flow velocity in excess of the cross-section averaged velocity (ω):

$$M = \varepsilon\omega \qquad (6)$$

Values of ε reflect a range of physical controls on riverbank erosion, but the variable is strongly determined by the material properties of the riverbank, including any effects exerted by the presence of riparian vegetation [*Constantine et al.*, 2009; *Perona et al.*, 2009]. I estimated ε for every river section across all study reaches as the ratio of M_R to the maximum value of ω located within the river section during conditions of bankfull flow.

3.2.2.1 Channel flow field

To approximate the near bank flow velocities along eroding bank faces, I used the numerical approximation to the first order solution of the St Vennant Equations proposed by *Sun et al.* [1996]:

$$\omega_j = \frac{b}{U/\Delta s + 2(U/h)F}\left[-U^2\left.\frac{\partial c}{\partial s}\right|_j + c_j F\left(\frac{U^4}{gh^2} + A\frac{U^2}{h}\right) + \frac{U}{\Delta s}\frac{\omega_{j-1}}{b}\right] \qquad (7)$$

Where $\omega_j = U_{b,j} - U$, which is the velocity perturbation at point *j* along the channel centreline, $U_{b,j}$ is the depth average velocity at the outer bank at point *j* along the channel centreline, *U* is the cross-section averaged velocity for the reach, *s* is the stream-wise distance, *h* is the average depth, *F* is the friction factor defined as $F = \frac{ghS}{U^2}$ where ρ is the density of water, *S* is average longitudinal water-surface slope and *g* is acceleration due to gravity. To better represent the secondary flow induced by the imbalance between the lateral pressure gradient and centripetal force, I used the modified *A'* to replace the original scour factor *A* [*Johannesson and Parker*, 1989], such that:

$$A' = A + A_s - 1 \qquad (8)$$

$$A_s = 181\left(\frac{h}{b}\right)^2 \frac{1}{\chi_1}\left(2\chi^2 + \frac{4}{5}\chi + \frac{1}{5}\right) \qquad (9)$$

$$\chi_1 = \frac{0.077}{\sqrt{F}} \qquad (10)$$

$$\chi = \chi_1 - \frac{1}{3}. \qquad (11)$$

The river centrelines were discretised as a sequence of points (s_i, i = 0, 1, 2, 3,…) separated by a constant stream-wise distance of Δs, and:

$$\left.\frac{\partial \omega}{\partial s}\right|_i = \frac{\omega_i - \omega_{i-1}}{\Delta s} \qquad (12)$$

$$\left.\frac{\partial c}{\partial s}\right|_i = \frac{c_i - c_{i-1}}{\Delta s}. \qquad (13)$$

The initial starting value ω_0 was taken to be 0 along a straight section of river upstream from the study reaches.

Bankfull discharges (Q_b) were estimated fitting a type-two Gumbel distribution to annual maxima data from the Balat gauging station, the more complete of the two data sets, assuming that Q_b corresponds to the 1.5 year recurrence event [*Dury*, 1976; *Castro and Jackson*, 2001]. Without sufficient annual maxima data from the Barik Menis gauging station to repeat this process there, the bankfull estimate at Balat gauging station was adjusted based on the ratio of average daily flow between the two gauging stations, and the increase between the two assumed to be linearly proportional to streamwise distance. The estimate of Q_b at Balat was then adjusted for each study reach based on the streamwise distance from Balat GS.

Average longitudinal water-surface slope (*S*) was estimated using the Manning formula:

$$U = \frac{R^{\frac{2}{3}}}{n} S^{\frac{1}{2}} \qquad (14)$$

where *R* is the hydraulic radius, and *n* is the manning's roughness coefficient, here taken as 0.035 [*Coon*, 1997]. Values are consistent with estimates of valley slope derived from SRTM digital elevation data for the region.

Reach averaged bankfull depths (*h*) for reaches **C** and **D** were taken from measured channel cross-sections, where bankfull stage was assumed to be the level at which vegetation ceased to grow on the point bar. Cross-sections were measured using a sonic depth gauge (Norcross Hawkeye H22PX) when the river was at or very near bankfull flow conditions. Access to reaches **A** and **B** was restricted, therefore a representative width to depth ratio was calculated from reaches **C** and **D**, and used to estimate bankfull depths for reaches A and B.

The automated process of identifying riverbank position from each Landsat derived NDVI mosaic resulted in a polygon outlining the river's extent in each of the four study reaches. These polygons were then used to estimate reach averaged bankfull widths (*2b*) by dividing the area of each by the length of the corresponding river centreline (**Table. A1**).

The scour factor (*A*) was determined from cross section data for reaches **C** and **D** using the equation:

$$A = -\frac{m}{hnc} \qquad (15)$$

where *n* is the cross-stream coordinate, *m* is the local bed elevation, *h* is bankfull depth, and *c* is local curvature [*Constantine et al.*, 2009]. At the channel centre, both *n* and *m* are 0. To better represent the secondary flow induced by the imbalance between the lateral pressure

gradient and centripetal force, I modify the scour factor according to *Johannesson and Parker* [1989].

Curvature was calculated at a spacing of 200 m along each centreline so as to capture the arc of the meander without being influenced by small-scale local variations. Curvature values were found by fitting a circle of radius *r* (units m) to three successive points along a river centreline (s_{i-1}, s_i, and s_{i+1}) such that all three points sit on the circle's circumference, with a curvature value of $\frac{1}{r}$ being assigned to the middle point s_i. This was achieved by providing an initial estimate for the center point of the circle ($\bar{s}$) and using a sequential least squares optimising algorithm [*Kraft*, 1988] to reduce the error in the difference between the distances from the estimated centre point to each of the three points (s_{i-1}, s_i, and s_{i+1}) to below 0.01 m. This optimised centre point yields three

estimates of *r*, the mean of which I used to define curvature (*c*) at point s_i (**Figure 7**). I report the maximum values of curvature for each river section.

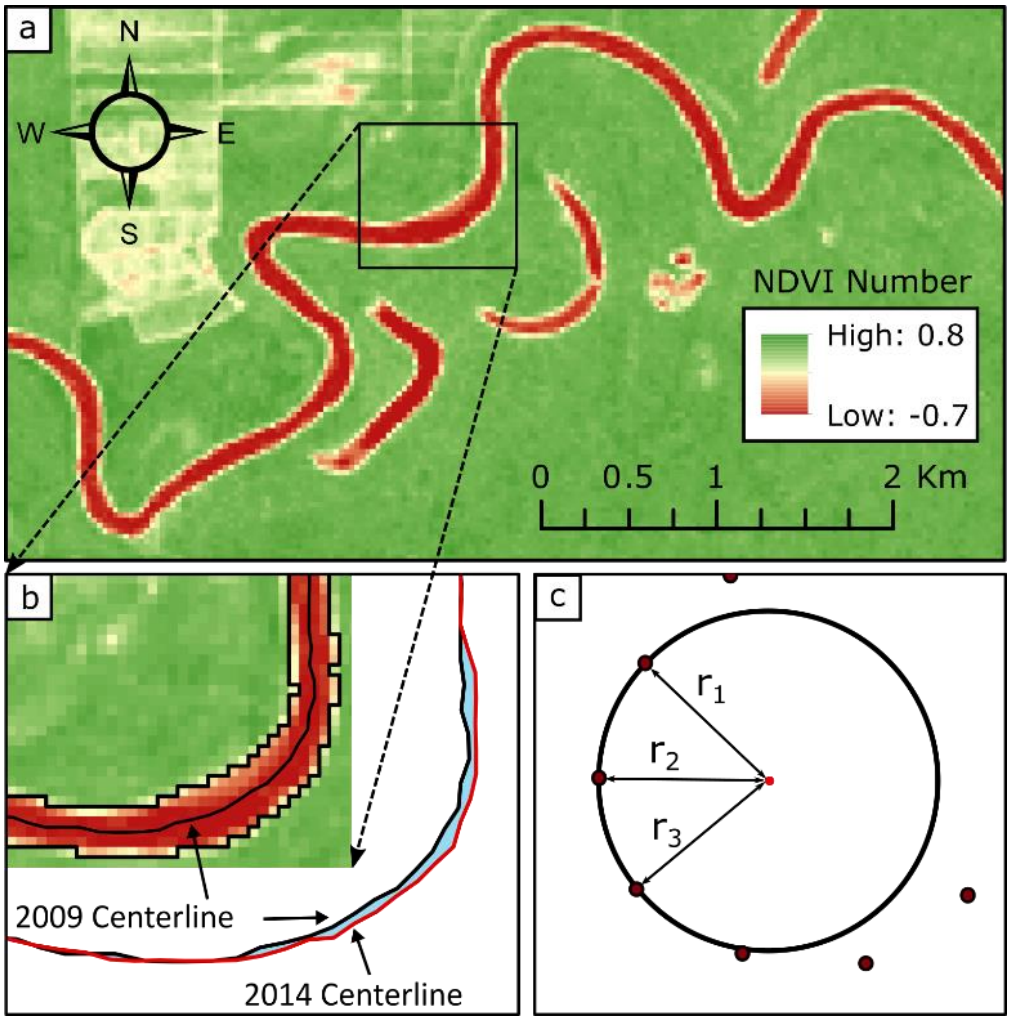

Figure 7: Meander migration and curvature calculation methodologies. a, NDVI mosaic derived from TM/Landsat-5 image (11/10/2009). b, Automatically derived river bank lines and associated river centreline for 2009 image, 2009 and 2014 centrelines superposed to form a polygon representing the area eroded. c, Fitting of circle to estimate curvature (1/r̄) at point r2.

The reported values of the velocity perturbation (ω) are taken as the maximum value within each river section, constituting a conservative estimate for the corresponding erodibility coefficient. Reach averaged parameter values used for the calculation of ω are listed in **Table 3**.

Table 3: Values used in calculation of ω

	Reach A	Reach B	Reach C	Reach D
Bankfull discharge Q_b [m^3 / s]	947.86	1242.27 (1428.61 after tributary)	1708.42	2198.64
Average bankfull width *2b* [m]	89.38	113.89	130.16	146.23
Average bankfull depth *h* [m]	5.2	6.7	7.83	8.33
Average Slope *S*	0.0004	0.0003	0.0003	0.0003
Manning's roughness coefficient *n*	0.035	0.035	0.035	0.035
Scour Factor *A*	3	3	3	3

I used two-tailed t-tests and Kruskal-Wallis tests (KW) to test the significance of differences in my measurements between *forested sections* and *cleared sections*. Kolmogorov-Smirnov (KS) tests were used to assess the distinctiveness of measurement distributions. Pearson product-moment correlation coefficient (*r*) and Spearman's rank correlation coefficients (ρ) provide measures of significance for correlations. The variable α defines the significance level of statistical tests.

3.3 Results

Rates of riverbank erosion along the Kinabatangan River were found to have increased after the total removal of its riparian cover, with M_R for cleared sections averaging significantly more than for forested sections (t-tests: $\alpha<0.01$; KW: $\alpha<0.001$) (**Figure 8A**).

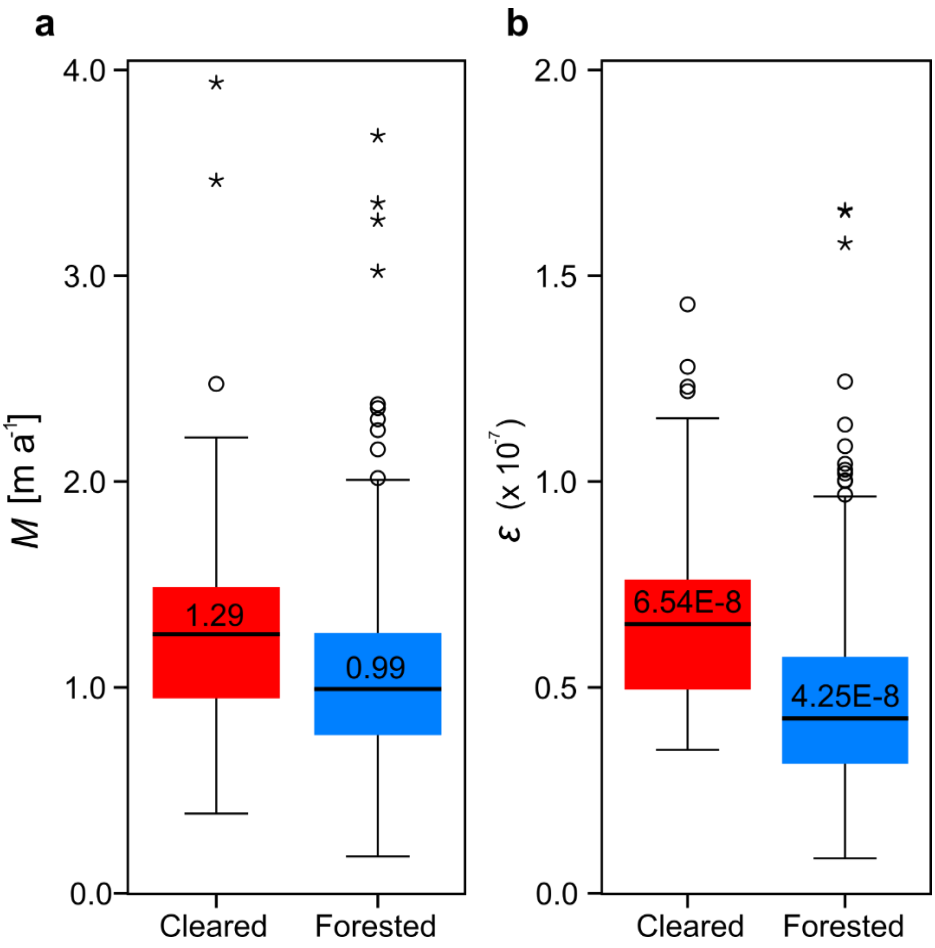

Figure 8: A: Box and whisker plot of distributions of measured values of average annual migration rates (MR) for both land-cover classifications, Kinabatangan River, Malaysia. B: Box and whisker plot of distributions of estimated values of dimensionless coefficient of riverbank erosion (ε). For all distributions, median is reported, outliers are denoted by circles, and extreme values are denoted by asterisks.

This is consistent with previous studies that have assessed the role of vegetation in riverbank erosion [*Beeson and Doyle*, 1995; *Micheli et al.*, 2004]. Increases in M_R following deforestation can be attributed to increases in riverbank erodibility, at least as reflected in the differences in ε. The average ε for forested sections was significantly less than the average for cleared sections (t-tests: $\alpha<0.001$; KW: $\alpha<0.001$) (**Figure 8B**), and KS tests confirm that the distributions of M_R and ε values for cleared sections are statistically distinct from the distributions for forested sections ($\alpha<0.001$).

To assess the error inherent in these measurements of meander migration, I identified 17 river sections located through reaches **B** and **C** where high resolution (60cm

pixel size) DigitalGlobe™ imagery was available for the years 2009 and 2014 via Google Earth™. By delineating bank lines from these high resolution images, and measuring the migration of the river centerline, I compared these results with those obtained from Landsat imagery for the same time span. The mean absolute difference in the centreline migrations derived from these two sources is 1.46 m (σ = 1.12), which, when averaged over the timespan of 5 years, provides an estimate for error in the measurements of meander migration rates of 0.29 m/yr. While I acknowledge that there is still error in the use of high resolution imagery to measure meander migration, the error associated with measurements taken from images with 60 cm resolution will be insignificant compared to those taken from images with 30 m resolution. (Due to the lack of available images spanning the study reaches, I was unable to extend the range of high resolution meander migration measurements.)

Our results suggest that the mechanisms responsible for riverbank retreat may be modified by deforestation, as the complete removal of riparian forest appears to allow near-bank flows to more effectively erode riverbank materials. To test that the measured differences in channel migration are not consequences of variation in river discharge between observations, I examined migration rates of river sections that have been cleared of forest before, and then after deforestation (**Figure 9**). To aid cross-comparison between river sections with differing magnitudes of migration, I normalized by mean migration rate across all time-steps (pairs of successive Landsat images) for individual river sections to give proportionate channel migration rates. As clearance events occur throughout the range of timesteps, the observed increase in migration rates following deforestation is not a consequence of a single large discharge event.

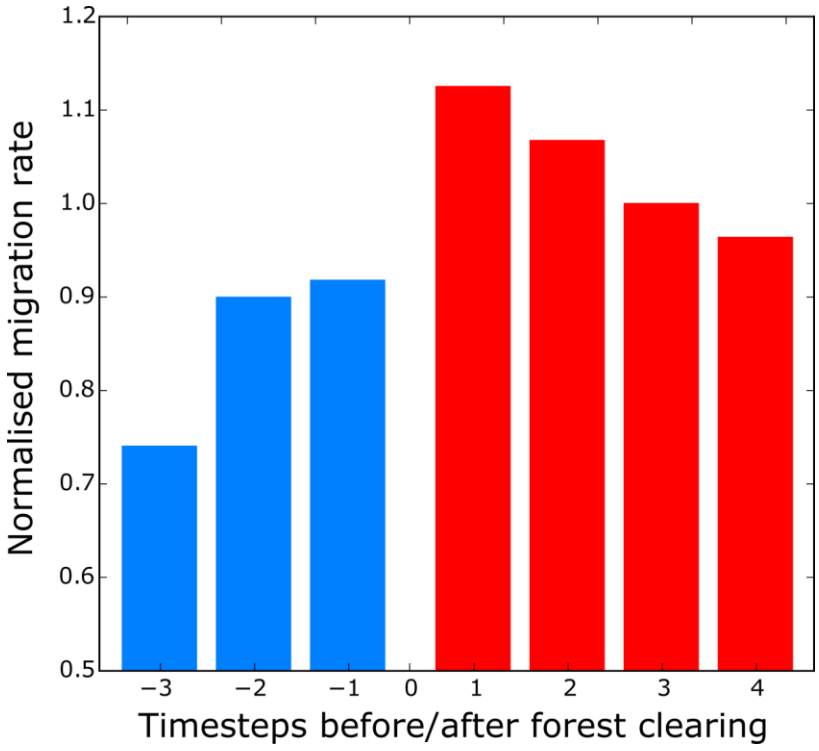

Figure 9: Mean migration rates for sections of river that have been cleared of forest, sorted by the number of time steps (successive pair of Landsat images i.e., 1989-1996, 1996-2001, 2001-2005, 2005-2009, 2009-2014) before and after forest clearing. Migration rates for individual river sections have been normalised by the mean migration rate across all time steps for that river section.

Figure 9 illustrates a temporal structure to the difference in proportionate migration between timesteps in which river sections were forested, to those when they are cleared, supporting the hypothesis of direct causality. Migration rates also show a clear recovery following the clearance event, suggesting that any alteration to the driving mechanisms of bank retreat as a result of deforestation aren't permanent.

The proximity of high-momentum fluid to the outer bank is thought to have an important control on rates of riverbank erosion [*Pizzuto and Meckelnburg*, 1989]. Values of M_R can therefore be expected to demonstrate some degree of correlation with measurements of local curvature (c) and modeled values of ω when the curvature-driven forcing of river flow induces the effective transport of riverbank materials. Within cleared river sections, mean migration rates (M_R) positively correlate with the maximum value of c located within the corresponding river section (r = 0.53, ρ = 0.45, α<0.001) and maximum

values of ω (r = 0.57, ρ = 0.53, α<0.001) (**Figure 10**). Conversely, values of M_R within forested river sections showed no such correlation with values of ω (α>0.22), and only a weak correlation with maximum values of c which may not be significant (r = 0.132, α = 0.035; ρ = 0.114, α > 0.05) (**Figure 10**). At least one other study, from the Sacramento River in California, USA, has quantified riverbank erosion as a function of planform curvature following deforestation, highlighting that erosion by curvature-driven forcing of river flow predominates only along sections of floodplain where the natural riparian cover was replaced by agriculture [*Micheli et al.*, 2004].

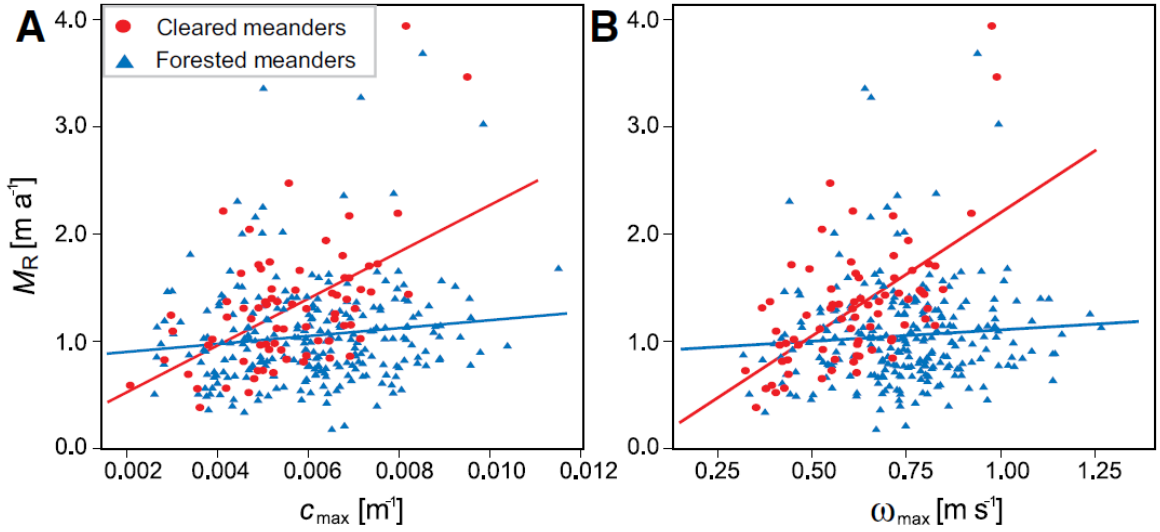

Figure 10: A: Average annual migration rates (M_R) plotted against maximum value of local curvature for individual meanders (c_{max}) for all sections within each study reach, Kinabatangan River, Malaysia. B: Values of M_R plotted against estimates of maximum velocity perturbation (ω_{max}) during bankfull-flow conditions for all sections. Values are plotted as function of history of land-cover change in both A and B.

3.4 Discussion

My hypothesis is that the increase in riverbank erosion sensitivity to curvature-driven forcing of river flows occurs because clearing riparian forest improves the ability of near-bank flows to remove riverbank materials (both intact and failed), and, by reducing riverbank shear strength, facilitates smaller more frequent mass failure events. Tropical forests are characterized by high rates of rainfall interception and evapotranspiration, which

reduce soil water content and pore-water pressures. If deforestation enhances wetting across the riverbank, causing pore-water pressures to increase, a reduction in the apparent cohesion of riverbank materials from a loss of matric suction will increase the susceptibility of exposed riverbank surfaces to fluvial scour [*Pollen-Bankhead and Simon*, 2010]. Furthermore, poorly rooted sediment is prone to disaggregation [*Dunaway et al.*, 1994], particularly sediment that lacks enough cohesion (i.e., from clays and other platy minerals) to withstand the boundary shear stresses applied by the near-bank current [*Simon and Collison*, 2002].

Alterations to the riverbank hydrology caused by deforestation may also exacerbate a mechanical reduction in riverbank shear strength [*Sidle et al.*, 2006]. Fiber reinforcement provided by tree roots increases riverbank shear strength [*Abernethy and Rutherfurd*, 2000]. Even when this root reinforcement has limited depth penetration, increased friction along the edges of a potential slide mass can control the size of individual failure events (e.g., slump blocks) [*Milledge et al.*, 2014]: the greater the root reinforcement, the larger the individual failure events. By extension, deforestation will tend to decrease the size of individual failure events, but the reduced shear strength of riverbank materials will tend to increase their frequency.

Finally, the additional fiber reinforcement provided by roots may prolong the residency time of failed slump blocks that armor and buttress the riverbank, impeding the ability of near-bank flows to remove material from the bank toe and face. The depleted presence of large woody material along the riverbank face may also reduce flow roughness, improving the potential for the near-bank current to sustain its momentum and thereby its erosive power [*Thorne and Furbish*, 1995a; *Daniels and Rhoads*, 2003].

Although future work is needed to fully evaluate the role of forests in controlling (1) the size and shape of riverbank mass failures and (2) the timescales for riverbank material removal, field observations provide a basis for the proposed hypotheses (**Figure 11**). Along many forested river sections, I observed that large failure blocks still retaining vegetation were present at the bank toe. Along sections that had been cleared of forest, such large blocks were almost entirely absent; instead I observed smaller, unconsolidated failure blocks with evidence of cantilever failure**.**

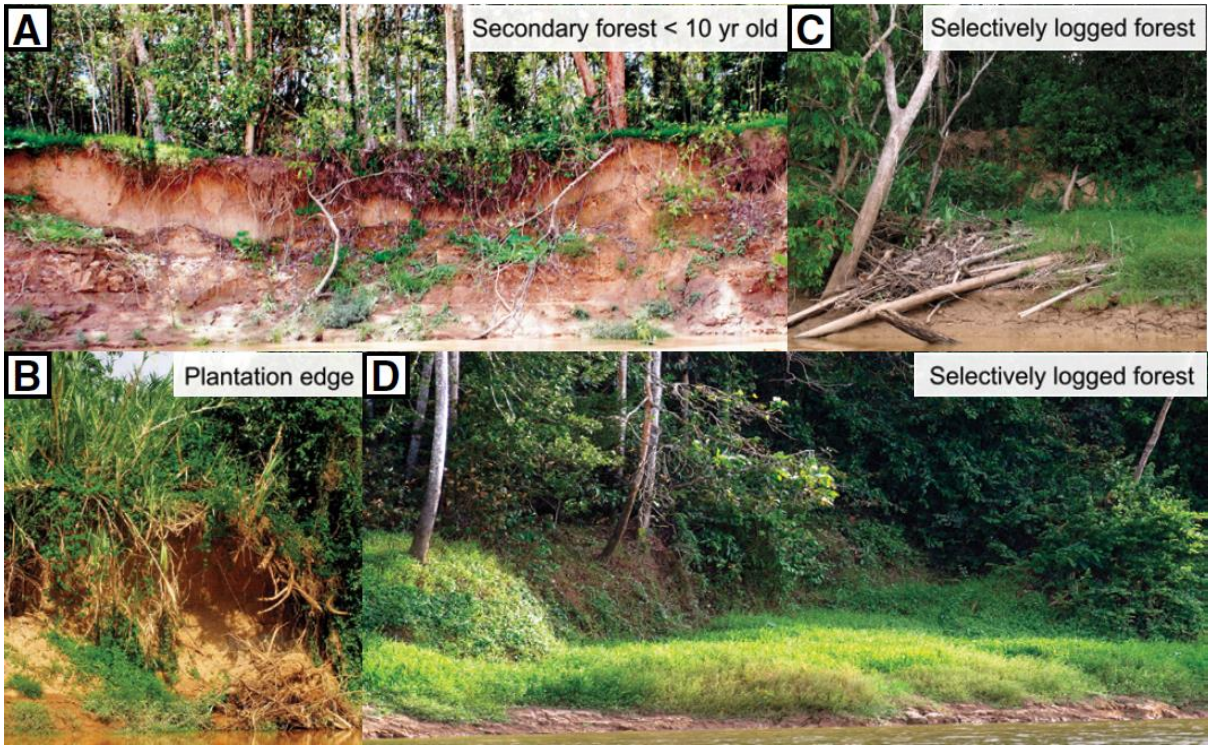

Figure 11: A,B: Examples of cleared meanders showing evidence of small mass-wasting events delivering unconsolidated material to Kinabatangan River, Malaysia. C,D: Examples of forested meanders showing evidence of large mass-wasting events with consolidated material accumulated at base of riverbank.

3.5 Conclusions

For the period between 1989–2014, sections along the Kinabatangan River that had been cleared of riparian forest show rates of channel migration >23% greater on average than those sections that remained forested. Furthermore, I find that those cleared sections exhibit a strong positive correlation between rates of riverbank erosion and estimated

curvature-influenced flow along the eroding bank, a correlation that is absent along forested sections. Removal of riparian forest may alter properties of the bank in ways that accelerate material disaggregation by fluvial scour, thus affecting the relationship between rates of channel migration and curvature-driven forcing of river flows. Implications for long-term evolution of tropical river meandering in the context of floodplain deforestation are a critical area for further investigation.

Chapter 4:

Can riparian forest reserves increase yields from oil-palm plantations?

Author Contributions

The main body of text presented here was originally drafted by myself, though many revisions and suggestions have been made by Dr Eli D. Lazarus. The original concept, data processing, model development and analysis are solely my own work.

4.1 Introduction

Agricultural expansion is driving deforestation and land conversion across tropical regions worldwide to meet growing demands for food production [*Rudel et al.* 2009; *Hosonuma et al.* 2012]. In Southeast Asia, which hosts some of the highest rates of tropical deforestation in the world *[Keenan et al.*, 2015], rapid agricultural expansion is dominated by the palm-oil industry [*Boucher et al.*, 2011; *Stibig et al.*, 2014]. In Malaysia and Indonesia, 9.5 million hectares (M ha) of land were converted to oil-palm plantations between 1990 and 2010 [*Wicke et al.*, 2011], with much of that expansion occurring at the expense of tropical forest [*Koh and Wilcove,* 2008]. Malaysia and Indonesia presently dominate the global palm-oil market, producing more than 85% of the world's supply [*USDA*, 2015]. Demand for palm oil and its derivatives is expected to increase with continued economic growth in India and China [*Murphy,* 2014], lending Indonesia incentive to expand its landholdings in Kalimantan and Papua in an effort to double its production capacity before 2030 [*Carlson et al.*, 2012]. Industrial palm oil production is not limited to Southeast Asia: Brazil, Colombia, and the Democratic Republic of Congo have a combined 102.9 M ha of lowland tropical forest identified as suitable for oil-palm cultivation [*Pirker et al.*, 2016].

Tropical deforestation is common near large meandering rivers [*Obidzinski et al.*, 2007; *Latrubesse et al.*, 2009], which provide both access to fertile floodplains and a ready-made transportation network [*Armenteras et al.*, 2006; *Renó et al.*, 2011]. Riparian corridors – protected habitat fringing the banks of river courses – represent a space where practicalities of land conversion and habitat preservation overlap [*Naiman et al.*, 1993]. The margins of river courses present opportunities for continuous habitat pathways, functioning as forest reserves unto themselves and as potential connectors between forest matrix

fragments. However, riparian forest buffers along rivers that run through oil-palm plantations occupy valuable land, and thus far have been found to provide no net positive ecosystem service to adjacent plantations [*Gray and Lewis,* 2014]. The assumption that total forest conversion along river boundaries will maximise profitability leaves little incentive to maintain riparian reserves within plantations. But what if the primary ecosystem service that riparian corridors provide is more geomorphic than ecologic? If riparian buffers protect plantations from losing land to riverbank erosion, how does that change their economic valuation?

Here I investigate the potential economic impact of expected geomorphic responses of a large tropical river to the removal and retention of its riparian forests. The results suggest a potentially synergistic relationship between meandering dynamics, riparian buffers, and expected yields from oil-palm cultivation near the river edge. Having quantified meander migration rates in the absence and presence of riparian forest, I now weigh the economic benefit of natural erosion protection against the cost of potential plantation, and evaluate the first-order role of riparian forests in maximising expected yields from proximal oil-palm plantations. Under certain conditions I find that maintaining riparian reserves could plausibly increase a plantation's long-term profitability, and that the optimum width of a riparian reserve depends upon the horizon of economic return.

4.2 Methods

For different hypothetical scenarios of forest removal along sections of unprotected riparian forest marked for future conversion to plantation (76 km total), I use a numerical model of river meander migration to simulate future channel planform position along a continuous 210 km stretch of the Kinabatangan (**Figure 12A**). I then assess the impact that riparian

buffers along these unprotected reaches could have on expected yield from oil palm cultivation adjacent to the river. Using a continuous river domain that encompasses the reaches of interest means that upstream/downstream boundary effects on planform evolution are negligible (within the context and constraints of this numerical model).

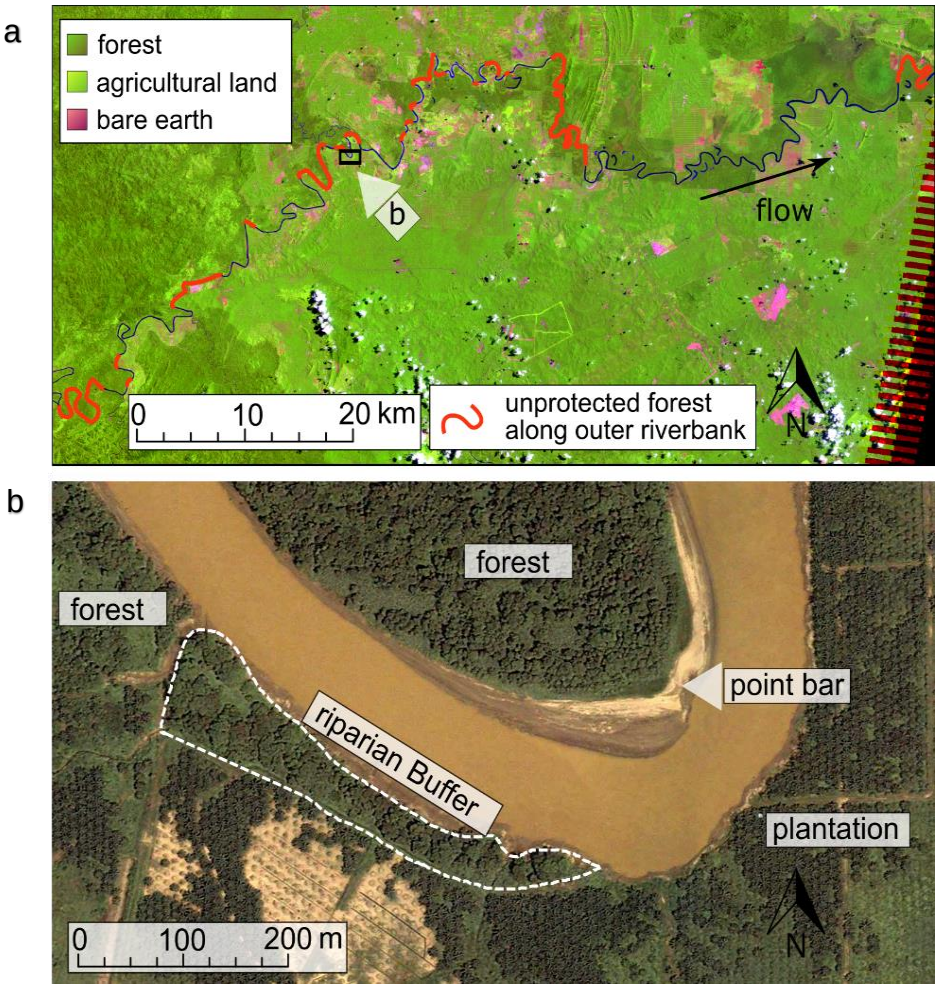

***Figure 12:** a, Landsat L5 image captured on 17/09/2005, showing the study domain, defined land-cover types, sections of the river with unprotected forest on the eroding bank, and the location of panel (b). b, A single meander exhibiting examples of each land cover type (forest, plantation, riparian buffer, and point bar) considered in this study. Dotted white line marks the remnants of a riparian buffer that originally lined the length of the meander. (Image from Google Earth™.)*

Although I model the full river planform, my analyses of crop yield only consider land directly affected by river migration, including (1) land at eroding river banks, and (2) new land accreted along inner (non-eroding) banks as a direct result of lateral river migration

(e.g., point bars). Eroding river banks are where the geomorphic ecosystem service of riparian protection against erosion actively functions. Newly accreted land in a migrating river meander may, after a temporal lag, partially offset losses to erosion on the opposite bank; the counter-argument is that, given the (multi-decadal) timeframe of the forecasting horizons, newly accreted land still might not have sufficient time to mature into a state suitable for plantation [*Leopold et al.*, 1964; *Lauer and Parker*, 2008a]. To address the balance of this dynamic, I cast two sets of simulations: one that ignores any contribution from land accreted to the inner bank, and one that takes it into account. (Both simulation premises are detailed below.) A static river bank has a net-zero effect on this analysis. I do not consider the net benefits of flood mitigation or other ecosystem services that riparian vegetation on both banks of the river can provide.

4.2.1 Fluvial model

Based on observations made in Chapter 3, I employ both linear and non-linear relations of meander migration to velocity perturbation in a deliberately simplified model of channel planform modification that accommodates relative vegetation effects via an adjustable coefficient of riverbank erodibility [*Ikeda et al*., 1981; *Johannesson and Parker*, 1989]. The numerical model of channel centreline migration includes three main components. The first component evaluates simplified river hydrodynamics and assigns a velocity perturbation to each point along the river. The second evaluates the vegetation along the eroding bank and assigns the appropriate erosion coefficient and corresponding migration rate. The third simulates channel migration by moving each point the ascribed distance normal to the river centreline.

Using a OLI/Landsat 8 image (LC81170562014365LGN00) from 2014, I generated an initial river centreline by delineating riverbank positions from an NDVI mosaic derived from

red and near-infrared spectral bands. The model first discretises the initial centreline at a point-spacing of 150 m to smooth out pixilation effects in the satellite imagery, then additional points are interpolated at a spacing of 50 m to improve the spatial resolution of the dynamic planform in the simulations.

As in Chapter 3, the velocity perturbation (ω) for all points along the river centreline is evaluated numerically [*Sun et al.*, 1996], then ascribed a migration rate according to the linear relation as purported by *Ikeda et al.* [1981]

$$M = \varepsilon\omega \qquad (16)$$

with the coefficient of riverbank erosion (ε) varying with bank vegetation type.

Applying the linear theory of meander migration to forested reaches is complicated to an extent by previous results showing that riparian vegetation exerts a control on rates of channel migration that effectively reduces the dominance of planform curvature along the Kinabatangan River [*Horton et al.*, 2017]. I therefore apply a second, non-linear relation to forested river sections that more faithfully represents these empirical observations

$$M = \varepsilon_s\omega; \qquad 0 \leq \omega < 0.5 \qquad (17)$$

$$M = C + k\omega; \qquad 0.5 \leq \omega \qquad (18)$$

where ε_s is the mean coefficient of riverbank erosion along forested sections with a maximum velocity perturbation less than 0.5 m s^{-1}, and the constants C and k describe the line of best fit for channel migration to velocity perturbations greater than 0.5 m s^{-1}. I assume channel migration diminishes as velocity perturbation decreases below the range of empirical measurements as this is a requisite of meander development, and apply a linear reduction in the absence of a well-defined relationship (Figure 13).

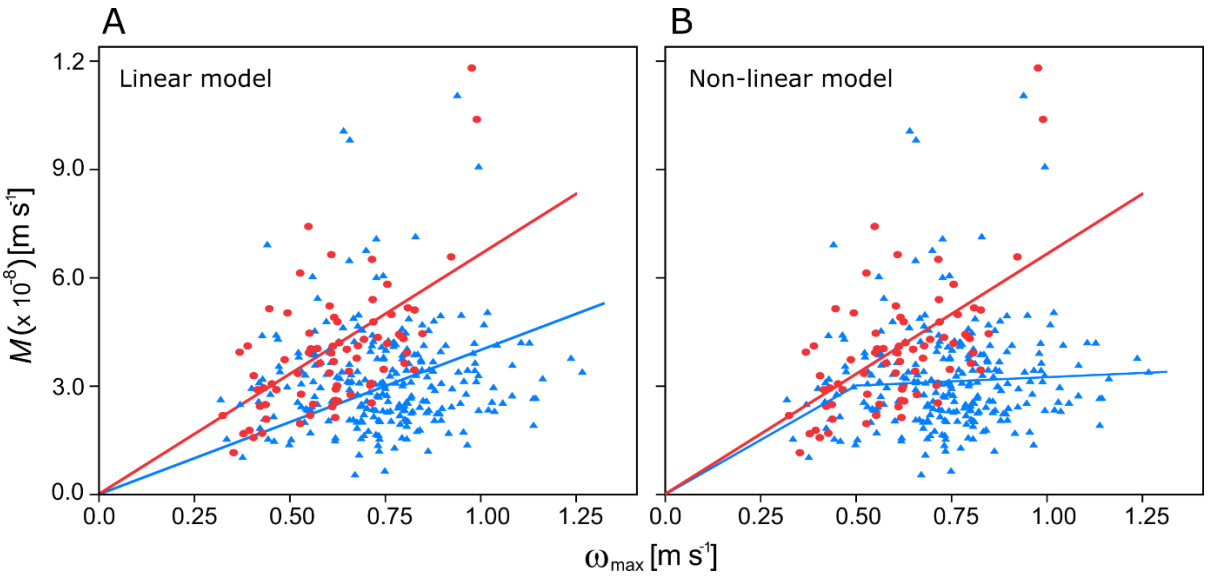

Figure 13: a. Linear fitting of migration rate to velocity perturbation for both forested and cleared sections of river. b.Non-linear fitting of migration rate to velocity perturbation for forested sections, and linear fitting for cleared sections.

Overall parameter values for the river (**Table 4**) are taken as the average of reach-specific values reported in Chapter 3, and an initial value of $\omega = 0$.

Table 4: Parameter values used in the calculation of meander migration

Parameter	Value
Q	1524.298
$2b$	119.92
h	7.02
n	0.035
A'	3
ε (cleared)	6.54×10^{-8}
ε (Forested)	4.25×10^{-8}
ε_s	6.0×10^{-8}
C	3.14×10^{-8}
k	3.14×10^{-9}

For the linear model I assign a coefficient of riverbank erosion (ε) based on bank vegetation type. A binary land-cover classification (forested or cleared) was evaluated using a polygon shapefile detailing the extent of forest cover evident in the 2014 Landsat 8 image, confirmed by field observations. Each point along the river centreline is assigned a migration value based on the coefficient of riverbank erosion corresponding to the land-cover

classification at an orthogonal distance *b* (half of one river width) in the direction of migration. For forested sections, $\varepsilon = 4.25 \times 10^{-8}$; for cleared sections, $\varepsilon = 6.54 \times 10^{-8}$, which reflects the observed increase in riverbank erodibility following riparian forest removal, and are mean estimated values specific to this study area as detailed in Chapter 2. The relative difference between these two parameter values (~1:1.5) is significantly lower than relative differences reported in other studies [*Micheli et al.*, 2004; *Perucca et al.*, 2007], which suggests that the formulation presented here is a conservative assessment of the linear model. For the non-linear model, points along the river centreline classified as forested are assigned migration values in accordance with equations 17 and 18.

After assigning migration values, each point along the river centreline is moved a distance of M in the direction of migration, simulating one iteration of channel migration. The direction of centreline point migration is orthogonal to the centreline curve [*Motta et al.*, 2012], found by numerically evaluating the unit tangent vector at each point and rotating it through 90° clockwise or anti-clockwise depending upon the sign of the velocity perturbation (ω). Modelled centreline position is re-discretised at a spacing of 50 m every 25 iterations to maintain a regular spacing between centreline points.

4.2.2 Measurement of bank erosion rates

From the annual modelled centreline migration rates, I calculate mean bank erosion rates at 25 year intervals, corresponding approximately to a full plantation cropping cycle (from planting to maturity to decline and replanting) [*Butler et al.*, 2009; *Abram et al.*, 2014]. To produce polygons that represent the area of eroded bank material, I superimpose two channel centrelines from model planforms 25 years apart [*Micheli et al.*, 2004; *Constantine et al.*, 2009]. I sum the areas of only those polygons that sit within reaches of unprotected

forest (assuming protected forest will remain so), and then divide the total area by the corresponding river length (using the original 2014 river centreline) to yield estimates for the mean area of riverbank eroded per unit length of river (m^2/m) per 25, 50, 75, and 100 years for each forest clearance scenario.

Each scenario imposes, within the reaches of unprotected forest, digitized polygons that represent a riparian buffer of a given width. I assume that any unprotected forest outside a given buffer zone is converted to oil-palm plantation. Each buffer width considered (**Table 5**) constitutes one scenario of forest clearing, and generates a distinct set of model outputs. For each scenario, I calculated distributions of centreline migration at 50 m increments along the channel length and mean land area lost from the eroding bank per unit length of river at 25 year intervals.

Table 5: Summary of notation.

Width of riparian buffer zone (m)	Scenario of forest clearing model outputs	Projection of expected yield with inner bank fallow (*SA*)	Projection of expected yield with inner bank cultivated (*SB*)
0	S_{F0}	SA_{F0}	SB_{F0}
10	S_{F10}	SA_{F10}	SB_{F10}
20	S_{F20}	SA_{F20}	SB_{F20}
30	S_{F30}	SA_{F30}	SB_{F30}
40	S_{F40}	SA_{F40}	SB_{F40}
50	S_{F50}	SA_{F50}	SB_{F50}
100	S_{F100}	SA_{F100}	SB_{F100}

4.2.3 Projections of expected yield

To model the expected yield from oil palm cultivated in close proximity to the river edge, I make two assumptions. First, I assume that a 3 m fallow buffer is maintained between the riverbank and productive plantation – a distance consistent with local field observations, and which approximately matches the typical radius of a single tree in plantation spacing (~7 m between any two trees). Second, I assume that land along the eroding bank is 100%

productive, which results in a conservative estimate for the impact riverbank erosion has on expected yields.

Using typical values of yields gained from existing oil palm plantations along the Kinabatangan floodplain [*Abram et al.*, 2014], I model the mean expected yield from land along the eroding bank within existing forested sections over a 100 year (a) period. I confine the calculations to 100 m distance from the riverbank position as of 2014 so as to give estimates of mean yield per hectare of adjacent land such that

$$Y = \sum_{t=1}^{r-1}(1-R)E_{100} + \sum_{t=r}^{100}(0.97 - Tt)E_{100} + IB \qquad (19)$$

$$\exists\, r \in \mathbb{N} : (T(r-1) - 0.03) < R \text{ and } (Tr - 0.03) > R$$

where *Y* is the total expected yield ($/100 m of river), *R* is the width of the initial riparian buffer zone (Ha/100 m), E_{100} is the net present value of 100% productive land with an 11% discount rate ($/Ha/a) [Abram *et al.* 2014], *T* is the model output of mean riverbank erosion per year (which varies with time in years *t*) (Ha/100 m/a), and *IB* is the contribution to yield from the conversion of new material accreted as a point-bar on the inner bank ($). The choice of discount rate is in keeping with the assessment of Kinabatangan oil-palm productivity by *Abram et al*. [2014], 0.97 reflects the 3 m fallow land extending from the river's edge, and the incorporation of *IB* is explained in detail below.

Field reconnaissance of the Kinabatangan River confirmed the presence of grasses and shrubs extending inland from bare point bars, transitioning to early successional forest. These areas of relatively sparse vegetation behind point bars may inundate several times a year for prolonged periods (>2 weeks), precluding the establishment of a canopy forest, but providing a suitable habitat for fast growing grasses and some flood resistant species. I consider two hypothetical circumstances for the contribution to the total expected yield

made by new land on the inner bank (*IB*). In the first, newly formed land on the inner bank (point bars) is left fallow, and is gradually colonised by successional riparian vegetation. In the second, land accreted on the inner bank is converted to oil-palm plantation.

If new land on the inner bank – "created" by meander migration and representative of point-bar accretion as the modelled channel maintains a constant width – is left fallow, then it contributes nothing to the expected yield of the domain (*IB* = 0). If the inner bank is cultivated, then *IB* depends upon the land productivity of newly formed point bars. Given the frequency and duration of in-channel bar inundation, I assume that oil palm planted in newly accreted land are marginally productive at 25% *[Abram et al., 2014; Corley and Tinker*, 2015]. Based on field observations of successional transitions, I also assume that as the river migrates away from the initial position of the inner bank, an increasing proportion of land on the inner bank becomes sufficiently distant from the river channel that it begins to gain productivity. For a conservative estimate of impact on yield, I assume productivity in these swathes increases from 25% to 100%. (High inner-bank productivity reduces the net effect of land loss at the eroding bank.)

To determine at each model iteration the proportion of inner bank that transitions to being productive, I identified inner-bank areas with mixed-stage vegetation in two Landsat images from 1989 and 2009. From the 2009 TM/Landsat-5 image (LT51170562009223BKT00), I used the software package eCognition to build an object-orientated classification scheme [*Baatz et al.*, 2000] to automatically differentiate between river, forest canopy, and any area of intermediate vegetation between the two. The scheme was calibrated using field-derived training data of point bars known to experience frequent inundation. The calibrated scheme was then applied to additional sections in the 2009 image, and to the corresponding river sections evident in the 1989 TM/Landsat-5 image

(LT51170561989264BKT00), allowing direct comparison between the rates of point bar growth and forest canopy advancement (**Figure 14**). A total of 17 meanders were included in the analysis, yielding mean point-bar migration of 31.2 m and mean forest-boundary migration of 6.1 m, suggesting that point bars growth rates far exceed the rates at which canopy forest advances into newly formed floodplain space (a ratio of 5:1).

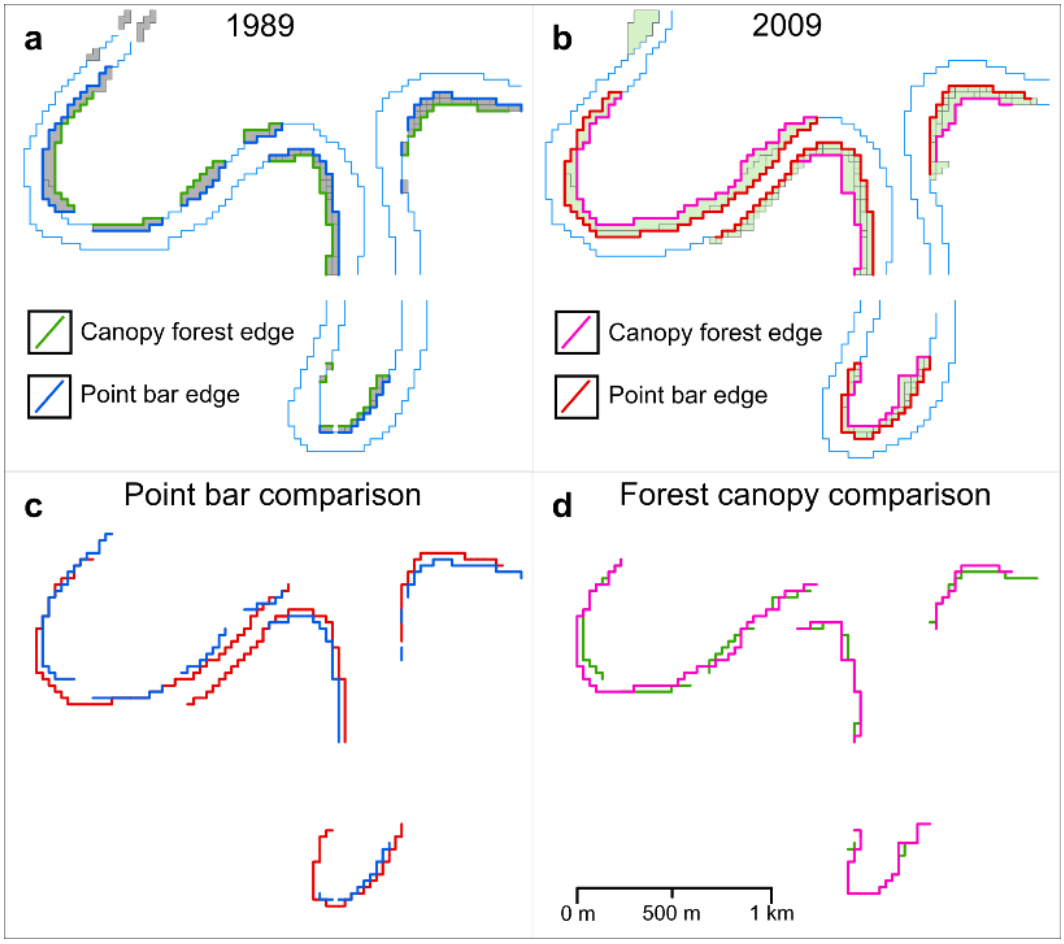

Figure 14: Comparison between rates of point bar growth and the advancement of the forest canopy. a, Region of non-forested land adjacent to the river's inner bank classified from a 1989 TM/Landsat-5 image using an object orientated classification scheme in eCognition. b, Region of non-forested land adjacent to the river's inner bank classified from a 2009 TM/Landsat-5 image. c, Relative positions of the river's inner bank in both 1989 and 2009. d, Relative positions of the forest's edge in both 1989 and 2009.

Contribution to the expected yield from cultivating newly accreted land on the inner-bank is expressed as

$$IB = \sum_{t=1}^{100} (TtE_{25} + 0.2TtE_{100}) \qquad (20)$$

where E_{25} is the net present value of 25% productive land with an 11% discount rate ($/Ha/a). I consider both formulations of *IB*, generating two estimates for the expected yields for each scenario of forest clearing. (A summary of the notation used to refer to each set of estimates is given in **Table 5**.)

4.2.4 Time-dependent profitability

Typically unproductive for the first 30 months, plantations are not considered mature until their third year [*Corley and Tinker*, 2003], after which yields rapidly increase reaching maximum productivity after nine years [*Butler et al.*, 2009]. Long-term estimates for expected yields are driven by mean annual values calculated over a full plantation life cycle [*Abram et al.*, 2014], and therefore do not incorporate the inherent variability of a plantation's productivity within its life cycle. To evaluate strategies for generating short-term profit within the first 10 years after implementing each forest-clearing scenario, I modify the E_{100} term in Eq. 6 to account for the time-dependent productivity of newly established plantations [*Abram et al.*, 2014] (assuming *IB* = 0).

4.3 Results

4.3.1 Simulated channel migration

4.3.1.1 Linear model

Figure 15 shows distributions of modelled bank migration distances at four successive time intervals (25, 50, 75, 100 years) for three hypothetical riparian buffer widths (0, 30, 100 m). The first-order consequence of removing all riparian forest is to affect larger incursions by river migration into the floodplain, both in the short and long term. The distribution of centreline migrations for S_{F0} (**Figure 15A**) shows fewer points migrating <10 m and more points migrating >50 m relative to the buffer scenarios S_{F30} (**Figure 15B**) and S_{F100} (**Figure**

15C). Although initially similar, after 25 years the distributions for S_{F30} and S_{F100} differentiate as the wider riparian reserve reduces the number of points migrating longer distances.

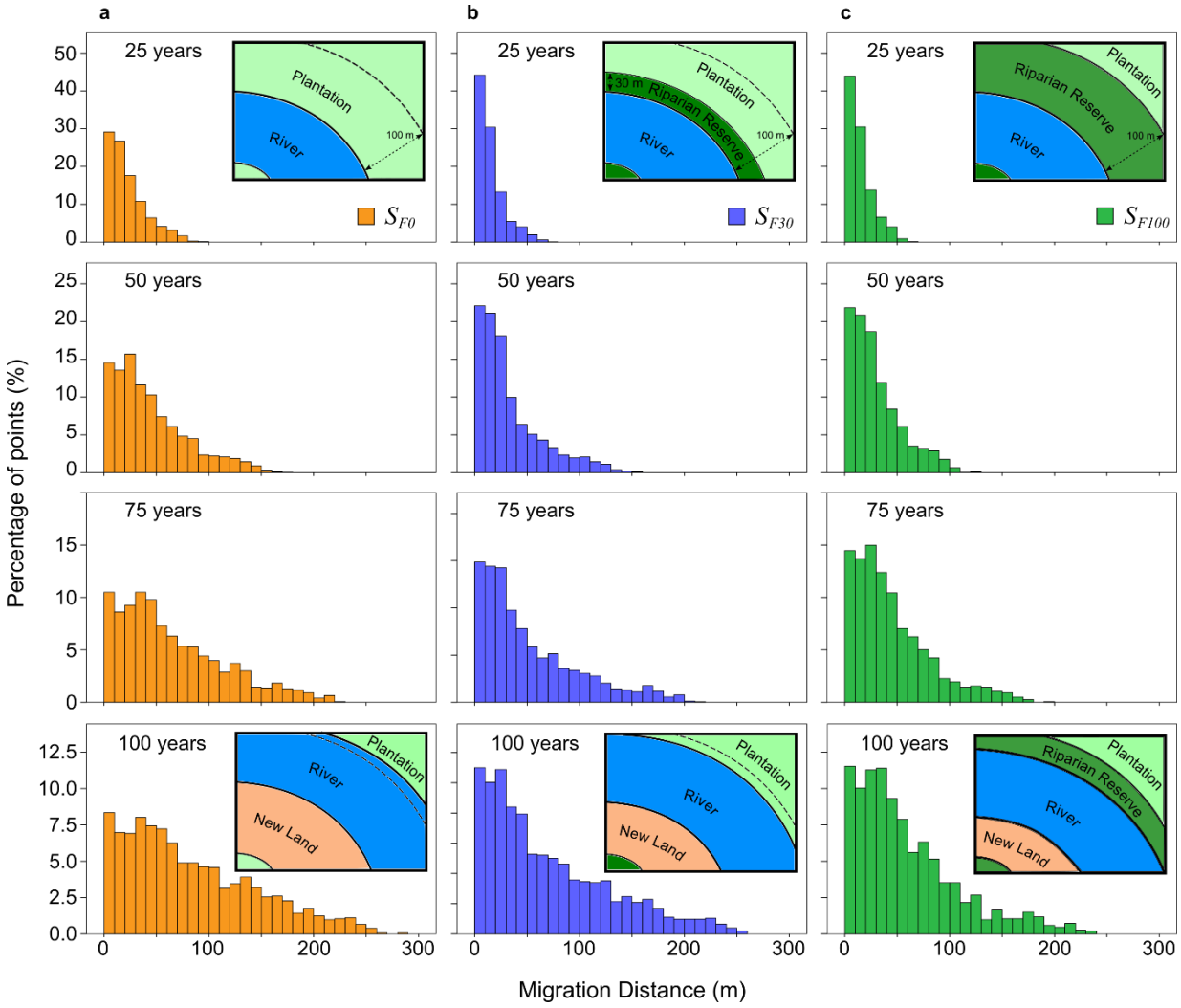

Figure 15: Distributions of centreline migrations for three forest clearance scenarios under the linear model. Model outputs for the distribution of centreline migrations taken at an along-channel spacing of 50 m after 25, 50, 75, and 100 years for a, SF0, b, SF30, and c, SF100.

Figure 16 (right-hand axis) shows the mean area of land lost per 100 m of river for each of the forest clearance scenarios after 25, 50, 75 and 100 years (see also **Table 6**). At each 25 year interval, the effect of maintaining a wide riparian buffer becomes more pronounced: after 100 years of migration, the mean area of land lost per unit length of river in S_{F10} is > 25 m^2/m greater than in S_{F100}, which equates to three rows of oil palms (**Figure**

16; **Table 6**). Migration rates are lower in the presence of a buffer, with land loss accelerating once the river has eroded through the buffer and into cleared plantation land.

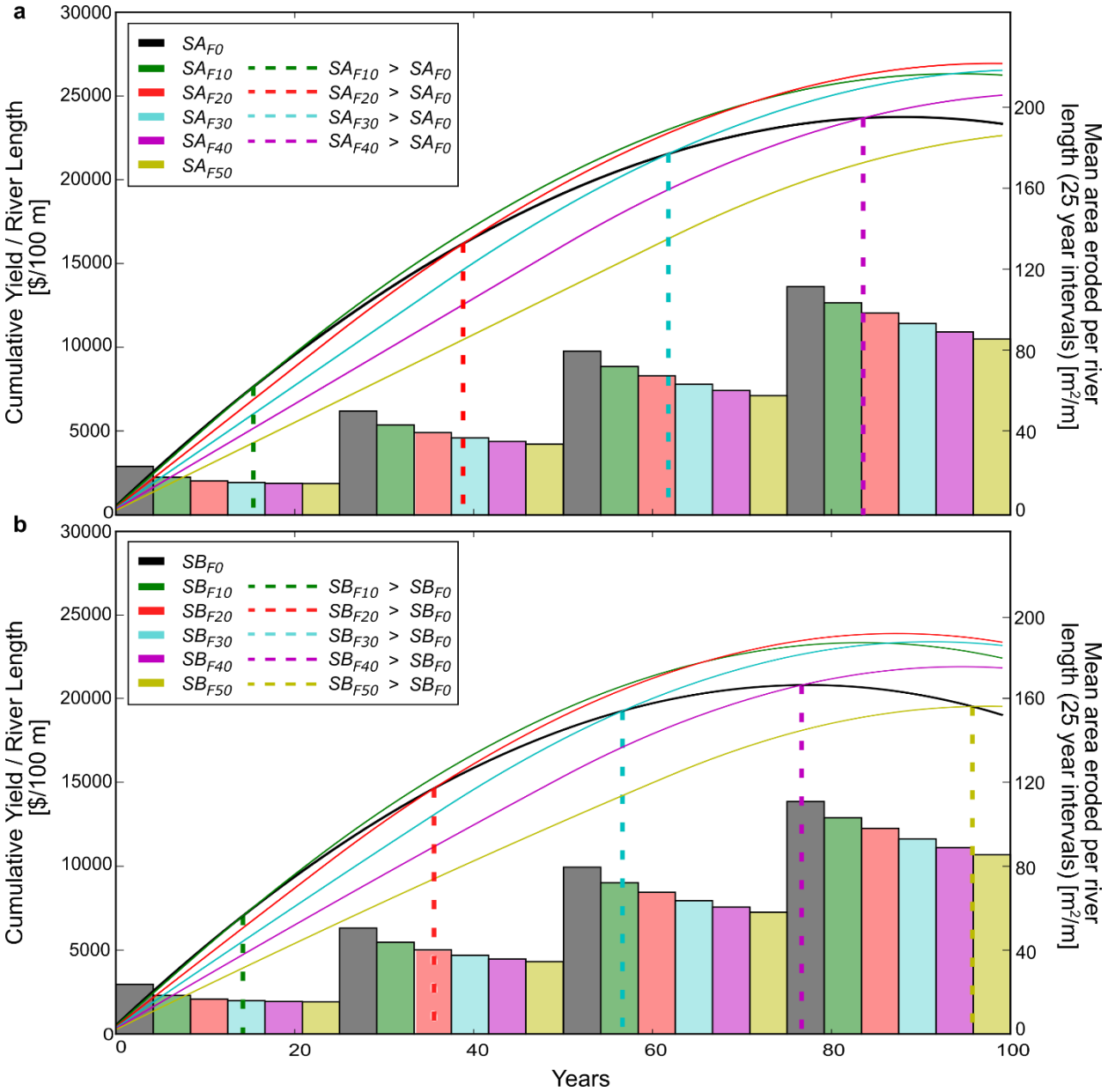

***Figure 16**: Expected cumulative yield for forest clearance scenarios. a. Model outputs of the expected cumulative yield for SA (no yield from land accreted on inner bank) applying the linear theory of meander migration for forested sections. b. Model outputs of the expected cumulative yield for SB (yield from accreted land). Markers show where each scenario exceeds S_{F0} (0 m riparian reserve). Bar charts show mean area of land lost per unit length of river (m/m²) for each forest clearance scenario after 25, 50, 75, and 100 years.*

Table 6: Mean area (m^2) of land eroded along the retreating bank per 100 m of river at 25 year intervals (relative to initial 2014 river position).

Scenario:	Mean area eroded per 100 m of river after 25 years (m2/m)	Mean area eroded per 100 m of river after 50 years (m2/m)	Mean area eroded per 100 m of river after 75 years (m2/m)	Mean area eroded per 100 m of river after 100 years (m2/m)
S_{F0}	23.54	50.21	79.07	110.20
S_{F10}	18.30	43.51	71.72	102.45
S_{F20}	16.56	39.92	67.17	97.50
S_{F30}	15.75	37.31	63.17	92.46
S_{F40}	15.37	35.56	60.14	88.35
S_{F50}	15.28	34.32	57.71	84.93
S_{F100}	15.27	32.37	51.82	74.51

4.3.1.2 Non-linear model

In contrast to the linear model, the retention of a riparian buffer under the non-linear modelling of forested reaches has little effect along sections where the expected migration is small, but greatly reduces the upper range of migration distances. Sections of river corresponding to the tail of the distribution evident in S_{F0} are limited to rates ≈ 1.0 m a^{-1} when migrating through riparian forest, resulting in a distribution of migration distances concentrated about this mean for S_{F100} (**Figure 17**).

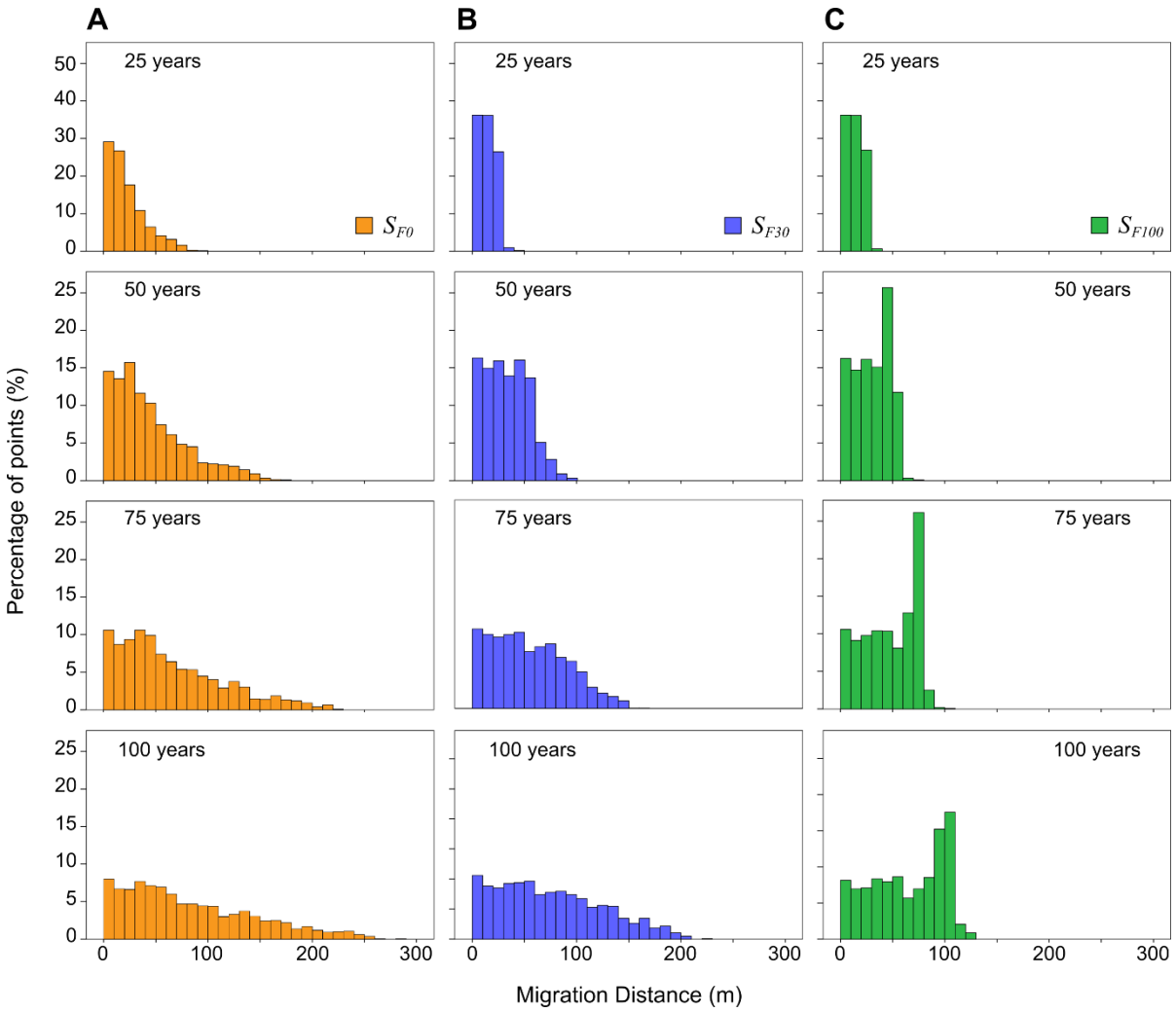

***Figure 17*: Distributions of centreline migrations for three forest clearance scenarios under the non-linear model. Model outputs for the distribution of centreline migrations taken at an along-channel spacing of 50 m after 25, 50, 75, and 100 years for a, SF0, b, SF30, and c, SF100.**

When averaged across all sections of river within the subsection of unprotected forest, the concentration of migration distances about a value corresponding to ≈ 1.0 m a^{-1} reduces the mean area of land eroded per 100 m of river compared to values derived from the linear model (**Table 7**). After each increment of 25 years, the model outputs from the non-linear modelling of forested sections are comparable to scenarios of buffer width 10 m wider under the linear model.

Table 7: Mean area (m^2) of land eroded along the retreating bank per 100 m of river at 25 year intervals (relative to initial 2014 river position).

Scenario:	Mean area eroded per 100 m of river after 25 years (m2/m)	Mean area eroded per 100 m of river after 50 years (m2/m)	Mean area eroded per 100 m of river after 75 years (m2/m)	Mean area eroded per 100 m of river after 100 years (m2/m)
S_{F0}	23.54	50.21	79.07	110.2
S_{F10}	16.35	40.81	68.04	97.09
S_{F20}	14.98	37.94	64.78	93.56
S_{F30}	14.52	35.44	61.53	89.81
S_{F40}	14.46	33.63	58.55	86.41
S_{F50}	14.47	32.67	55.89	83.33
S_{F100}	14.46	32.41	51.26	71.25

4.3.2 Expected yields from land in close proximity to the river edge

Using estimates of expected yields from existing oil-palm plantations on the Kinabatangan floodplain [*Abram et al.*, 2014] I quantify the potential impact of river migration on the mean long-term yield from land in close proximity to the eroding bank (≤100 m from the 2014 river position).

4.3.2.1 Linear model

Figure 16A shows projections for mean cumulative yield per unit length of river ($/100 m) from each forest clearance scenario assuming no contribution from cultivation along the inner bank, and applying the linear theory of meander migration for forested sections (*SA* projections; *IB* = 0); the dashed lines mark the point in time at which each scenario becomes economically advantageous relative to total forest removal (SA_{F0}). For SA_{F0}, the initial increase in yield from replacing all forest with oil palm is ultimately counteracted by the increase in riverbank erosion, reducing the long-term return. Given a 10 m buffer (SA_{F10}), the mean cumulative yield from land within 100 m of the eroding bank exceeds yield from SA_{F0} after ~15 years (**Figure 16A**; **Table 8**). Buffers >30 m wide appear to affect migration distances to similar extents over multiple decades (<50 years), preserving high-yield areas

for the longest periods. Wider buffers are good for conservation purposes but may have diminishing returns for efficient use of plantation land.

In **Figure 16B** the projections of mean cumulative yield per unit length of river ($/100 m) from land within 100 m of the eroding bank account for contributions to yield from cultivation of new land on the inner bank (*SB* projections; *IB* = cultivated). Cultivation of the inner bank adds planted area but reduces expected yields: newly accreted, frequently inundated land is only marginally productive (25%), and cannot offset the fixed costs of palm planting and maintenance [*Abrams et al*., 2014]. For projections of cumulative yield under *SB*, the negative effect of high migration rates are compounded as land accreted to the inner bank yields a net loss when converted to oil palm; the positive net benefit derived from buffers arrives earlier relative to the *SA* scenarios **Figure 16B**; **Table 8**). Note that SA_{F0} and SB_{F0} both exhibit a local maximum for cumulative yield. Because the initial condition describes a generic 100 x 100 m box extending inland from the riverbank with a mean yield value (see Eq. 19), the trend in cumulative yield from cultivated land (at 100% productivity) within that box is positive until the river erodes into cultivated land beyond 100 m from the initial position and the net effect on yield becomes only negative. The maximum for SB_{F0} occurs earlier than for SA_{F0} because yield from land within 100 m of the eroding bank must offset the net loss from cultivation of newly accreted land along the inner bank.

Table 8: Time before forest clearance scenarios become economically advantageous relative to total forest removal S_{F0} under each set of assumptions (SA, SB, and productivity proportional to river proximity).

Width of riparian buffer (m)	Time before scenario > SA_{F0} (a)	Time before scenario > SB_{F0} (a)	Time before scenario > S_{F0} assuming proportional productivity (a)
10	15.2	14.0	3.0
20	38.6	35.3	7.0
30	61.5	56.4	23.9
40	83.2	76.3	44.4
50	NA	95.4	63.8

4.3.2.2 Non-linear model

Figure 18 shows projections of mean cumulative yield per unit length of river ($/100 m) for scenarios of forest clearing resulting from the application of a non-linear model to forested river sections, and assuming the inner bank is left fallow (*SA*).

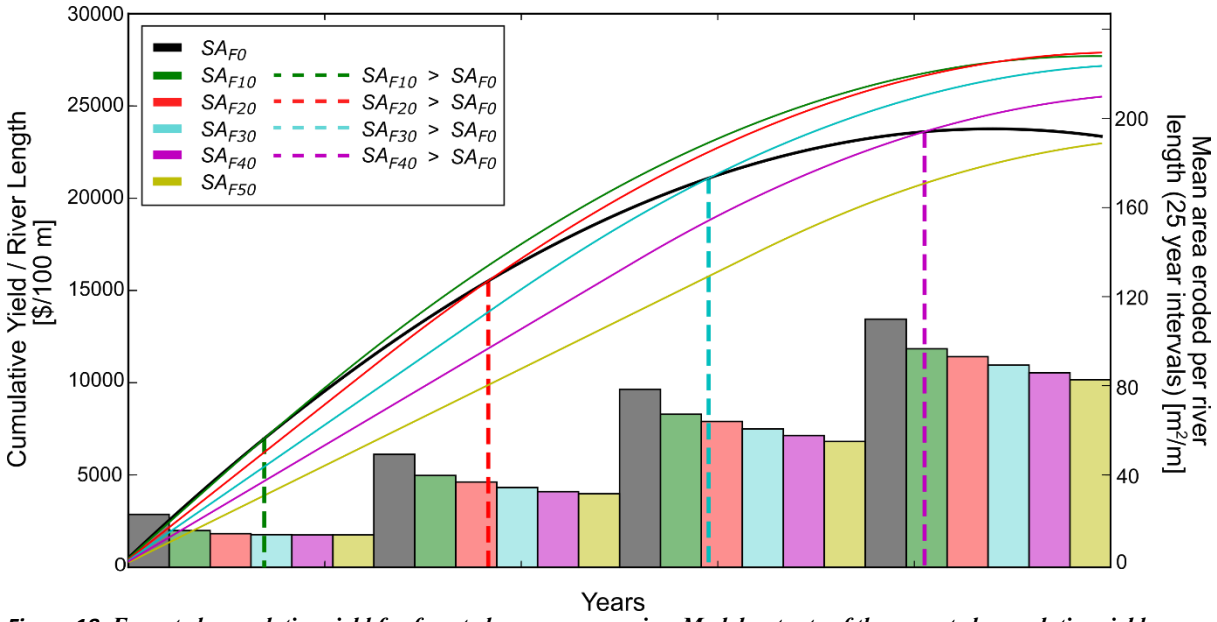

Figure 18: Expected cumulative yield for forest clearance scenarios. Model outputs of the expected cumulative yield for SA (no yield from land accreted on inner bank) applying the non-linear model for forested sections. Markers show where each scenario exceeds SA_{F0} (0 m riparian reserve). Bar chart shows mean area of land lost per unit length of river (m/m^2) for each forest clearance scenario after 25, 50, 75, and 100 years.

Scenarios retaining wider riparian buffers become economically advantageous relative to total forest removal (SA_{F0}) as the initial investment of maintaining forest on potential plantation pays dividend by protecting yield generating land from an advancing river. Compared to the results generated by the application of the linear theory to forested section, each scenario of forest clearing surpasses the expected yield generated by SA_{F0} earlier in the simulation when applying the non-linear model (**Table 9**).

Table 9: Time before forest clearance scenarios become economically advantageous relative to total forest removal S_{F0} for both linear and non-linear models of forested river sections

Width of riparian buffer (m)	Time before scenario > SA_{F0} : Linear Model (a)	Time before scenario > SA_{F0} : Non-linear Model (a)
10	15.2	13.7
20	38.6	36.4
30	61.5	58.8
40	83.2	80.6
50	NA	NA

4.3.3 Fast migrating river sections

For velocity perturbations less than 0.5 m s^{-1}, the non-linear model assigns migration values to forested sections of river that are comparable to those of cleared sections – it is along sections of river where velocity perturbations exceed this value that the non-linear model distinguishes between vegetation types. That the non-linear model should generate smaller estimates for the mean area of land eroded per unit length of river suggests that the influence of riparian buffers is most significant along sections of the river migrating larger distances – for they dictate the reach scale average. As velocity perturbation is primarily a function of planform curvature, riparian forest bordering straighter sections of river exert less control on reach scale averages than forest bordering meander bends, despite being a larger proportion of the total river length.

Confining my analysis to sections of the river that experience higher velocity perturbations, I applied both the linear and non-linear models to a 30 km subsection of the 76 km of unprotected forest, consisting of the apex and downstream exit of meander bends. **Figure 19** shows the mean area of land eroded per 100 m of river (also in

Table 10), and projections of cumulative yield assuming no inner bank cultivation (*SA*), for sections of the river where the geomorphic function of riparian buffers exerts the greatest degree of control.

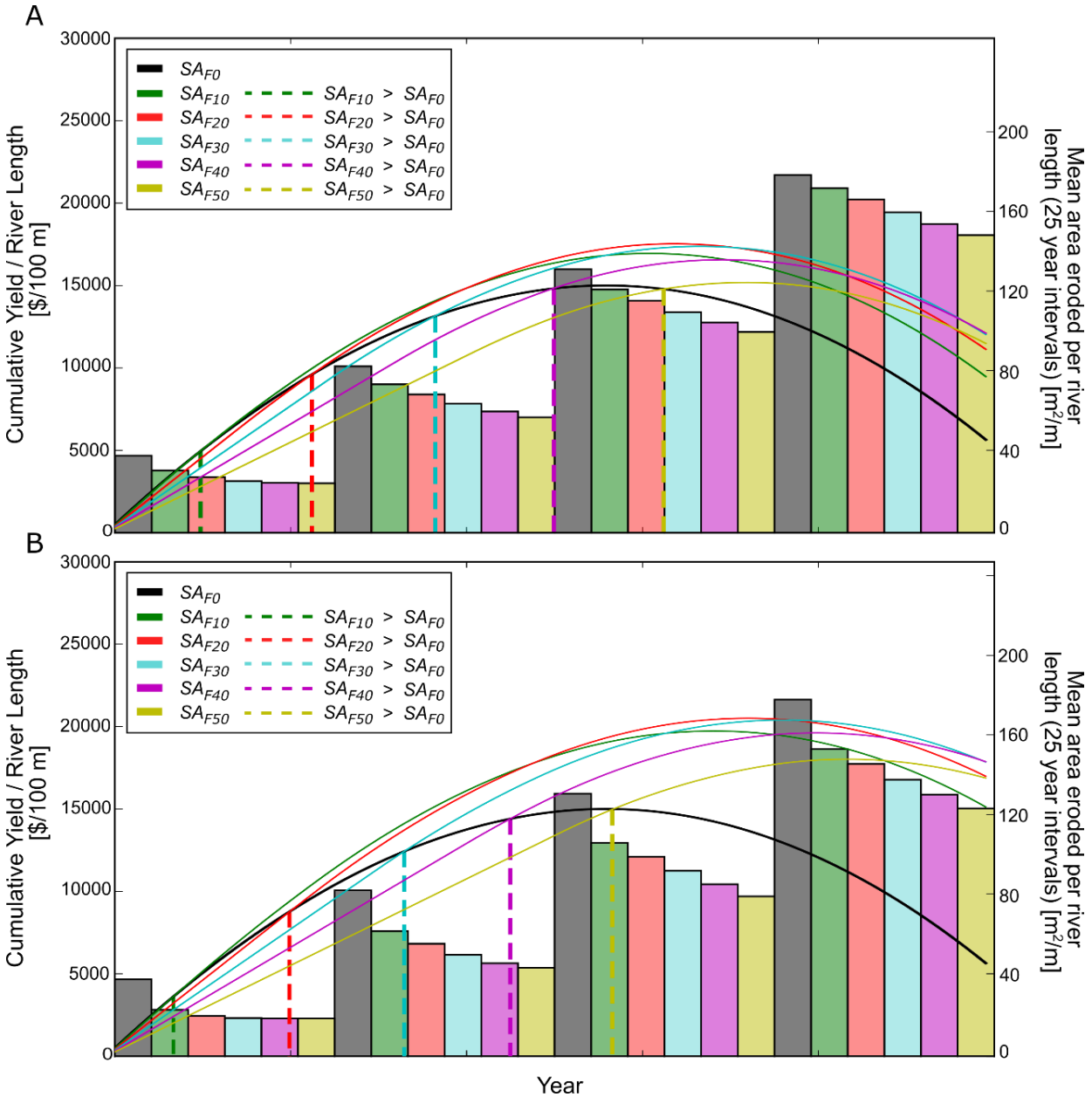

***Figure 19**: Expected cumulative yield for forest clearance scenarios along high velocity perturbation river sections. a. Model outputs of the expected cumulative yield for SA (no yield from land accreted on inner bank) applying the linear theory of meander migration for forested sections. b. Model outputs of the expected cumulative yield for SA applying the non-linear model for forested sections. Markers show where each scenario exceeds SA_{F0} (0 m riparian reserve). Bar charts show mean area of land lost per unit length of river (m/m^2) for each forest clearance scenario after 25, 50, 75, and 100 years.*

Table 10: Mean area (m^2) of land eroded along the retreating bank per 100 m of river at 25 year intervals (relative to initial 2014 river position) along high velocity perturbation river sections for both linear and non-linear models.

Scenario:	Mean area eroded per 100 m of river after 25 years (m^2/m)		Mean area eroded per 100 m of river after 50 years (m^2/m)		Mean area eroded per 100 m of river after 75 years (m^2/m)		Mean area eroded per 100 m of river after 100 years (m^2/m)	
	Linear	Non-linear	Linear	Non-linear	Linear	Non-linear	Linear	Non-linear
S_{F0}	38.38	38.38	82.79	82.79	131.09	131.09	178.02	178.02
S_{F10}	31.00	23.18	73.84	62.40	121.03	106.52	171.42	153.26
S_{F20}	27.61	20.14	68.84	56.16	115.50	99.56	165.82	145.89
S_{F30}	25.75	19.05	64.18	50.62	109.73	92.56	159.46	138.06
S_{F40}	24.86	18.92	60.38	46.40	104.63	85.85	153.55	130.58
S_{F50}	24.62	18.93	57.48	44.13	99.88	79.81	148.12	123.72

Higher migration rates around the apex and downstream exit of meander bends reduces the area of land available for yield generation more rapidly, significantly diminishing both the magnitude, and the time required to reach the maximum cumulative yield for all scenarios of forest clearing. At higher velocity perturbations the proportionate reduction in the rate of land lost to the river as it advances through riparian forest is greater when applying the non-linear model - the positive net benefit derived from buffers then arrives earlier relative to the linear model (**Table 11**).

Table 11: Time before forest clearance scenarios become economically advantageous relative to total forest removal SA_{F0} along high velocity perturbation sections of river for both linear and non-linear models.

Width of riparian buffer (m)	Time before scenario > SA_{F0}: Linear Model (a)	Time before scenario > SA_{F0}: Non-linear Model (a)
10	9.5	6.5
20	22.2	19.7
30	36.2	32.7
40	49.6	44.7
50	62.1	56.3

Irrespective of the model, the retention of riparian forest around the outer bank of meander bends has the potential to increase the return from adjacent plantation within timeframes corresponding to less than one crop rotation (25 years).

4.3.4 Short term profitability

When averaged across the reach scale for the total length of unprotected forest, the discrepancies between model outputs are small, therefore I apply only the linear model for the subsequent analyses, constituting a conservative estimate for the economic return derived from riparian buffers.

For time scales <10 years, SA_{F0} and SB_{F0} produce the highest revenues as the initial increase in yield, generated by converting all available land to oil-palm planation, compensates for the negative consequence of accelerated meander migration (**Figure 16**). However, this apparent short-term profitability changes if the fact that newly established oil-palm plantations are typically unproductive for the first three years is taken into consideration *[Corley and Tinker*, 2003; *Butler et al.*, 2009]. **Figure 20** shows projections of the mean cumulative yield per unit length of river ($/100 m) for the first 10 years of a plantation lifecycle (applying the linear model with no contribution from the inner bank), modified to incorporate the time-dependant productivity of a newly established plantation. Under these conditions, a riparian buffer is necessary to maximise the potential return from land in close proximity to the eroding bank. By reducing the initial planting expenditure and safeguarding young palms from being lost to erosion before they generate revenue, riparian buffer zones have the potential to increase the short-term profitability of newly established plantations.

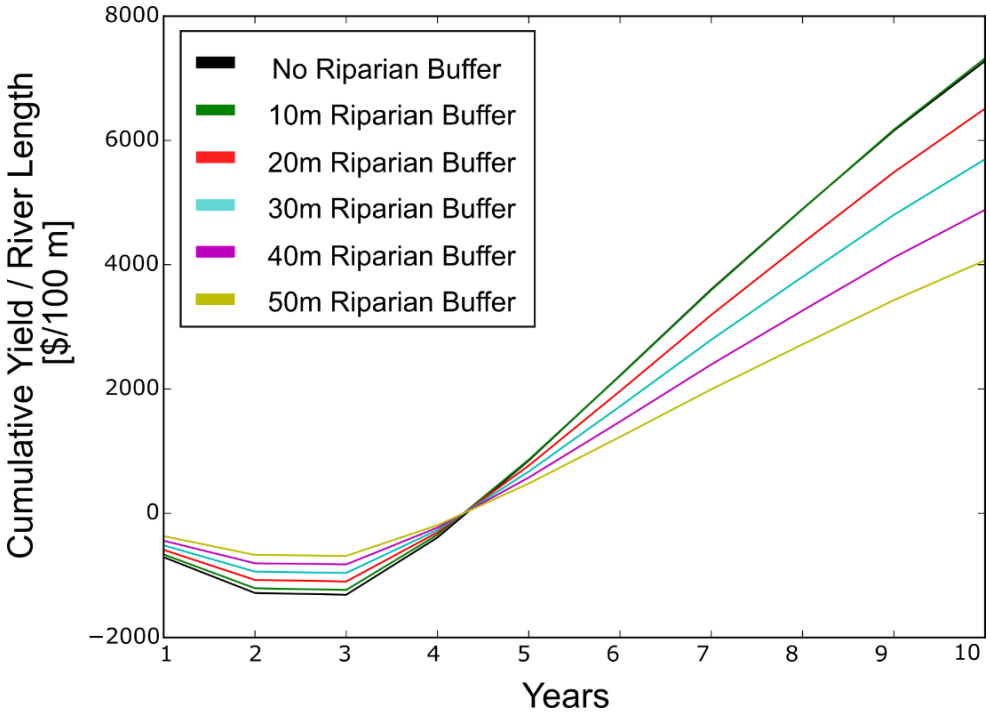

***Figure 20**: Expected yields from newly established plantations. a, Results for the first 10 years of SA using annual yield values that account for the time dependant productivity of a plantation over its expected life cycle.*

4.3.5 Propagating edge effect

Because regular inundation and excess soil moisture content is detrimental to the cultivation of oil palm, it is likely that plant productivity increases with distance from the river [*Abram et al.*, 2014; *Corley and Tinker*, 2015]. Therefore, yield estimates that assume all land on the eroding bank is productive at 100% probably underestimate the impact of river migration. To examine the possible effect of productivity being proportional to river distance, I consider the simple, hypothetical case that assumes (1) land within 20 m of the eroding bank is 50% productive, and (2) that this reduced productivity tracks inland with the eroding bank as the river migrates through the floodplain, akin to a "propagating edge effect" or "spatial externality" [*Parker*, 2007] (**Figure 21**). Although the choice of spatial gradient is arbitrary, **Figure 21** demonstrates that any gradient of reduced productivity extending inland from the riverbank intensifies the impact of river migration on expected yields, and thus increases the long-term economic value of riparian forest reserves.

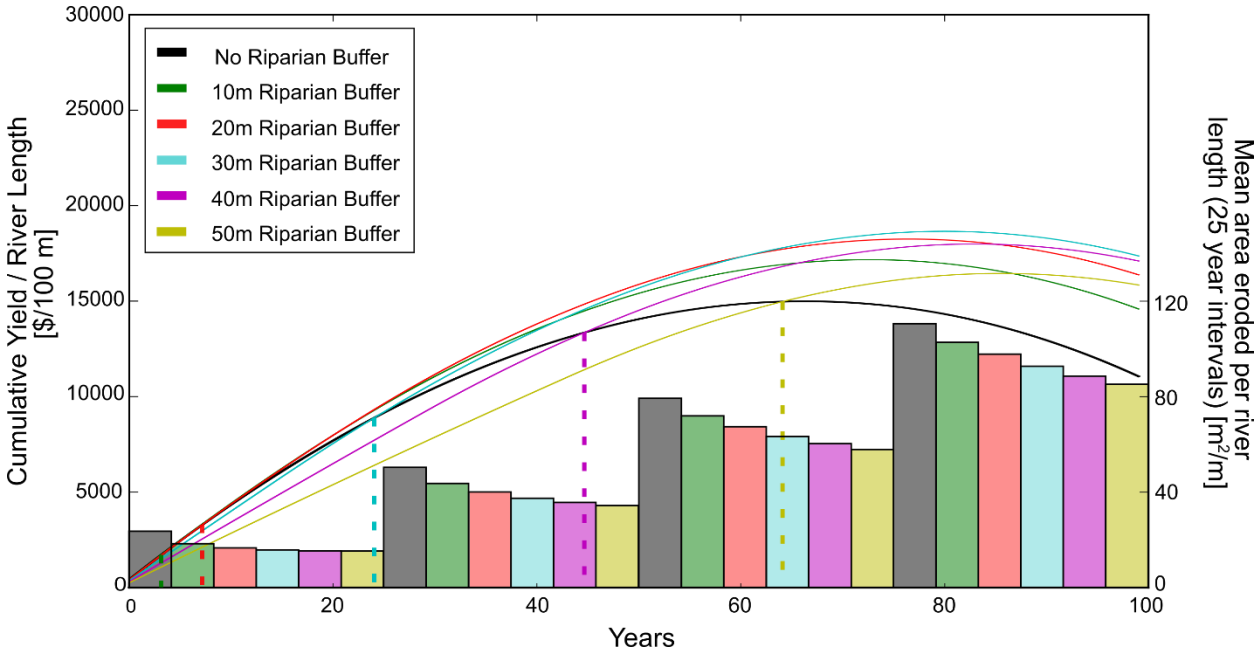

Figure 21: Expected cumulative yield for forest clearance scenarios with an edge-effect externality. Model outputs of the expected cumulative yield assuming a reduction in productivity proportional to river proximity, applying the linear model and assuming no yield from land accreted on the inner bank. Markers show model year that each scenario exceeds the no-buffer scenario; bar charts show mean area of land lost per unit length of river (m/m^2) for each forest clearance scenario after 25, 50, 75, and 100 years.

4.3.6 Highest-yield scenarios

The forest-clearing scenarios (i.e., recommended buffer widths) that produce the highest expected yields over short (0–10 years), medium (10–50 years), and long terms (50–100 years) are summarised in **Table 12**. When assuming lower productivity in close proximity to the riverbank (**Figure 21**), the highest-yield scenarios require a wider riparian buffer. Although the maximum yields for *SA* and *SB* are of different magnitudes, the recommended buffer widths are the same for both scenario sets.

Table 12: Actions to maximise expected yields based on range of economic forecast and productivity of land adjacent to the river's eroding bank.

Range of Forecast	Action assuming 100% productivity along eroding bank	Action assuming a reduction in productivity proportional to river proximity
Short term (0 - 10 years)	Maintain an initial 0 – 10 m riparian reserve	Maintain an initial 10 – 20 m riparian reserve
Mid-term (10 - 50 years)	Maintain an initial 10 m riparian reserve	Maintain an initial 20 m riparian reserve
Long-term (50 - 100 years)	Maintain an initial 20 m riparian reserve	Maintain an initial 30 m riparian reserve

4.4 Discussion

4.4.1 Conservative estimates

Because several components of this analysis involve conservative estimates of rates and effects, the assessments likely under-represent the potential for riparian forest reserves to enhance the economic return from floodplain plantation.

First, the model underestimates rates of meander migration. The values used for the coefficient of erosion, taken as the ratio of mean migration rate to the maximum velocity perturbation along aggregated sections of river, are themselves conservative estimates. I then apply this aggregated ratio to local velocity perturbation values at points along the river centreline. This results in an underestimation of meander migration along both forested and cleared sections of the river. Riparian reserves derive their economic worth from slowing the migration of the river through the floodplain; underestimating migration will thus tend to undervalue the economic worth attributed to riparian reserves.

Second, meander migration rates represented in the model only account for riverbank erodibility as a function of riparian forest absence or presence. I don't consider any secondary effects of forest removal, such as increased sediment loading, increased mean average discharge, magnitude and frequency of peak flows, or the duration of high flows that can affect bank erosion, migration rates, and otherwise alter the river's internal flow regime [*Costa et al.*, 2003; *Liu et al.*, 2015]. Forest removal from tropical floodplains has been shown to increase sediment delivery to river systems [*Gomi et al.*, 2006; *Annammala et al.*, 2012], which in turn may drive more rapid river evolution (including increased migration rates) *[Dunne et al., 2010; Wickert et al., 2013; Constantine et al.*, 2014] . Scenarios of forest clearing involving narrower riparian reserves might entail increased

sediment loading to the river system, which would further increase meander migration rates and accelerate the loss of converted plantation to bank erosion. Because this effect would propagate downstream, the full economic benefit of maintaining riparian reserves – both upstream and down – would increase.

Third, reduced meander migration rates as an ecosystem service provision for land in close proximity (≤100 m) to the river's edge are considered, but flood impacts following the removal of floodplain forests may also adversely affect the productivity of established plantations at larger scales [*Liu et al.*, 2015; *Corley and Tinker,* 2015]. Flood events along the Kinabatangan can extend hundreds of meters inland from the river's banks; persistent flood impacts, whether through increased frequency or duration, are likely to be far more economically detrimental than those caused by meander migration, particularly over short (multi-annual) time scales.

4.4.2 Maximising return from floodplain plantations

By reducing meander migration rates, riparian reserves have the potential to increase the expected yield from plantations adjacent to eroding riverbanks. How best to utilise this provision to maximise economic return from floodplain plantations depends upon the duration of the desired return, and the level of productivity along the eroding riverbank (**Table 12**).

Our results suggest that irrespective of whether newly accreted land is converted to planation, preserving a riparian forest buffer can enhance the expected return from converted land along the river's eroding bank. For a given scenario, the simulations assume a uniform buffer width along each unprotected reach of the river. However, a more efficient application of a buffer – that is, a more nuanced use of the geomorphic ecosystem service that a buffer provides – might involve linking local buffer width to local bank erosion rate.

Given a buffer of uniform width, sections of river that undergo little migration lose potential yield to a redundant service; similarly, plantations especially vulnerable to rapid river migration could make better use of a wider buffer as has been demonstrated (**Figure 19**). Initial widths of riverbank forest reserves could vary according to expected distances of bank migration over a given time span. This would reduce the area of land lost to the river along sections that migrate rapidly, and would allow forest conversion along relatively static reaches. This is particularly pertinent when considering the results from the non-linear model, as the geomorphic function of riparian buffers is entirely localised along sections of the river that experience higher velocity perturbations. If the non-linear model is a more faithful representation of the observed data, then redistributing the allocation of riparian forest reserves around the apex and downstream exit of meander bends will dramatically increase the economic return from forest retention. In addition, forest connectivity could be better maintained along the length of the river (at least until broken by meander migration), providing the benefits of a continuous forest corridor [*Bruford et al.*, 2010; *Gregory et al.*, 2014].

4.4.3 Geomorphic Ecosystem Function

Ecosystem functions and services constitute flows of materials, energy, and information from natural capital stocks to the benefit of human welfare. Ecosystem functions refer to the habitat, properties, or processes of an ecosystem, whereas ecosystem services are the end benefit derived from ecosystem functions, such as food production or waste assimilation [*Costanza et al.*, 1997]. Major ecosystem services studies have tended to focus on the functional interaction between biodiversity (living) rather than geodiversity (non-living) ecosystem elements, undervaluing the contribution of geomorphic processes to human wellbeing [*Everard and Quinn*, 2017]. Whilst geomorphological processes directly

contribute to two of the four broad categories of ecosystem services defined within the Millennium Ecosystem Assessment [2005] (Supporting and Regulating), the functional links between biodiversity and geodiversity are not explicitly recognised [*Gordon and Barron*, 2013]. Fluvial geomorphology is an integral part of an ecosystem's geodiversity, as the processes of erosion, deposition and transportation of sediment through a fluvial system constantly reshape the physical landscape, and influence the structure, functioning, and biodiversity of an ecosystem [*Naiman et al.*, 2010]. There is a need to better understand and describe the reciprocal influences between linked habitat types and services provided by fluvial forms and processes [*Everard and Quinn*, 2017].

Here I offer a quantification of the potential benefit arising from the interaction of the riparian ecosystem with fluvial geomorphic processes. These results demonstrate that the functional interaction of the natural riparian environment with riverine processes result in the service of reducing land lost to the river to the benefit of adjacent plantations. These results are intended to constitute a case study for future research that seeks to map the associated ecosystem service within a formal Ecosystem Approach policy framework.

4.5 Conclusion

The main purpose of this investigation was to quantify effects of riparian forest reserves on expected yield from an adjacent tropical oil-palm planation, given the capacity for riparian forest to reduce rates of riverbank erosion, meander migration, and loss of arable land. Although further work is needed to identify and quantify the full range of ecosystem services afforded to oil-palm plantations by riparian reserves, the results suggest that preservation of riparian buffers can enhance profitability of adjacent plantations by slowing

land loss (while also reducing carbon emissions, maintaining forest connectivity, and supporting ecosystem biodiversity).

Because rapid, large-scale land conversions – including tropical deforestation – have geomorphic consequences [*Lazarus*, 2014], geomorphic ecosystem services have an important role to play in efforts to guide long-term environmental sustainability. "Building with nature" efforts have a long legacy in in floodplain management and river restoration research [*Darby and Sear,* 2008], but also extend to other geomorphic systems, including deltas [*Paola et al.*, 2011] and coastlines *[Cheong et al., 2013; Temmerman et al., 2013; van Slobbe et al.*, 2013]. Insight into the dynamics of management interventions that make use of natural processes is essential to understanding how human-dominated landscapes [*Werner and McNamara*, 2007; *Di Baldassarre et al.*, 2013] and novel ecosystems [*Ellis*, 2011] will evolve in the future.

Chapter 5:

Riparian forest as a primary control on meander migration

Author Contributions

The main body of text presented here was originally drafted by myself, though many revisions and suggestions have been made by Dr Tristram C. Hales. The original concept, model formulation and development, and analysis are solely my own work.

5.1 Introduction

Rates of riverbank retreat are governed by the balancing of two distinct events: the delivery of failed riverbank material to the channel margins by abrupt riverbank collapse (mass wasting), and the rate of removal of sediment by lift and drag forces applied by the channel flow (fluvial entrainment) [*Thorne*, 1991; *Lawler et al.*, 1997]. Whilst residing at the bank toe, failed material armours and buttresses the bank face , impeding further retreat until its removal by fluvial entrainment [*Thorne*, 1991]. Along rivers that have composite banks comprised of both cohesive and non-cohesive materials, mass wasting takes place by one of three failure mechanisms; cantilever, planar, or rotational [*Pizzuto*, 1984; *ASCE Task Committee*, 1998]. Preferential scouring of lower bank material can lead to undercutting, causing an overhanging cohesive block to form in the upper layers, which then collapses by cantilever failure [*Thorne et al.*, 1981]. Riverbanks where cantilever failure predominates are characterized by small frequent collapses, evidenced by irregular blocks accumulating at the toe of a steep bank face. Where the geotechnical properties of the composite bank promote larger mass wasting events, riverbanks most commonly fail by planar shearing [*ASCE Task Committee*, 1998] as stresses imposed by the weight of a failure block exceed the shear strength of the soil along the most critical planar surface [*Lawler*, 1992, 1995]. Riverbanks where planar failure predominate are characterized by less frequent mass wasting events evidenced by large slump blocks buttressing the lower bank face.

By providing root reinforcement and reducing pore water pressures [*Simon et al.*, 2000; *Pollen-Bankhead and Simon*, 2010], riparian forests stabilise riverbanks and contribute to the size of mass wasting events [*Milledge et al.*, 2014; *Wang et al.*, 2016]. Observations made along the Kinabatangan River in northern Borneo suggest that the removal of riparian

forest can alter the style of mass wasting, with evidence of more frequent, smaller failure events following deforestation [*Horton et al.*, 2017]. Furthermore, rates of channel migration following the removal of floodplain forest are significantly increased, and exhibit a shift in process dominance so that planform curvature ceases to be a first order control [*Horton et al.*, 2017]. Similar observations have been made along forested sections of the Sacramento River in California, where rates of channel migration along forested reaches are seemingly independent of velocity perturbation until the river transitions into agricultural land [*Micheli et al.*, 2004]. Both the Kinabatangan and the Sacramento are large rivers, with bank heights far in excess of rooting depths, confining the influence of a root network to the upper portion of riverbank. Material entrained by fluvial scour from the lower portion of the bank face is not, therefore, directly affected by the presence of riparian forest, but may indirectly be affected as the upper portion of riverbank is episodically delivered to the channel margins by mass wasting. I propose that the observed shift in rates of channel migration following deforestation are a consequence of alterations to either the style of mass wasting, or the fate of failed material once delivered to the bank toe.

Assuming rates of fluvial entrainment are constant, then over long timeframes the total volume of material delivered to the channel margins should be independent of the size of individual mass wasting events [*Constantine et al.*, 2009]. Therefore, mean rates of channel migration should be unaffected by the style of mass wasting unless the residency time per unit volume of failed material is altered as a consequence. This may indeed be the case, for slump blocks resulting from mass wasting are in effect small scale topographic features that add roughness and create form drag altering the near-bank flow structure [*Kean and Smith*, 2006]. Accounting for the effect of slump-block size and shape on the flow field around a meander bend may play an important role in predicting rates of riverbank

retreat [*Hackney et al.*, 2015]. In addition to altering the characteristic size of individual failure events, riparian vegetation might control the residency time of slump blocks by altering the composition of failed material, providing resistance to fluvial scouring [*Dunaway et al.*, 1994]. Whilst it is likely that these two influences work in combination, I examine the latter in isolation to assess whether it may plausibly account for the non-linearity displayed in the relationship between planform curvature and channel migration observed along both the Kinabatangan and Sacramento Rivers. Recent intensification of research into the importance of slump block armouring to the long term migration patterns of alluvial rivers has focused on either the self-organising nature of channel geometry [*Asahi et al.*, 2013; *Eke et al.*, 2013, 2014], or the effect of structural heterogeneity within floodplains [*Xu et al.*, 2011; *Motta et al.*, 2014], but hasn't explicitly represented the effect of riparian vegetation on slump block dynamics. I develop a formulation of slump block armament that represents the effect of a dense root network, and accounts for the decomposition of roots over time.

I hypothesize that altering the composition of failed riverbank material delivered to the bank toe by mass wasting has the potential to affect rates of channel migration, and alter the dominant control on riverbank retreat. Furthermore, the influence of root decomposition within the dynamics of slump block armouring introduces a constraint on residency times that is independent of the flow field around a meander bend, altering the relationship between planform curvature and channel migration. To test this hypothesis I develop a model of channel migration that incorporates vegetation dynamics within a representation of slump block armouring, and examine the impact of varying root density on rates and patterns of channel migration. I then attempt to reproduce observed patterns of meander migration relating to planform curvature along the Kinabatangan River to assess

whether a formulation of slump block decay that incorporates plant mortality might account for the observed non-linearity.

Our hypotheses assume that rates of channel migration are determined by the progression of the outer bank, and that alterations to the driving mechanisms of bank retreat are responsible for the observed shift in the relationship between planform curvature and channel migration. By examining the dynamic width adjustment of the river channel as it migrates through its floodplain, and the effect of root density on the relative dominance of either bar push or bank pull, I assess the merits of this assumption.

5.2 Methods

The model framework describing slump block armament set out by *Parker et al.* [2011] combines a 2D model of the morphodynamic flow field within a central channel region with a description of non-cohesive sediment transport from the outer to inner banks moderated by the influence of cohesive slump blocks, which are periodically delivered from the upper layer to the bank toe by either cantilever or planar/rotational failure. The slump blocks are assumed to prevent the entrainment of non-cohesive material from the protected portion of bank face until they are entirely removed piecemeal by fluvial scour, at which point the transport of non-cohesive sediment from the lower bank face can progress unhindered until mass wasting replenishes the cover of cohesive slump blocks from the upper layer. The rate of slump block production is controlled by the unhindered rate of lateral migration – the rate of slump block decay is proportional to the shear stress applied by the (unmodified) flow field in excess of a formative threshold. By modifying this model framework to represent the effect of riparian vegetation on slump block characteristics and decay, I examine the role of a dense root network in controlling rates of channel migration along

large river systems by means of altering the composition of failed material alone. Within the formulation of slump block armament, I incorporate a function of plant mortality to assess whether rates of root decomposition might account for the reduction in planform curvature as the dominant control on rates of meander migration in the presence of riparian vegetation. I then examine the patterns of dynamic width adjustment as the river migrates through its floodplain to assess the role of riparian forest in controlling the relative dominance of either bar push or bank pull.

5.2.1 Model framework

I adopt the same computational arrangement as *Eke et al.* [2014] in the application of the modeling framework, dividing the river channel into three distinct regions: inner bank, outer bank, and central channel. I define the channel geometry and expressions that govern the morphodynamics of each region, linking these through the application of a global formative Shield's number.

Based on the continuity of sediment transport, the framework develops an expression based on the Exner equation that describes the transport of non-cohesive sediment through a channel cross-section [*Parker et al.,* 2011]. Evaluating the integral of the Exner equation across the bank face at the boundary between the bank and bed regions yields Equation 21, which demonstrates a linear relation between the rate of riverbank migration ($\dot{n}_e$) and the rate of sediment delivery from an eroding bank face to the bed region ($\tilde{q}_{e,J}$) plus the net aggregation/degradation of the channel bed

$$\dot{n}_e = \frac{1}{(S_e + S_{tb})}\left[\frac{\frac{\partial}{\partial s}\int_{n_e}^{n_{ee}} q_{e,s}\, dn + (1 + Cn_e)\tilde{q}_{e,J}}{(1-\lambda_p)B_e(1 + C\bar{n}_e)} + \left.\frac{\partial \eta}{\partial t}\right|_{n=n_e}\right], \qquad EQ\ (21)$$

where *n* denotes the transverse coordinate from the river centrepoint, the subscript *e* denotes the eroding bank face, the subscript *s* denotes the longitudinal coordinate, S_e is the slope of the bank region, S_{tb} is the transverse bed slope at the bank toe, $q_{e,s}$ is the longitudinal sediment flux in the bank region, $\tilde{q}_{e,j}$ is the combined longitudinal and transverse transport rate of sediment across the boundary between the bank and bed regions, *C* is channel curvature, λ_p is the porosity of the non-cohesive bank material, B_e is the width of the bank region $(n_{ee} - n_e)$, $\bar{n}_e$ is the coordinate of the midpoint in the bank region $\frac{1}{2}(n_{ee} + n_e)$, t is time, and η is the bed elevation.

Assuming $|S_e| \gg |S_{tb}|$, and the net flux of sediment in the longitudinal direction to be zero [*Eke et al.* 2014], Equation 1 reduces to

$$\dot{n}_e = \frac{(1 + Cn_e)q_{e,n}}{S_e B_e(1 - \lambda_p)(1 + C\bar{n}_e)} + \frac{1}{S_e}\frac{\partial \eta}{\partial t}\Big|_{n=n_e}, \qquad EQ\ (22)$$

$$= \xi_{E/D} + \frac{1}{S_e}\frac{\partial \eta}{\partial t}\Big|_{n=n_e},$$

where $q_{e,n}$ is the transverse sediment transport rate from the bank to bed region. This formulation of Equation 22 holds true for both the inner and outer banks, though quantification of the term relating to channel migration due to sediment transport (the first term on right hand side) will depend upon the bank either moving away from the centre (eroding) or towards the centre (depositing).

5.2.1.1 Quantification of bank erosion by sediment transport - ξ_E

Rather than explicitly evaluate the combined flux of both cohesive and non-cohesive sediment represented by the $q_{e,n}$ term in ξ_E; *Parker et al.* [2011] first specify an erosion rate based on the transport of purely non-cohesive sediment from the bank face (ξ_{Enon}), then modify this default rate by representing the natural armouring effect of cohesive vegetated

slump-blocks. In accordance with EQ (22), the lateral migration of an unprotected bank can be expressed as

$$\xi_{Enon} = \frac{1}{(1-\lambda_p)} \frac{q_{Enon,n}}{H_e} \frac{(1+Cn_e)}{(1+C\bar{n}_e)}, \qquad EQ\ (23)$$

where H_e is the height of the non-cohesive portion of bank face, and $q_{Enon,n}$ is the transverse supply rate of sediment from the non-cohesive portion of bank face to the bed region. ξ_{Enon} is then modified to account for the effect of cohesive material reducing rates of lateral migration by the inclusion of an armouring coefficient $K_{armor} \leq 1$ modelled as a function of slump-block characteristics

$$\xi_E = I_f K_{armor} \xi_{Enon} \qquad EQ\ (24)$$

where I_f is a ratio of flood intermittency – a proportion of time the river is deemed morphodynamically active.

The rate of bedload supply from the non-cohesive portion of the eroding bank face can be expressed as a function of sediment and flow characteristics applied to the sloping bank face [*Eke et al.*, 2014]

$$q_{Enon,n} = \phi \beta S_e \sqrt{RgD_s{}^3} \qquad EQ\ (25)$$

where *g* denotes acceleration due to gravity, *R* is the submerged specific gravity of the sediment, D_s is a characteristic grain size, and ϕ is the intensity of bedload transport as described in [*Einstein*, 1950] here approximated due to *Parker* [1979] as

$$\phi = 11.2\left(\tau^*_{tb,E}\right)^{1.5}\left[1 - \frac{\tau^*_c}{\tau^*_{tb,E}}\right]^{4.5} \qquad EQ\ (26)$$

and

$$\beta = \frac{1+\omega\mu}{\mu}\sqrt{\frac{\tau^*_c}{\tau^*_{tb,E}}} \qquad EQ\ (27)$$

where ω is the lift coefficient assumed to be 0.178 [*Einstein*, 1950], μ is the Coulomb friction coefficient taken as 1.0 [*Asahi et al.*, 2013], τ_c^* is the Shield's number relating to the critical shear stress at the threshold of motion, and $\tau_{tb,E}^*$ is the Shield's number relating to the shear stress acting on an eroding bank face taken to be a fraction (φ) of the streamwise Shield's number acting on the channel bed evaluated at the bank toe, which I take to be 0.6 [*Eke et al.*, 2014]. $\tau_{tb,E}^*$ is found by evaluating a sub model for the morphodynamic flow field around the central channel based on the linear numerical approximation for the velocity perturbation of *Sun et al.* [1996].

5.2.1.2 Slump-block Armouring

The dampening effect of slump-block armouring is described as a simple function of the proportion of slump-block cover afforded to the exposed bank face as [*Parker et al.*, 2011]

$$K_{armor} = 1 - \frac{A_c}{D_c L_e} \qquad EQ\ (28)$$

where A_c is the volume of failed cohesive material armouring the bank face per unit length of channel, D_c is the characteristic size of slump-blocks so that $\frac{A_c}{D_c}$ relates to the height of stacked slump-blocks at a given time, and L_e is the length of the non-cohesive portion of bank face

$$L_e = H_e\sqrt{1 + (S_e)^{-2}}. \qquad EQ\ (29)$$

As a greater proportion of the bank face is covered by slump-blocks, $\frac{A_c}{D_c} \rightarrow L_e$, $K_{armor} \rightarrow 0$, and so $\xi_E \rightarrow 0$. The delivery of cohesive sediment to the bank toe is modelled as mass failure caused by the removal of underlying non-cohesive bank material. The style of mass wasting is not specified, but the rate of slump block production is assumed to be directly proportional to the rate of non-cohesive sediment removal. Therefore, the

volume of cohesive material delivered to the bank toe per unit channel length over time can be expressed as

$$q_c = H_c|\xi_E|(1-\lambda_c) \qquad EQ\ (30)$$

where H_c is the height of the cohesive layer, and λ_c is porosity of the cohesive material. Assuming that in situ slump-blocks decay by disaggregation, the total volume of failed material at the bank toe can be said to change with respect to time as

$$\frac{dA_c}{dt} = q_c - \frac{A_c}{T_c} \qquad EQ\ (31)$$

where T_c is a characteristic slump-block residency time. The volume of failed material at the bank toe is likely to fluctuate over time as mass wasting periodically delivers large deposits that are subsequently removed. However, taken as an average over the timeframe of planform evolution, it is reasonable to assume a quasi-steady state in which $\frac{dA_c}{dt} = 0$. The total volume of failed material at the bank toe can then be expressed as a relation between the rate of slump-block production, and the characteristic residency time, such that

$$A_c = H_c|\xi_E|(1-\lambda_c)T_c \qquad EQ\ (32)$$

and from Eq. 28 I get

$$K_{armor} = 1 - \frac{H_c|\xi_E|(1-\lambda_c)T_c}{D_c L_e}. \qquad EQ\ (33)$$

Substituting Eq. 23 into Eq. 24 and solving for ξ_E, I find that

$$\xi_E = \frac{I_f \xi_{Enon}}{\left(1+\frac{1}{\delta}\right)}, \qquad \delta = \frac{D_c L_e}{H_c(1-\lambda_c)T_c I_f|\xi_{Enon}|}. \qquad EQ\ (34a,b)$$

Eke et al. [2014] demonstrate that δ represents the relative control slump-block armouring exerts on rates of riverbank erosion, so that as $\delta \to 0$,

$$\xi_E = kT_c^{-1}, \qquad k = \frac{D_c L_e}{H_c(1-\lambda_c)}\mathrm{sgn}(\xi_{Enon}) \qquad EQ\ (35)$$

corresponding to the case where lateral migration is entirely mediated by slump-block armouring, and becomes a function of residency time alone. Therefore, if the residency time of slump blocks fails to correlate with planform curvature, so too will rates of channel migration for systems where delta is small. This result has the counter-intuitive consequence of rendering ξ_{Enon} irrelevant for systems where it takes very large values, for as ξ_{Enon} increases, δ decreases, diminishing its importance. Taking the extreme case as an example, we can see this to be true, for if ξ_{Enon} were large enough that non-cohesive sediment transport was effectively instantaneous, then the instant slump block cover was removed by fluvial scour, the lower bank would retreat the distance required to trigger mass wasting of the upper layer and replenish slump block protection. The rate of channel migration then becomes entirely dependent upon the characteristic dimensions of slump block production, and the subsequent rate their removal, i.e. when $\delta = 0$.

5.2.1.3 Slump-block residency time

In order to avoid the case where channel migration can be expressed independently of a flow field (as in Eq. 35), *Eke et al.* [2014] suggest representing the residency time of slump-blocks as a function of boundary shear stresses

$$T_c = T_{ref}\left(\frac{\tau^*_{tb,E}}{\tau^*_{form}} - 1\right)^{-1} \qquad EQ\ (36)$$

where T_{ref} is a reference slump-block residency time to be proportionally mediated by the ratio of bank Shield's number to a formative Shield's number: τ^*_{form}. The formative Shield's number stipulates the shear stress required to initiate bank erosion; should the bank Shield's number fall below this threshold, then erosion ceases, and deposition occurs along the bank face, which requires an alternative quantification of channel migration (discussed below). It is the imposition of a threshold Shield's number governing the formation of both

banks that closes the relationship between erosional and depositional processes [*Eke et al.*, 2014]. This formulation of slump-block residency time reduces riverbank erosion as $\tau^*_{tb,E} \rightarrow \tau^*_{form}$, halting entirely as the two become equal.

The formative Shield's number is the Shield's number applied to the bank face at bankfull conditions along a straight channel

$$\tau^*_{form} = \varphi \tau^*_{bf} \qquad EQ\ (37)$$

where τ^*_{bf} is the bankfull Shield's number acting on the channel bed along a straight section. This formulation of the model satisfies the conditions necessary to reproduce observed patterns of meander formation. Although T_{ref} describes the expected residency time of a slump-block along a channel section where $\tau^*_{tb,E} = 2\tau^*_{form}$, it effectively acts as an arbitrary scaling parameter that needs calibration. Rather than define T_c by referring to an expected value – I present a formulation that incorporates the effect of riparian vegetation, and explicitly describes the process of slump-block decay.

In order for cohesive sediment from the upper layer to afford any protection to the non-cohesive bank face, the material delivered to the channel margin must be sufficiently consolidated to form slump-blocks large enough to preclude entrainment by river flows. First let's consider the case where cohesive particulates constitute a small fraction of the cohesive layer, and the required consolidation is primarily a consequence of the binding effect of a riparian root network.

From the excess shear strength equation [*Kandiah*, 1974; *Krone*, 1999] we can derive an expression for the erodibility (k_d) of non-cohesive sediment as

$$k_{d,non} = \xi_{Enon}\left(\frac{\tau^*_{tb,E}}{\tau^*_c} - 1\right)^{-n} \qquad EQ\ (38)$$

where *n* is usually assumed to be 1, though other values may used for smaller grained sediments [*Fernandez Luque and Van Beek*, 1976; *Van Rijn*, 1984].

As the definition of τ^*_{form} is the limit below which bank erosion does not take place, we can reinterpret τ^*_{form} as the critical Shield's number of slump-blocks, and thus

$$\xi_{slump} = f\left(k_{d,non}\right)\left(\frac{\tau^*_{tb,E}}{\tau^*_{form}} - 1\right)^n \qquad EQ\ (39)$$

where ξ_{slump} is the erosion rate of slump-blocks, and $f\left(k_{d,non}\right)$ is some function of $k_{d,non}$that incorporates particulate cohesion and the effect of a riparian root network.

The inclusion of root biomass to a soil matrix rapidly decreases erodibility relative to bare earth [*Dunaway et al.*, 1994; *Mamo and Bubenzer*, 2001; *Gyssels et al.*, 2005; *De Baets et al.*, 2006; *De Baets and Poesen*, 2010; *Vannoppen et al.*, 2015] and can be expressed as function of root density

$$k_d = k_0 e^{-aRd} \qquad EQ\ (40)$$

where k_0 is the erodibility of the soil without the addition of roots, *Rd* is root density [kg m^{-3}], and *a* is a decay constant that varies widely between empirical studies (0.41 [*Zhang et al.*, 2013] – 2.58 [*Gyssels et al.*, 2006]). Though many of these studies quantify the effect of roots in reducing the erodibility of topsoil by overland flow, a dense root network has also been shown to reduce the erodibility of exposed streambanks [*Smith*, 1976; *Wynn*, 2004; *Pollen-Bankhead and Simon*, 2010]. Applying a water jet testing device to rooted streambanks, *Wynn and Mostaghimi* [2006] found that reductions in bank erodibility best correlated with volumetric increases in larger roots (2 to 20 mm diameter) such as those found along forested riverbanks.

Reported values of root density for different biomes are often derived from measurements of the upper 10 – 30 cm and extrapolated to the unit cubic meter, resulting

in values that are far in excess of total in situ biomass. As the complete removal of slump-blocks by fluvial scour requires the disaggregation of material throughout the entire soil column – *Rd* is represented as a total biomass per area [kg m^{-2}] and the exponent in Eq. 40 is adjusted to account for the unit conversion [*Flanagan and Nearing*, 1995].

The reduction of erodibility in newly formed slump-blocks by a sufficiently dense root network prohibits fluvial scour, resulting in residency times large enough to halt channel migration. However, once delivered to the channel margins, slump-block erodibility begins to recover as root material decays. We can then describe the decline in root matter over time using an exponential decay from an initial root density as proposed by *O'Loughlin and Watson* [1979] to describe the decline in root tensile strengths assuming that the observed reduction in tensile strengths was the result of root death

$$Rd(t) = Rd_0 e^{-b12t} \qquad EQ\ (41)$$

where Rd_0 is the root density at t = 0, and b = decay constant. As the decline in root tensile strength is likely to be more rapid than root decomposition, this formulation constitutes a conservative estimate for the role plant mortality might play in controlling slump block residency times. The significance of the uncertainty within both the decay exponents *a* and *b* from equations 40 and 41 is discussed later.

For the case where cohesive particulates constitute a small fraction of the bank material, we can assume k_0 = $k_{d,non}$, thus the erosion rate of slump-blocks as a function of time can be defined as

$$\xi_{slump}(t) = \left(\frac{\tau^*_{tb,E}}{\tau^*_{form}} - 1\right)^n \left(k_{d,non} e^{-a\left(Rd_0 e^{-b12t}\right)}\right). \qquad EQ\ (42)$$

The residency time of a slump-block is then the time taken to erode its width

$$\int_0^{T_c} \xi_{slump}(t)\ dt = D_c, \qquad EQ\ (43)$$

which yields the solution

$$\left[\frac{E_1(aRd_0e^{-b12t})}{12b}\right]_0^{T_c} = \frac{D_c}{k_{d,non}}\left(\frac{\tau^*_{tb,E}}{\tau^*_{form}} - 1\right)^{-n} \qquad EQ\ (44)$$

where E_1 is the exponential integral on the complex plane

$$-\int \frac{e^{-t}}{t}dt \qquad EQ\ (45)$$

which requires a numerical approximation.

Although the inclusion of root biomass within a soil matrix reduces erodibility, and has been show to increase the shear strength of riverbanks [*Abernethy and Rutherfurd*, 2001], as well as the apparent cohesion of soil [*Pollen-Bankhead and Simon*, 2010], it is unclear whether the addition of roots alters the critical shear stress of sediments [*Wynn and Mostaghimi*, 2006]. If the addition of roots to a soil matrix doesn't significantly affect the critical shear stress, then the increase in slump-block critical shear compared to non-cohesive sediment can be attributed to the inclusion of clay and silt particulates. If slump blocks contain cohesive particulates, then the erodibility of slump blocks devoid of root matter (k_0) will differ from the erodibility of non-cohesive sediment ($k_{d,non}$). *Hanson and Simon* [2001] propose a relation for the erodibility of cohesive material based on the critical shear stress (τ_c [cm^3 / N s]) as

$$k_d = 0.2{\tau_c}^{-0.5}. \qquad EQ\ (46)$$

Approximating the critical shear stress of slump-blocks as the shear stress relating to the formative Shield's number, an estimate for k_0 inclusive of cohesive particulates within slump-blocks is then

$$k_0 = 0.2U{\tau_{form}}^{-0.5} \qquad EQ\ (47)$$

where *U* is a unit conversion factor.

5.2.1.4 Quantification of bank deposition by sediment transport – ξ_D

Migration directed away from the channel centre (erosion) is initiated when the streamwise Shield's number acting on the bed at the bank's toe is above the formative Shield's number, should the bank Shield's number fall below the formative Shield's number, then the bank undergoes deposition, and migrates towards the channel centre. Bank deposition is quantified as a function of vegetation encroachment, assuming a constant upper bound of vegetation growth on newly formed point bars, mediated by flood events and higher flows [*Eke et al.*, 2014]

$$\xi_D = \xi_{Veg}\left(1 - I_f\right)\left(1 - \frac{\tau^*_{tb,D}}{\tau^*_{form}}\right) \qquad EQ\ (48)$$

where $\tau^*_{tb,D}$ is a fraction (φ) of the streamwise Shield's number acting on the channel bed evaluated at the toe of a depositing bank face, and ξ_{Veg} is the rate of vegetation colonization along point bars. In the absence of field measurements I have taken ξ_{Veg} to be ~5% of the bankfull channel width [*Lauer and Parker*, 2008b].

5.2.2 Model implementation

The implementation of the model framework as outlined above requires a submodel that simulates the in-channel morphodynamics to provide estimates for boundary shear stresses, water elevation, flow depths, and near bank velocities. I use the linear solution to the equations of motion in an open channel with constant curvature as presented by *Johannesson and Parker* [1989], but evaluate the solution with a numerical approximation [*Sun et al.*, 1996], as the analytical solution is only valid for small curvatures.

Running the model over multiple iterations requires three global constraints; constant bankfull discharge (Q), homogeneous bed friction factor (c_f), and a constant

adjustment to the centerline height with respect to angle change around the meander bend [*Eke et al.*, 2014]

$$S_0(t)R_c(t) = \frac{\Delta z}{\Delta \theta}, \qquad EQ\ (49)$$

where R_c is the radius of curvature, S_0 is the streamwise bed slope, z is the centerline elevation, and ϑ is the angle around the meander bend.

Initial inputs of straight channel morphology are then required to specify c_f, and the cross-sectionally averaged Shield's number acting on the bed at bank full conditions

$$c_f = \frac{gH_{0,bf}S_{0,bf}}{{U_{0,bf}}^2}, \qquad \tau^*_{bf} = \frac{H_{0,bf}S_{0,bf}}{RD_s}, \qquad EQ\ (50, 51)$$

where $H_{0,bf}$ is the mean channel depth along a straight channel at bankfull, $U_{0,bf}$ is the mean channel velocity along a straight channel at bankfull, and $S_{0,bf}$ is the streamwise slope along a straight channel at bankfull. The initial formative Shield's number is then $\varphi\tau^*_{bf}$.

If the initial bankfull width of the curved channel differs from that of the straight section, then initial values of mean depth, velocity, and streamwise slope are determined by assuming cross-sectionally averaged bedload transport rates (Qs) are consistent (this assumption is made just once to approximate initial conditions and isn't a global constraint throughout the model)

$$Qs_{bf} = 11.2B(\tau^*_0)^{1.5}\left[1 - \frac{\tau^*_c}{\tau^*_0}\right]^{4.5}\sqrt{RgD_s{}^3}, \qquad EQ\ (52)$$

where B is the width of the curved channel, and τ^*_0 is the cross-sectionally averaged Shield's number acting on the bed corresponding to the initial conditions of the curved channel.

At each iteration of the model, the velocity perturbation resulting from the present channel morphology is evaluated along each bank using the numerical approximation of *Sun et al.* [1996]. These approximations then yield left and right bank Shield's numbers

($\tau^*_{tb,L}, \tau^*_{tb,R}$) to be evaluated against the formative Shield's number and used to derive values of bank migration according to either EQ (34a,b) or (38).

Flow depth ($H_{L/R}$) and water surface elevation perturbation ($\zeta_{L/R}$) at each bank are calculated assuming constant curvature according to *Johannesson and Parker* [1989]

$$H_{L/R} = \frac{RD_s\tau^*_{tb,L/R}}{S_0}, \qquad \zeta_{L/R} = H_0\chi_{20}F^2 n_e C, \qquad EQ\ (53,54)$$

where *F* is the Froude number, and χ_{20} is a function of c_f defined in *Johannesson and Parker* [1989]. The depth of the channel bed is then

$$\eta_{L/R} = H_{L/R} - \zeta_{L/R} \qquad EQ\ (55)$$

providing all necessary components to compute bank migration rates from EQ (2).

After each iteration, the radius of curvature and bankfull width are recalculated according to the new bank positions, the new streamwise bed slope is calculated according to the global constraint of EQ (49), and subsequently

$$U_0 = \left(\frac{gQS_0}{c_f B}\right)^{\frac{1}{3}}, \qquad H_0 = \frac{Q}{U_0 B}, \qquad EQ\ (56,57)$$

which redefines the channel geometry ready for the next iteration. Finally, the formative Shield's number is adjusted to account for the reduction in streamwise slope [*Eke et al.*, 2014]

$$\tau^*_{form} = \tau^*_{form,1}\left(\frac{S_0}{S_{0,1}}\right)^{0.54}, \qquad EQ\ (58)$$

where $\tau^*_{form,1}$, and $S_{0,1}$ are values from the first iteration derived from the initial channel geometry.

In its original conception, the model framework of *Parker et al.* [2011] was formulated to describe compound banks typical of smaller gravel bed rivers, with larger

grained, non-cohesive material forming a basal portion overlain by fine grained, cohesive alluvial deposits, which differs from the large sand bedded river of the Kinabatangan. However, *Eke et al.* [2014] successfully applied the model framework to the Trinity River in Texas, the composition and dimensions of which are similar to the Kinabatangan River, suggesting that its application in this case is valid. Using input parameters and initial conditions that are representative of the Kinabatangan, I generated two sets of model outputs for comparison: one set using the formulation of slump-block decay described by *Eke et al.* [2014] (hence forth referred to as 'EPS' (Eke, Parker, Shimizu)), and one set using the formulation of slump-block decay detailed above (hence forth referred to as 'HHC' (Horton, Hales, Constantine)). When comparing between sets of results I hold all parameters common to both formulations of slump-block armouring constant, and adjust only those that are distinct as part of a sensitivity analysis presented in the results. Where available, I have used measured values from a low lying meandering section of the river ('Reach B' in Chapter 3). A full description of parameter values and their origin can be found in **Table 13**.

Table 13: Slump block Parameter symbols and values

Parameter	Symbol	Value	Unit	
Initial curvature	C	0.003 – 0.024	m^{-1}	
Initial slump-block root Density	Rd_0	0.5 – 10.0	Kg m^{-2}	
Reference slump-block residency time	T_{ref}	0.5 – 10.0	yr.	
Vegetation encroachment rate	E_{veg}	4.0	m yr^{-1}	%5 of bankfull width – [*Eke et al.,* 2014]
Exponent a in eq (40)	a	5.7		[*Flanagan and Nearing*, 1995]
Exponent b in eq (41)	b	0.023		[*O'Loughlin and Watson*, 1979]
Exponent n in eq (38)	n	1.0		
Bankfull discharge	Q	1450	m s^{-1}	[*Horton et al, 2017*]
Bankfull width (including bank regions)		110	m	[*Horton et al, 2017*]
Bankfull depth (initial)	H_0	6.5	m	[*Horton et al, 2017*]
Bankfull streamwise Slope	S_0	0.0003		[*Horton et al, 2017*]
Eroding bank slope	S_e	0.6		Measured cross-sections
Porosity of bank	λ_p	0.4		
Critical Shield's number	τ^*_{form}	0.048		Shield's diagram
Fraction of bed shear stress on bank	φ	0.6		[*Eke et al.,* 2014]
Grain size	D_s	0.00035	m	Field observations
Density of sediment	ρ_s	2650	Kg m^{-3}	density of quartz from literature
Flood intermittency	I_f	0.154		ratio of days > 55% bankfull discharge
Characteristic size of failure blocks	D_c	0.5	m	
Height of cohesive layer	H_c	1.0	m	
Porosity of failed material	λ_c	0.4		

5.3 Results

5.3.1 Slump-block residency times

The degree to which root density moderates the erodibility of slump-blocks is controlled by the exponents *a* and *b* from equations 40 and 41 respectively, where *a* relates to the magnitude of the initial reduction, and *b* relates to the rate of recovery via the decay of root material. **Figure 22** illustrates how the proportional reduction in erodibility varies through time according to the relation described by equations 40 and 41 as the exponents *a* and *b* vary across an order of magnitude whilst maintaining a constant root density.

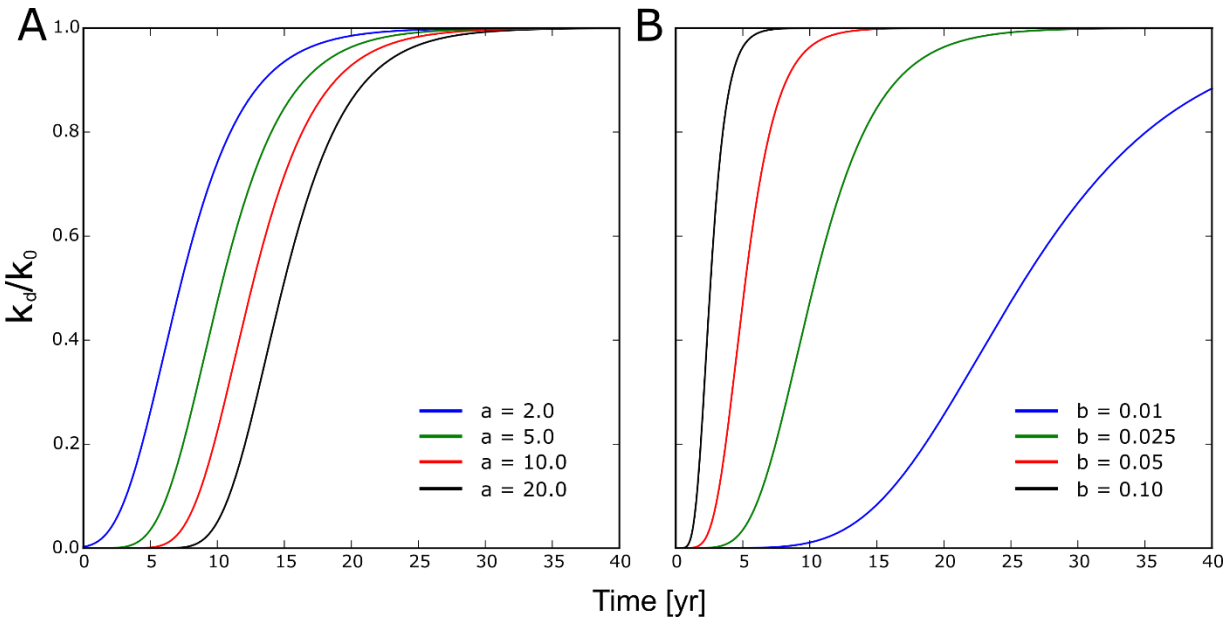

Figure 22: a. Proportional erodibility as a function of time with constant root density (3.0 kg m^{-2}), varying exponent* a *from eq. 40 (2, 5, 10, 20), and constant exponent* b *from eq. 41 (0.25). b. Proportional erodibility as a function of time with constant root density (3.0 kg m^{-2}), constant exponent* a *from eq. 19 (5.0), and varying exponent* b *from eq. 20 (0.01, 0.025, 0.05, 0.10).

Increasing the exponent controlling the magnitude of the initial reduction in erodibility has the effect of prolonging the onset of recovery, though the pattern and timescale of recovery is maintained (**Figure 22A**). Increasing the exponent controlling the decay of root material dramatically alters the pattern of proportional recovery, suggesting it to be the more significant of the two exponents in controlling slump block residency times. In the absence of field data I refer to the empirical findings of *Flanagan and Nearing* [1995], who propose using the value a = 5.7 for the reduction in soil erodibility due to the combined effects of live and dead roots, and from *O'Loughlin and Watson* [1979] I take the exponent controlling the decay rate of roots to be b = 0.023. These values correspond to median patterns of proportional reductions within the range each displays in **Figure 22**. I examine the significance of the uncertainty within each of these exponents by conducting a sensitivity analysis observing the alteration to the relationship between curvature and migration of the outer bank in the subsequent section.

Figure 23 shows the proportional reduction in erodibility as root densities vary between the extremes observed across global terrestrial biomes: 0.125 – 16.0 kg m^{-2} [*Klinge and Herrera*, 1978; *Jackson et al.*, 1996].

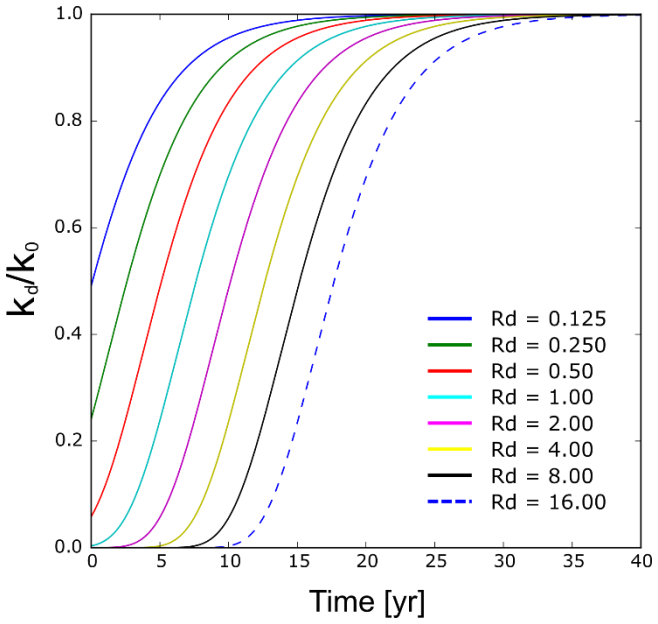

Figure 23: Proportional reduction in erodibility through time varying initial root density.

Root densities at the lower bounds of the defined range do not sufficiently impair the erodibility of slump-blocks to altogether halt their degradation. For the case where $k_0 = k_{d,non}$, the initial erosion rate of slump-blocks with small root densities is a significant proportion of ξ_{Enon}, which, even along straight channels, has been shown to be orders of magnitude larger than observed rates of channel migration [*Eke et al.*, 2014]. For root densities larger than 0.6 kg m^{-2}, erodibility is reduced to the extent that slump-block degradation doesn't initially take place, delaying the breakdown of slump-blocks until a sufficient quantity of root matter has been removed by decay to enable the disaggregation of material by fluvial scour.

Altering the formulation of slump-block armouring to incorporate a time dependent erodibility function changes the relationship between residency times and the excess boundary shear stress acting on the eroding bank face. To examine this relationship, I assign

arbitrary values to τ^*_{form} and ξ_{Enon}, and holding these constant, compare slump-block residency times across a range of $\tau^*_{tb,E}$ ($\tau^*_{form} < \tau^*_{tb,E} \leq 3\tau^*_{form}$) for both HHC and EPS (**Figure 24**).

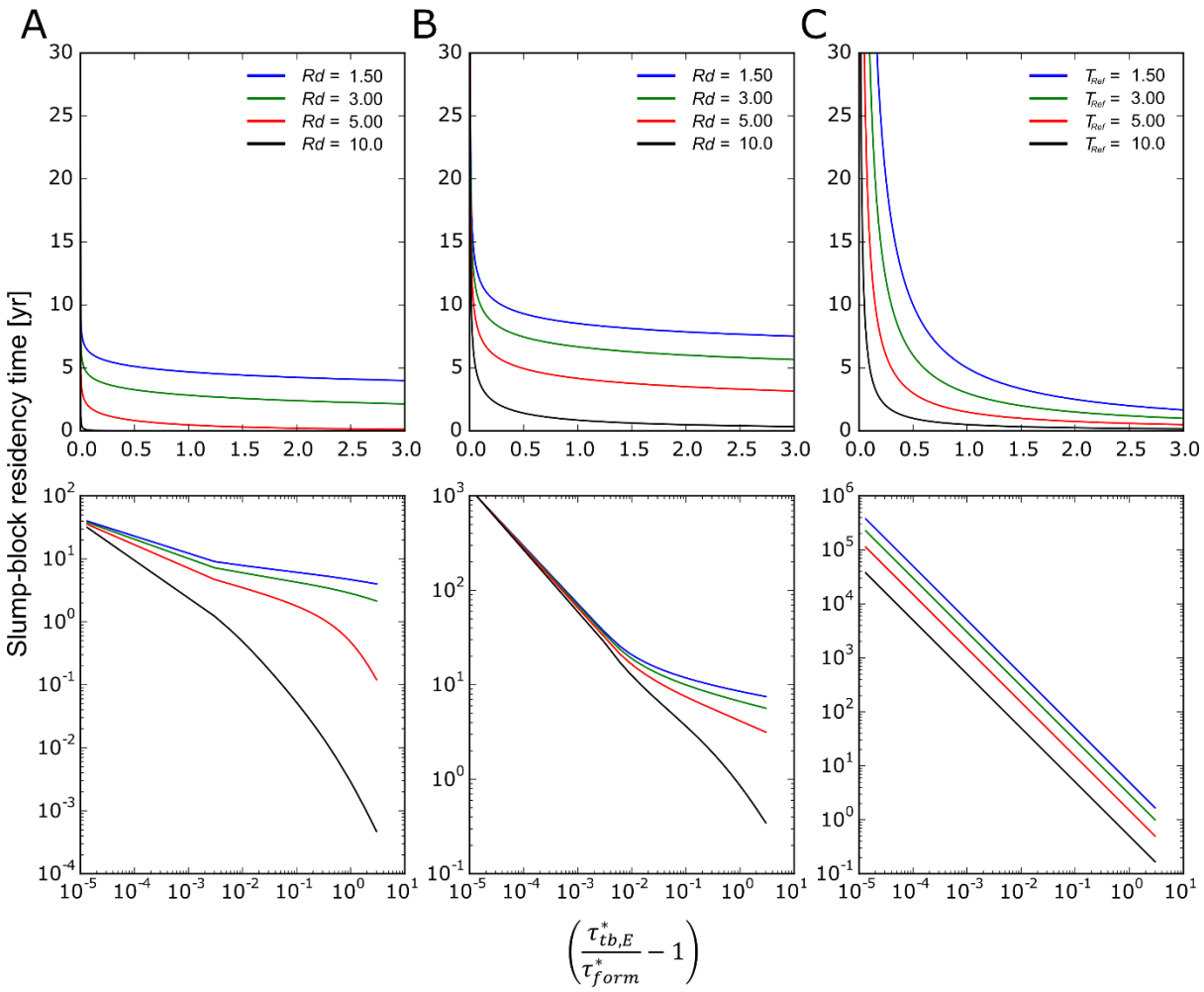

Figure 24: a. Slump block residency times across the range of proportional excess shear stress [0, 3] with varying initial root densities [1.5, 3.0, 5.0, 10.0] under slump block formulation HHC assuming cohesion due to rooted sediment alone ($k_0 = k_{d,non}$). b. Slump block residency times across the range of proportional excess shear stress [0, 3] with varying initial root densities [1.5, 3.0, 5.0, 10.0] under slump block formulation HHC assuming the presence of cohesive particulates within slump blocks ($k_0 = 0.2U{\tau_{form}}^{-0.5}$). Slump block residency times across the range of proportional excess shear stress [0, 3] with varying reference residency times [1.5, 3.0, 5.0, 10.0] under slump block formulation EPS. Lower panels depict log-log relationships.

Deriving an expression for the residency time of slump blocks that incorporates root decay causes an almost constant (slightly reducing) residence time across the range of shear stresses. **Figure 24A** and **Figure 24B** show residency times as defined by HHC quickly tend towards a lower limit as excess shear stresses increase. The effect of altering initial values of

root density is to shift this lower bound upwards with increasing density. Although there is an asymptote where excess shear stress is zero, the exponential decay from this asymptote is very rapid for all values of root density, so that small values of $\frac{\tau^*_{tb,E}}{\tau^*_{form}}$ correspond to residency times that are the same order of magnitude as larger values. By contrast, the residency time of slump-blocks as defined by EPS decay by power laws from an asymptote towards zero as excess shear stresses increase, with the rate of decay being inversely proportional to the parameter T_{ref}. This slow decay means that residency times of slump-blocks increase by several orders of magnitude at lower values of $\frac{\tau^*_{tb,E}}{\tau^*_{form}}$, and that irrespective of sump-block properties, residency times will always tend towards 0 as excess shear stresses increase, which is not the case for HHC.

5.3.2 Planform curvature

The principal consequence of including vegetation characteristics in the representation of slump-block residency times is to alter the relationship between rates of outer bank retreat and planform curvature. This is of central importance to this investigation as my hypothesis maintains that riparian vegetation along the outer bank modulates slump block armament to the extent that planform curvature ceases to be a first order control on rates of channel migration. To examine the relationship between outer bank retreat and planform curvature in isolation, I apply both HHC and EPS to the case of the Kinabatangan River, but fix the progression of the inner bank to that of the outer. Using parameter values listed in **Table 13**, and an initial channel curvature of 0.01, I vary slump-block characteristics ($Rd_0, T_{ref} = 1.5, 3.0, 5.0, 10.0$) whilst maintaining a constant channel width by fixing $\dot{n}_{e,Inner} = \dot{n}_{e,Outer}$. Running each model formulation for a period of 500 years, I then compare rates of outer

bank migration as the channel adjusts to a reduction in curvature resulting from continual centerline expansion (**Figure 25**).

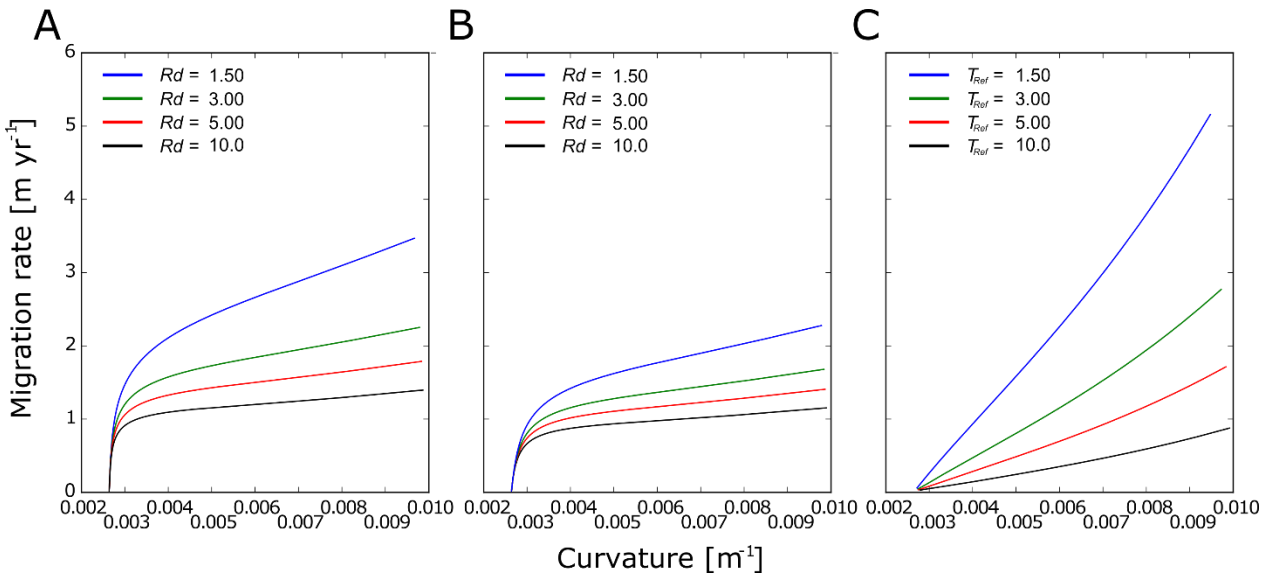

Figure 25: Rates of outer bank migration relative to planform curvature with fixed channel width across a range of slump block parameters. a. Under slump block formulation HHC assuming $k_0 = k_{d,non}$ for root initial root densities [1.5, 3.0, 5.0, 10.0]. b. Under slump block formulation HHC assuming $k_0 = 0.2U\tau_{form}^{-0.5}$ for root initial root densities [1.5, 3.0, 5.0, 10.0]. c. Under slump block formulation EPS for reference residency times [1.5, 3.0, 5.0, 10.0].

For both HHC and EPS, rates of channel migration tend towards zero as curvature tends towards 0.0025, which marks the point where the outer bank Shield's number exceeds the formative. For curvature values that are greater than this threshold, channel migration for HHC rapidly increases as the residency time of slump-blocks digress from the asymptote at $\frac{\tau^*_{tb,E}}{\tau^*_{form}} = 1$, then gradually increases with a linear proportionality controlled by the parameter Rd_0. By contrast, rates of channel migration in EPS deviate only slightly from constant linearity, with the rate of proportional increase being controlled by the parameter T_{ref}. The deviation from linearity is a result of streamwise slope reducing with planform curvature as the channel extends outwards according to the relation described by Eq. 49.

We can now examine the significance of the uncertainty within the selection of the exponents controlling the proportional reduction in slump block erodibility (*a, b* in eq. 40, 41) on the relationship between curvature and the retreat of the outer riverbank.

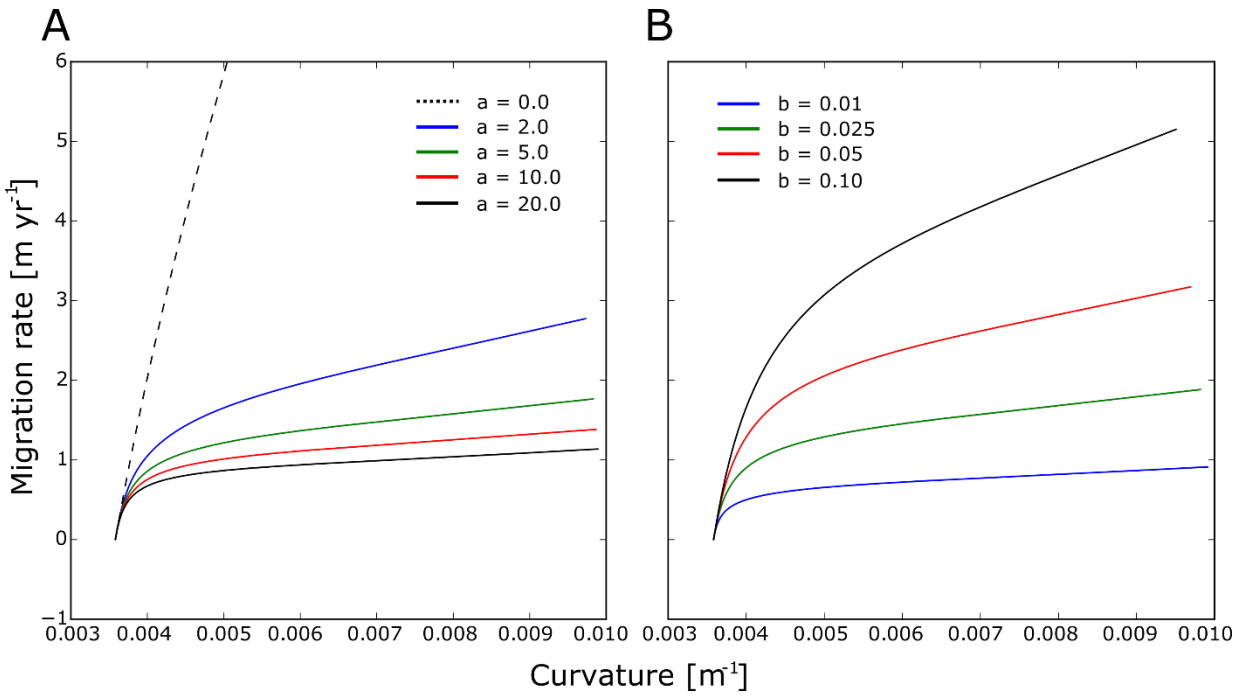

Figure 26: a. Migration of the outer bank relative to planform curvature varying the exponent controlling the initial reduction in slump block erodibility (a = 0.0, 2.0, 5.0, 10.0, and 20.0); b = 0.025, Rd = 3.0. b. Migration of the outer bank relative to planform curvature varying the exponent controlling the decay of root material (b = 0.01, 0.025, 0.05, 0.10); a = 5.0, Rd = 3.0. Both figures a and b implement the HHC formulation assuming $k_0 = 0.2U\tau_{form}^{-0.5}$. In both a and b the green line represents the assumed values taken from literature.

Varying the exponent controlling the magnitude of the initial reduction in erodibility (a in eq. 40) through the rage [5, 20] has relatively limited impact on the relationship between curvature and migration of the outer bank when compared to the significance of varying the exponent in the range [0, 5) (**Figure 26A**). Reducing the exponent below 5.0 raises the proportional increase of migration with curvature, restoring the role of curvature as the dominant control on channel migration. Setting *a* = 0, we recover a linear relationship as migration rates are a function of excess shear stress alone, though the proportional increase with curvature is far higher than EPS as it describes the un-moderated rate of non-cohesive sediment transport. Varying the exponent controlling the decay of rooted material

significantly alters the magnitude of outer bank migration throughout the range [0.01, 0.1], as well as raising the proportionate increase of outer migration with respect to curvature (**Figure 26B**). To observe the effect of varying these two exponents in combination, we can examine the relationship between outer bank migration and curvature for varying root densities at the extreme ends of the ranges defined within **Figure 26**. **Figure 27A** shows migration of the outer bank relative to planform curvature taking exponent values that represent the strongest degree of proportional reduction in slump block erodibility (a = 20.0, b = 0.01), whilst varying root density (Rd = 0.5, 1.5, 3.0, 5.0). The exponent values in **Figure 27B** represent the weakest degree of proportional reduction in slump block erodibility within the range defined in **Figure 26** (a = 2.0, b = 0.1).

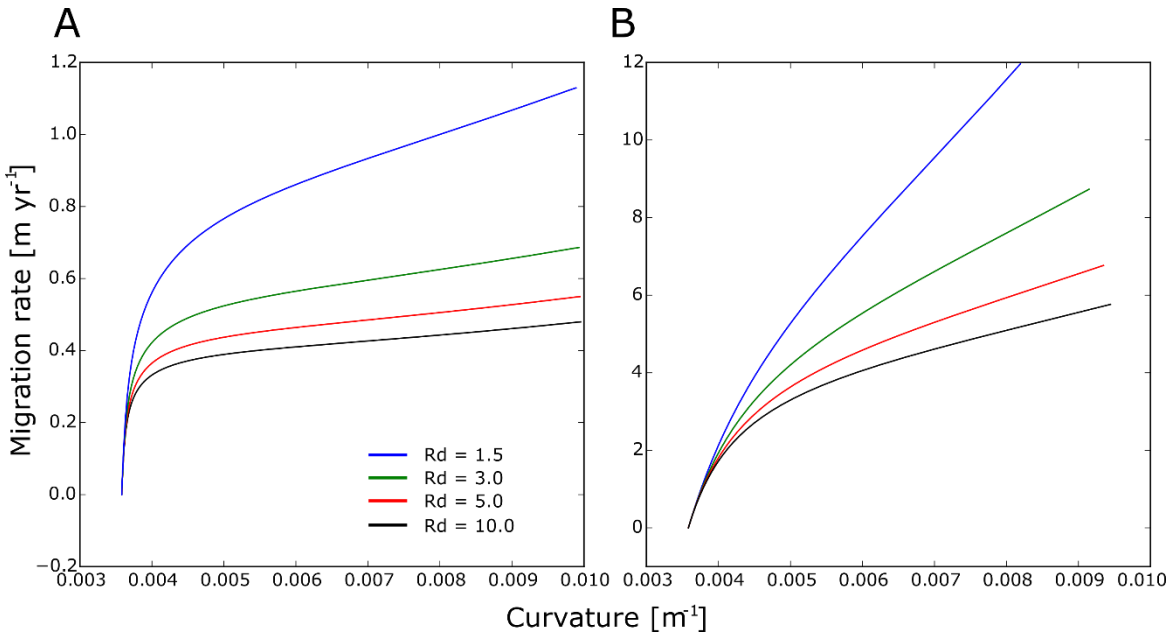

Figure 27: a. Migration of the outer bank relative to planform curvature strongly influenced by the exponents* a *and* b *(*a *= 20.0,* b *= 0.01), varying root density (Rd = [1.5, 3.0, 5.0, and 10.0]). b. Migration of the outer bank relative to planform curvature weakly influenced by the exponents* a *and* b *(*a *= 2.0,* b *= 0.1), varying root density (Rd =[1.5, 3.0, 5.0, and 10.0]). Both figures a and b implement the HHC formulation assuming $k_0 = 0.2U\tau_{form}^{-0.5}$.

Whilst the selection of exponent values is crucial to determining the domain for the relationship between outer bank migration and planform curvature, it is root density that moderates the relative dominance of curvature as a first order control within that domain.

Relating the residency time of slump-blocks to the decay of root matter via an erodibility function reduces the dominance of boundary shear stress in controlling rates of outer bank retreat by introducing a constraint on residency times that is independent of a flow field, i.e. plant mortality. However, channel migration is not determined by outer bank retreat in isolation. It is the combined adjustment of both inner and outer banks as the channel width dynamically adjusts that determines rates of channel migration. **Figure 28** shows rates of channel migration relative to planform curvature under the same parameterization as **Figure 25**, but without fixing the inner bank progression to that of the outer, allowing the channel width to adjust as it extends outward through the floodplain and curvature reduces.

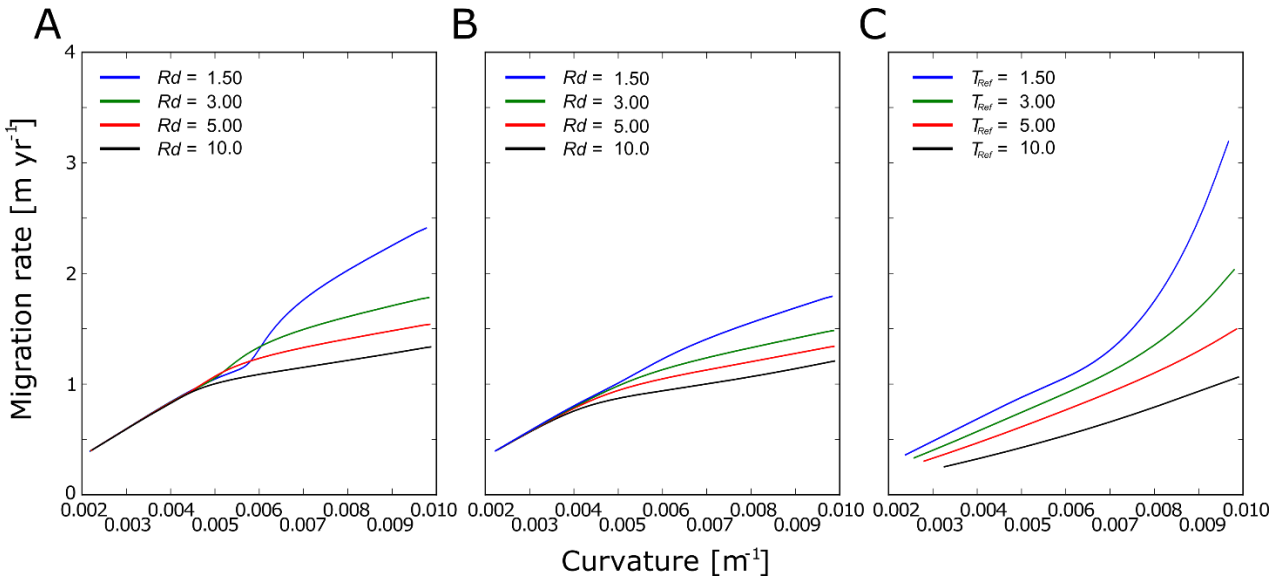

Figure 28: Rates of channel migration relative to planform curvature with dynamically adjusting width across a range of slump block parameters. a. Under slump block formulation HHC assuming $k_0 = k_{d,non}$ for root initial root densities [1.5, 3.0, 5.0, 10.0]. b. Under slump block formulation HHC assuming $k_0 = 0.2U\tau_{form}^{-0.5}$ for root initial root densities [1.5, 3.0, 5.0, 10.0]. c. Under slump block formulation EPS for reference residency times [1.5, 3.0, 5.0, 10.0].

For curvature values above ≈ 0.004 the pattern of channel migration for both formulations of HHC (**Figure 28A** and **B**) closely resemble the corresponding pattern depicted in **Figure 25**, where increasing root density reduces the dominance of planform curvature so that migration rates approach a consistent value with high root densities.

Below curvature values of ≈ 0.004 migration rates are strongly controlled by planform curvature, displaying the same relation irrespective of root density, suggesting that channel migration is controlled by the progression of the inner bank alone. Where the residency time of slump blocks are purely a function of excess shear stress, as in EPS (**Figure 28C**), allowing the width to adjust brings the patterns of migration into closer alignment across the range of T_{ref} parameter values at lower curvature values, and deforms the relation away from linear at higher curvature values as T_{ref} reduces (**Figure 25C**).

In order to understand the full impact of riparian forest removal on rates and patterns of channel migration, we need to examine how river width dynamically alters through time, and assess the relative dominance of either bank push or bar pull across a range of root densities.

5.3.3 Dynamic width adjustment

When applying each formulation of slump-block armouring to the case of the Kinabatangan, maintaining all initial values constant (**Table 13**), and varying only those relating to the regulation of slump-block residency times; both HHC and EPS display the same general pattern of width adjustment. Initially the channel undergoes a period of rapid widening until reaching a maximum, followed by channel narrowing as the inner bank adjusts, then a gradual narrowing towards a stable limit as the channel expands outwards and curvature decreases (**Figure 29**).

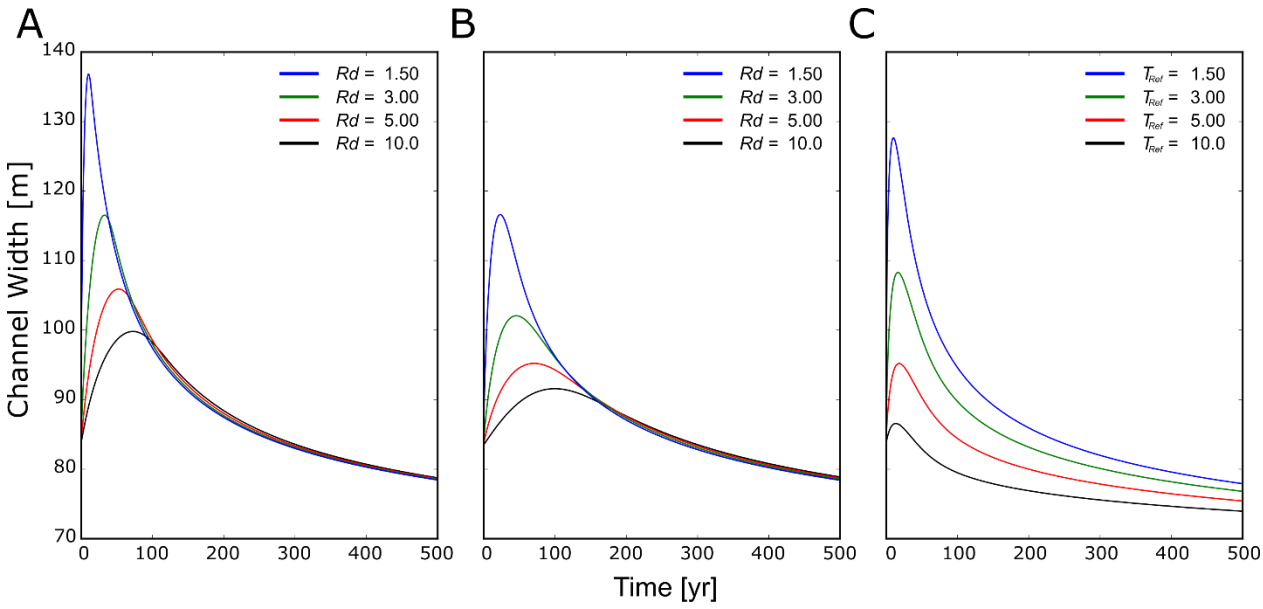

Figure 29: Channel width as it adjusts over time across a range of slump block parameters. a. Under slump block formulation HHC assuming $k_0 = k_{d,non}$ for root initial root densities [1.5, 3.0, 5.0, 10.0]. b. Under slump block formulation HHC assuming $k_0 = 0.2U{\tau_{form}}^{-0.5}$ for root initial root densities [1.5, 3.0, 5.0, 10.0]. c. Under slump block formulation EPS for reference residency times [1.5, 3.0, 5.0, 10.0].

As the formative Shield's number is defined by the bankfull geometry of a straight channel, the introduction of curvature will necessitate a channel adjustment to realign each of the bank Shield's numbers. For both HHC and EPS, reducing the slump-block parameters Rd_0 and T_{ref} increases the magnitude of the initial expansion, as the outer bank migrates at rates far in excess of the inner bank, which has an upper limit imposed by the parameter E_{veg}.

The timing of the maximum is also affected by slump-block properties - increasing T_{ref} in EPS reduces the time taken to reach the maximum width, whereas increasing Rd_0 in HHC has the opposite effect. These responses are governed by the ratio of residency times generated by small values of excess shear stresses to those generated by large $(S{:}\,L)$. Boundary shear stresses acting on the outer bank are greatest upon model initiation, as curvature is high and bankfull width has yet to adjust. In subsequent iterations, channel width increases whilst curvature decreases, reducing the shear stress acting on the outer

bank. For the case where $S{:}\,L$ is very large, even a small reduction in excess shear stress will greatly increase the residency time of slump-blocks, retarding the retreat of the outer bank, and reducing the time till the maximum is reached. We can see from **Figure 24C** that as T_{ref} increases in EPS, so too does $S{:}\,L$, which have the combined effect of reducing the initial rate of expansion, and increasing the proportionate reduction of that expansion after each iteration, resulting in a smaller maximum width achieved sooner. For HHC, however, $S{:}\,L$ is consistently low across the range of root densities (**Figure 24A**, **2B**), as small excess shear stresses correspond to residency times that are comparable to large values, implying rates of outer bank retreat remain relatively consistent whilst $\frac{\tau^*_{tb,E}}{\tau^*_{form}} > 1$ (**Figure 25**). The outer bank, therefore, continues to retreat at a rate approaching the upper limit until channel width is sufficiently large and curvature sufficiently low that $\frac{\tau^*_{tb,E}}{\tau^*_{form}} \approx 1$, at which point the rate of outer bank retreat rapidly drops below that of inner bank migration, and channel narrowing takes place. Increasing Rd_0 in HHC reduces the upper limit of outer bank retreat, and by extension, the rate of channel expansion. As the model then progresses through iterations, and the radius of curvature expands, the channel remains narrow for longer, and so the limit of $\frac{\tau^*_{tb,E}}{\tau^*_{form}} \approx 1$ is reached later in the simulation (**Figure 30**).

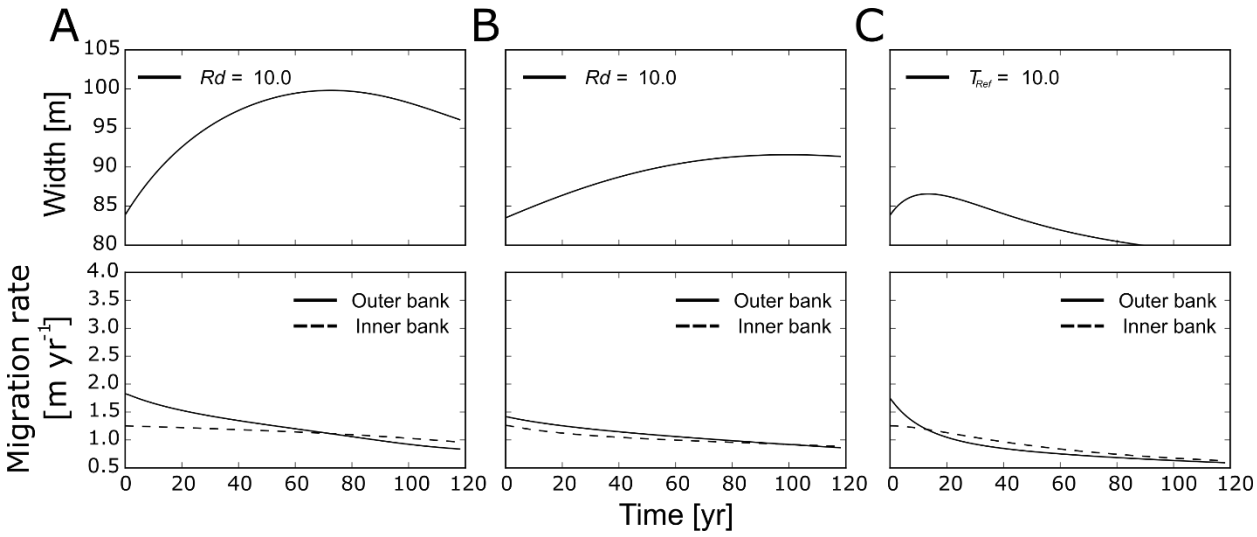

Figure 30: Upper panel – Channel width as it adjusts over the initial 120 years. Lower panel – Migration of outer (solid line) and inner (dotted line) banks for initial 120 years. a. Under slump block formulation HHC assuming $k_0 = k_{d,non}$ for $Rd_0 = 10.0$. b. Under slump block formulation HHC assuming $k_0 = 0.2U\tau_{form}^{-0.5}$ for $Rd_0 = 10.0$. c. Under slump block formulation EPS for $T_{ref} = 10.0$.

Figure 31A shows channel width as it adjusts over time with constant initial parameters (**Table 13**, $Rd_0 = 2.5, T_{ref} = 3.0$), and initial channel curvature values that double from 0.003 to 0.024.

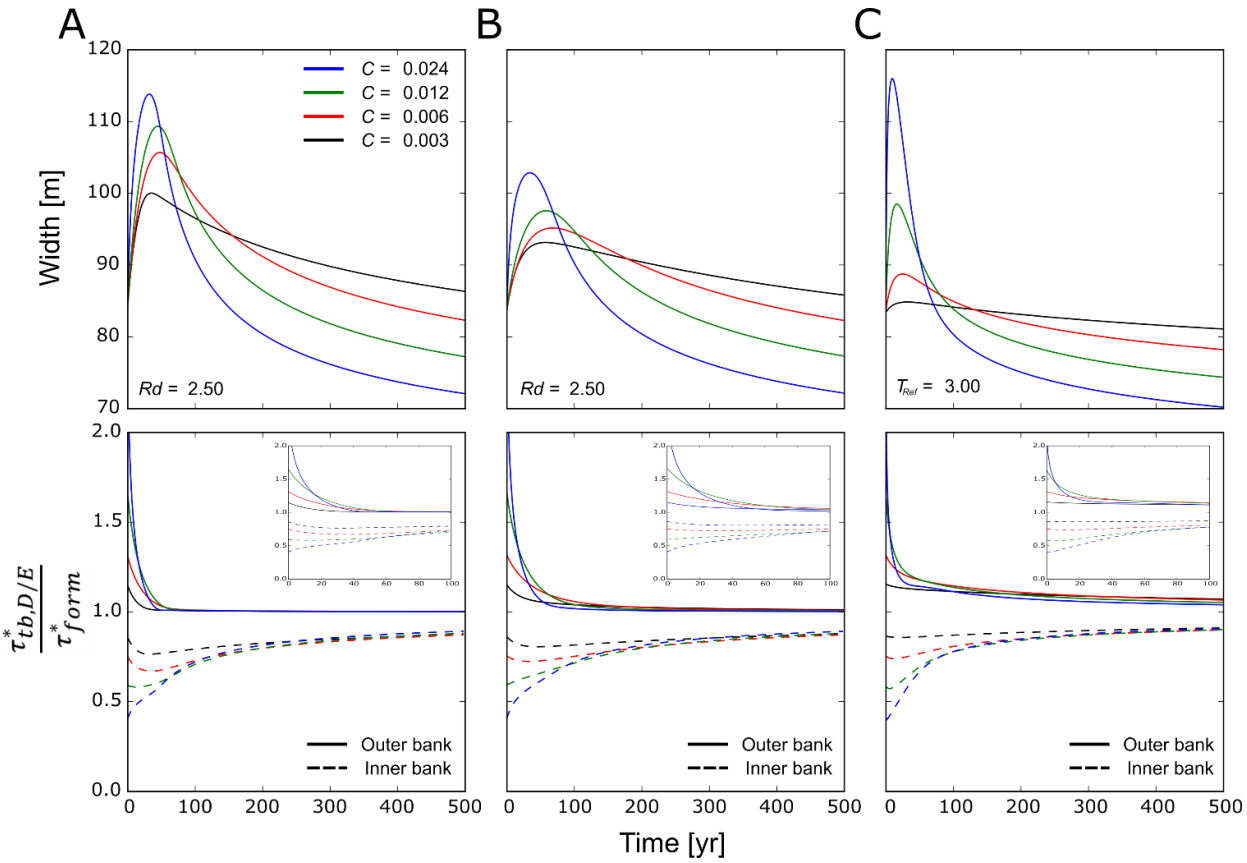

Figure 31: Upper panel – Channel width as it adjusts over time varying initial curvature. Lower panel – proportion of bank shear stress to formative shear stress for outer (solid line) and inner (dotted line) banks. Close up panel in top right shows initial 100 years. a. Under slump block formulation HHC assuming $k_0 = k_{d,non}$ for $Rd_0 = 2.5$. b. Under slump block formulation HHC assuming $k_0 = 0.2U{\tau_{form}}^{-0.5}$ for $Rd_0 = 2.5$. c. Under slump block formulation EPS for $T_{ref} = 3.0$.

Changing initial channel curvature modulates the magnitude of the initial expansion, and alters the asymptote of the lower limit. This latter effect is a consequence of there being multiple states of equilibrium, and each asymptotic width is approached with its balanced curvature so that $\frac{\tau^*_{tb,D}}{\tau^*_{form}}, \frac{\tau^*_{tb,E}}{\tau^*_{form}} \rightarrow 1$ (**Figure 31B**).

5.3.4 Bank pull, bar push

Although patterns of channel widening differ markedly between model formulations, the driving motivations behind their production are the same, and can be characterized into two phases; one of bank pull and one of bar push. Within the HHC formulation of slump block armouring there is a clear distinction between these two phases evident in the relation

between channel migration and planform curvature (**Figure 28A** and **B**). Bar push relates to the phase below curvature values of ≈ 0.004, and bank pull corresponds to the phase above, where patterns of migration differ with root density. That this phase distinction is clearly evident in HHC, but not in EPS suggests that the balance between these two controls on channel migration can be altered by the nature of failed bank material residing along the bank toe.

For both formulations of slump block armaring, the model framework is constructed in such a way that the system is self-organizing, and tends towards a state of equilibrium, which is defined as the channel morphology that replicates the formative Shield's number along both banks. As the formative Shield's number is defined by a straight channel, any system that includes a modicum of planform curvature will, by definition, be in disequilibrium. Upon model initiation both outer and inner bank Shield's numbers are deviated from the formative (**Figure 31B**), and so the system adjusts. A reduction in planform curvature aligns both inner and outer banks with the formative, and so for simulations that have high initial migration rates (large initial reductions in planform curvature), the Shield's numbers along both banks tend towards the formative. However, for simulations that have lower rates of initial migration, bank alignment is a consequence of width adjustment; channel widening aligns the outer bank Shield's number towards the formative, whilst narrowing aligns the inner. Each model simulation thus far has undergone an initial period of channel expansion, which is a preferential alignment of the outer bank. This initial phase of bank pull quickly reduces the outer bank Shield's number towards the formative, bringing it close to the point of equilibrium. Once this initial phase of outer bank alignment is complete, the inner bank slowly narrows towards its state of equilibrium as the continual reduction in curvature allows.

The apparent dominance of the outer bank in modulating channel geometry may be a consequence of the initial width being equal to that used for the calculation of the formative Shield's number along a straight channel. To examine whether bar push becomes the dominant control under different initial conditions, I hold all channel geometry and slump-block armouring parameters constant and vary the initial channel width taking values of $\frac{2}{3}B$, B, $2B$, and $3B$, where B is the width of a straight channel at bankfull conditions (**Figure 32**).

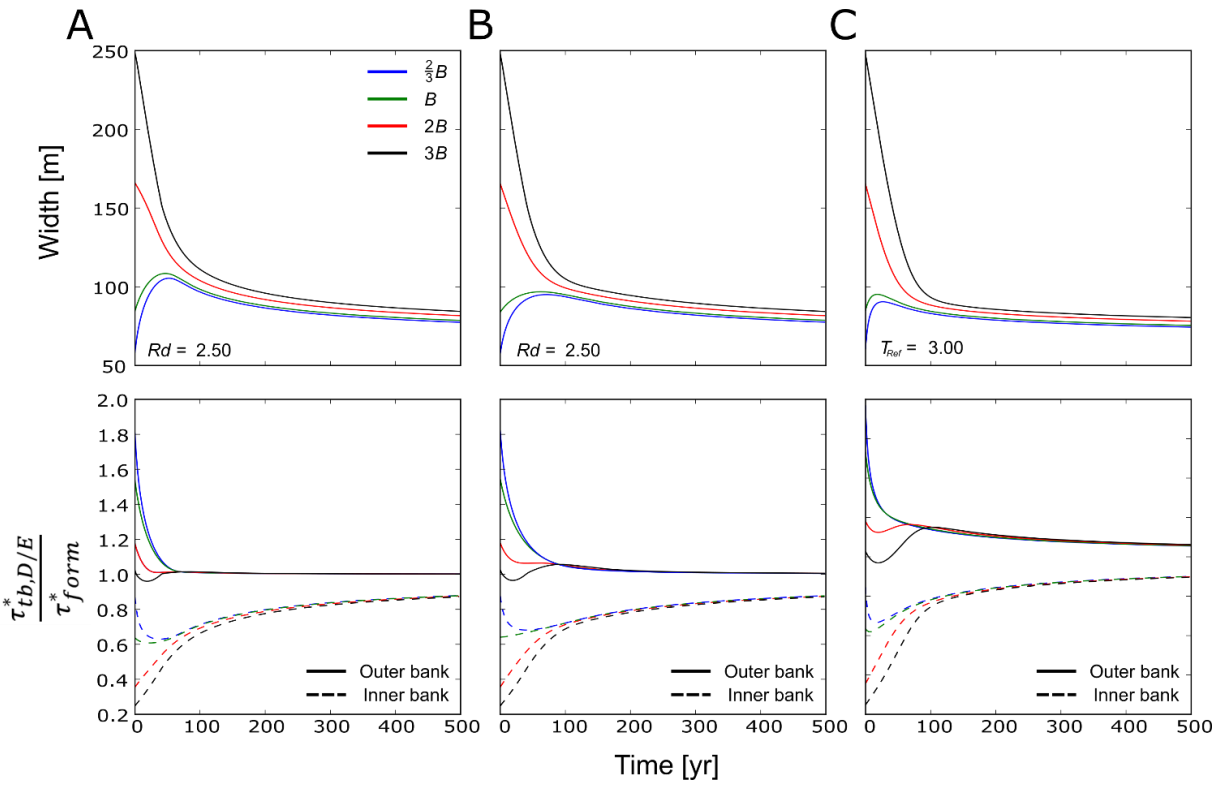

Figure 32: Upper panel – Channel width as it adjusts over time across a range of initial widths. Lower panel – proportion of bank shear stress to formative shear stress for outer (solid line) and inner (dotted line) banks. a. Under slump block formulation HHC assuming $k_0 = k_{d,non}$ for $Rd_0 = 2.5$. b. Under slump block formulation HHC assuming $k_0 = 0.2U\tau_{form}{}^{-0.5}$ for $Rd_0 = 2.5$. c. Under slump block formulation EPS for $T_{ref} = 3.0$.

The dominance of the outer bank in controlling channel width is more apparent for HHC – only when the initial width is extended to three times that of a straight channel does the outer bank Shield's number tend away from the formative to accommodate an adjustment of the inner bank. The phase shift between bank pull and bar push is less distinct

in EPS – irrespective of the initial channel width, the adjustment of the outer bank Shield's number towards the formative is more gradual than for HHC, and more closely resembles that of the inner bank. Where initial channel width is $3B$, the outer bank migrates towards the channel centre to facilitate narrowing, before increasing away from the formative as the inner bank dominates and continues to narrow the channel until inner and outer bank Shield's numbers balance.

Outer and inner bank migration rates corresponding to the pattern of bank stresses described in **Figure 32B** for overly wide initial channels illustrate the bi-modal construct of HHC in contrast to EPS, as rates of outer bank migration rapidly reduce to zero, and then sharply return toward a consistent limit, as the bank Shield's number crosses the threshold of the formative (**Figure 33**).

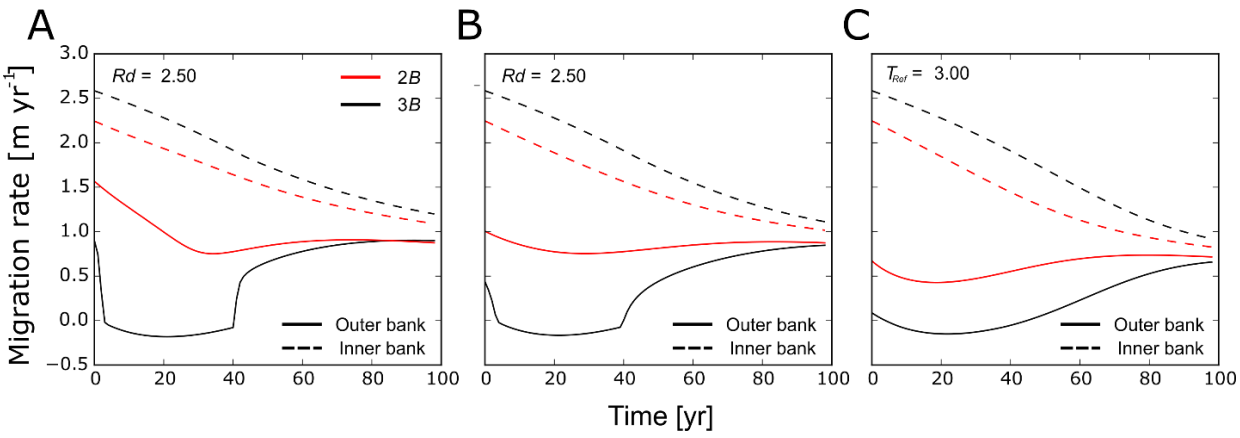

Figure 33: Migration rate as it changes through time for outer (solid line) and inner (dotted line) banks for initial widths of 2B (red line) and 3B (black line). a. Under slump block formulation HHC assuming $k_0 = k_{d,non}$ for $Rd_0 = 2.5$. b. Under slump block formulation HHC assuming $k_0 = 0.2U\tau_{form}^{-0.5}$ for $Rd_0 = 2.5$. c. Under slump block formulation EPS for $T_{ref} = 3.0$.

5.3.5 Migration rates

Upon model initiation, planform curvature is at its highest value, resulting in large deviations from the formative Shield's number along both banks, which consistently induces an initial centerline adjustment amounting to the highest rate of channel migration for all parameter sets (**Figure 34**). As the channel expands outwards, curvature decreases and the

channel widths adjust, reducing the deviation from the formative Shield's number along both banks, and thus rates of centerline migration.

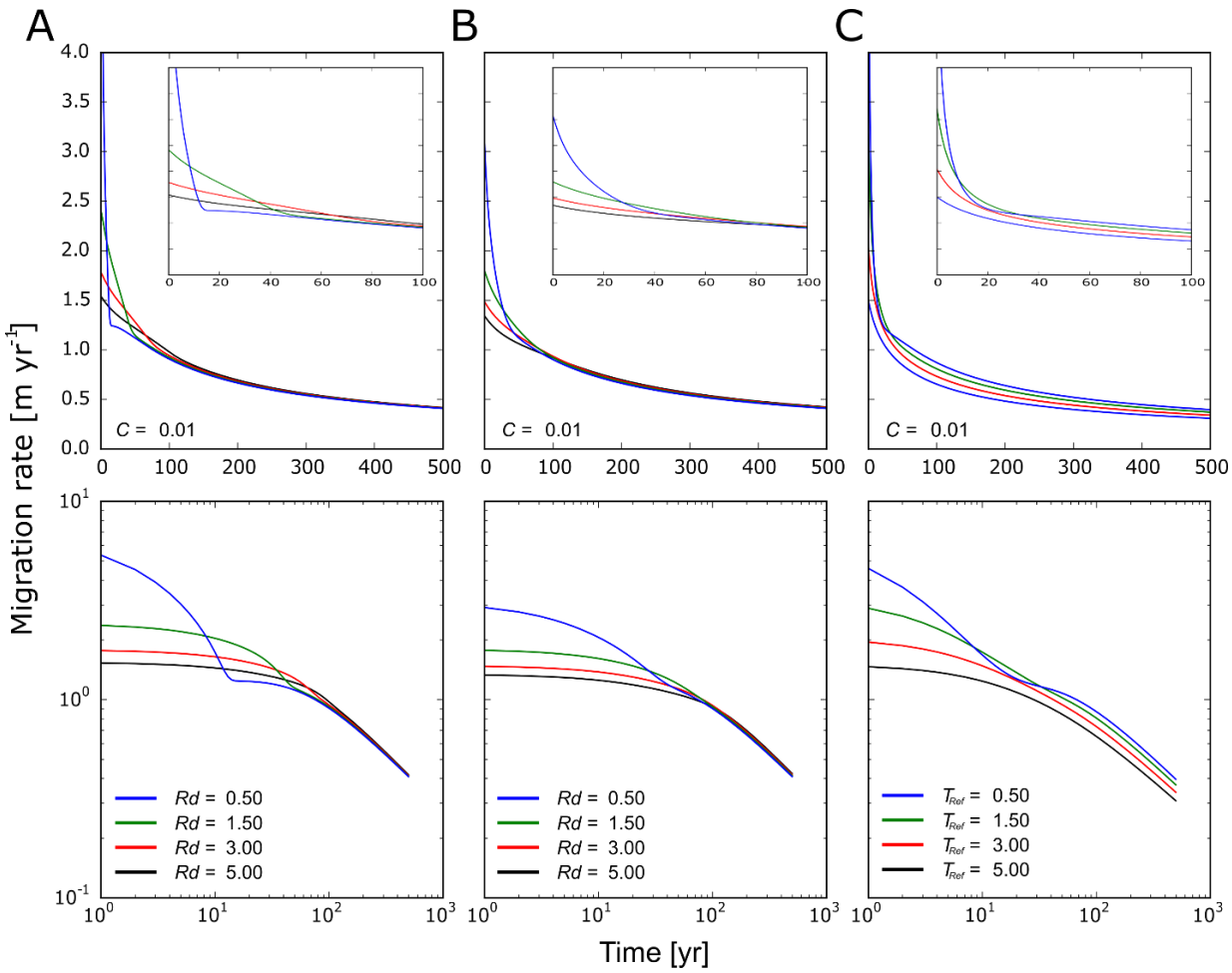

Figure 34: Upper panel - Channel migration rates through time across a range of initial root densities. Zoomed section showing initial 100 years. Lower panel – log-log relationship of channel migration over time. a. Under slump block formulation HHC assuming $k_0 = k_{d,non}$ for root initial root densities [0.5, 1.5, 3.0, 5.0]. b. Under slump block formulation HHC assuming $k_0 = 0.2U\tau_{form}^{-0.5}$ for root initial root densities [0.5, 1.5, 3.0, 5.0]. c. Under slump block formulation EPS for reference residency times [0.5, 1.5, 3.0, 5.0].

Varying slump-block properties within both HHC and EPS alters the magnitude of the initial migration, as well as the pattern of its subsequent reduction.

Adjusting the parameter E_{veg} to allow the inner bank to keep pace with a retreating outer bank prevents over widening, and maintains a more consistent width as the channel migrates rapidly outwards (**Figure 35**).

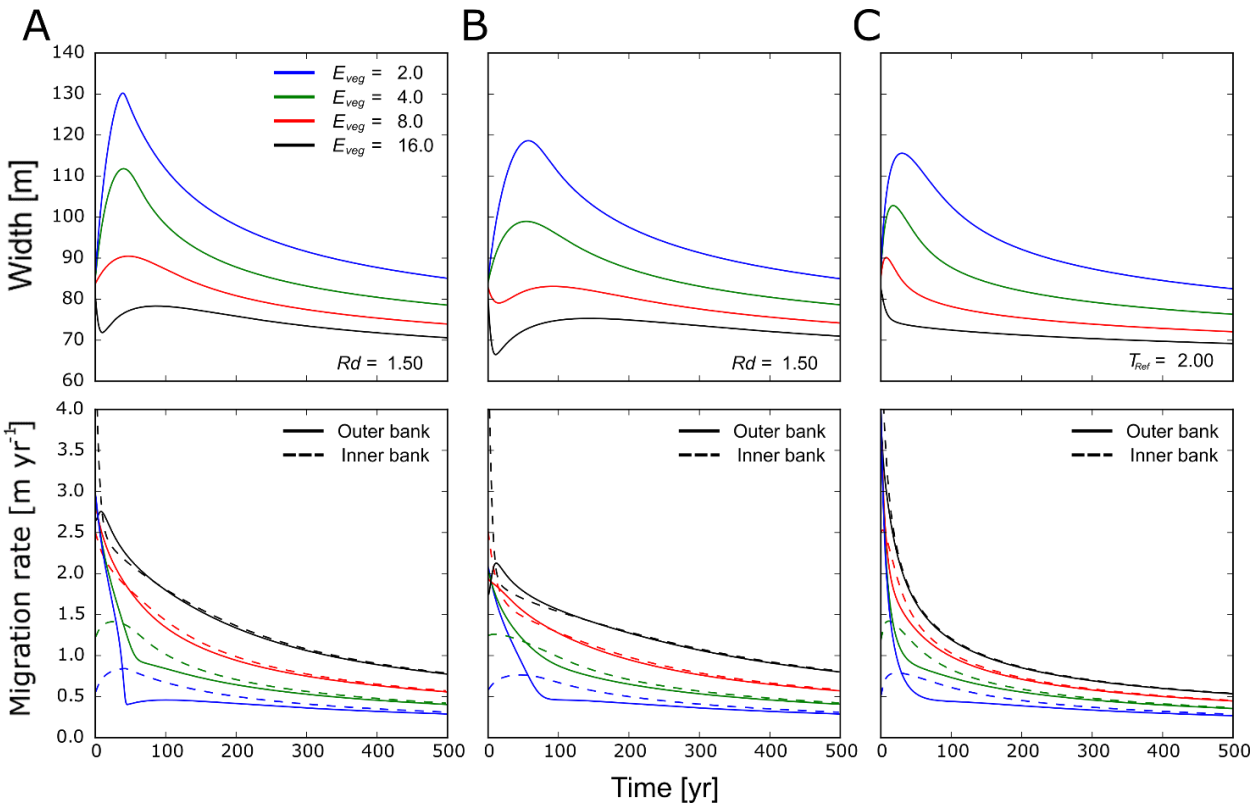

Figure 35: Upper panel – Channel width as it adjusts over time across a range of vegetation encroachment rates (E_{veg}). Lower panel – Migration of outer (solid line) and inner (dotted line) banks with varying E_{veg}. a. Under slump block formulation HHC assuming $k_0 = k_{d,non}$ for $Rd_0 = 1.5$. b. Under slump block formulation HHC assuming $k_0 = 0.2U{\tau_{form}}^{-0.5}$ for $Rd_0 = 1.5$. c. Under slump block formulation EPS for $T_{ref} = 2.0$.

As the parameters controlling slump-block residency times and vegetation encroachment rates approach a balance, so that inner bank progression matches that of the outer bank, channel width is preserved and rates of channel migration reduce to a function of $\frac{\tau^*_{tb,E}}{\tau^*_{form}}$; recovering patterns of channel migration that closely resemble those described in **Figure 25** (**Figure 36**).

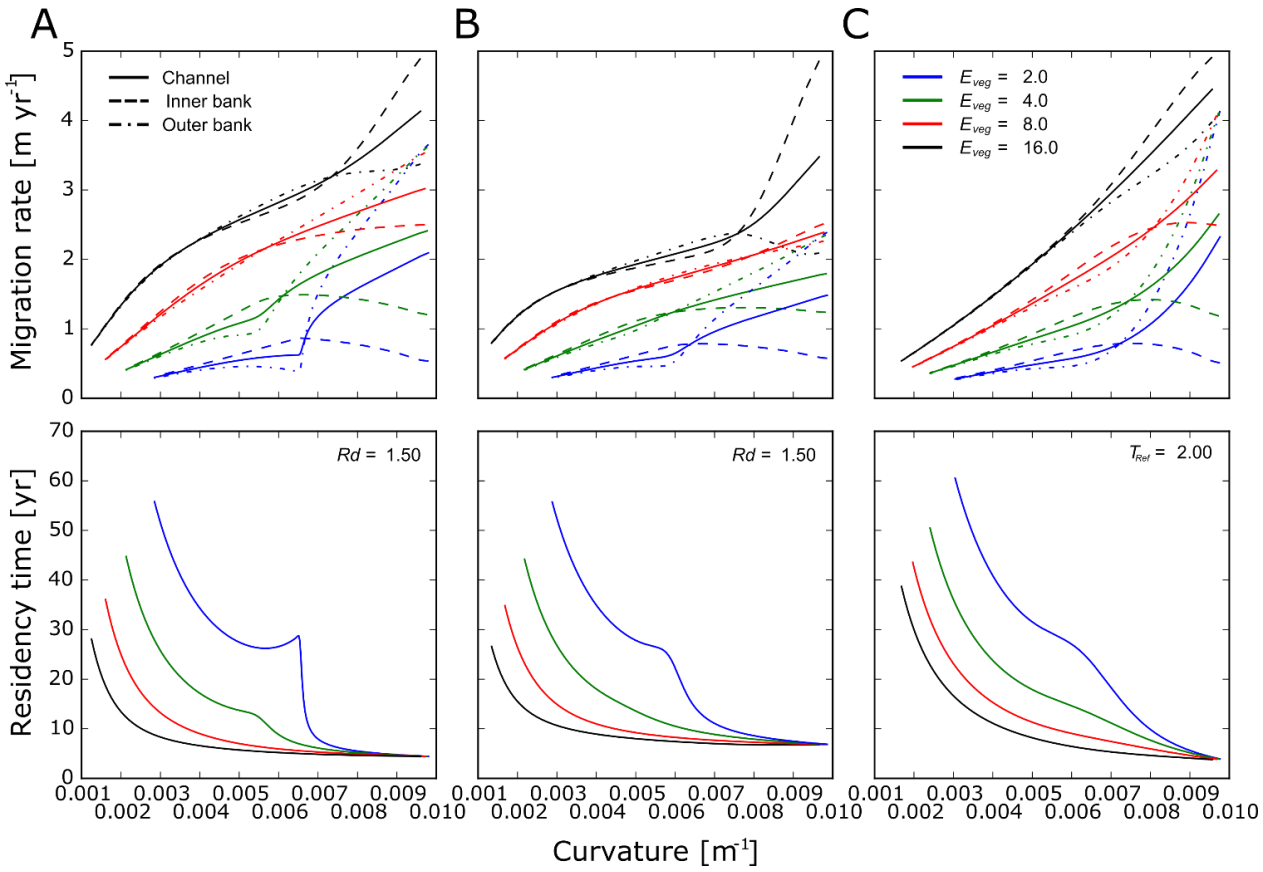

Figure 36: Upper panel – Channel centreline migration (solid line), outer bank migration (dash dot dash line), and inner bank migration (dotted line) as curvature varies across a range of vegetation encroachment rates (E_{veg}). Lower panel – Slump block residency time as curvature varies across a range of vegetation encroachment rates. a. Under slump block formulation HHC assuming $k_0 = k_{d,non}$ for $Rd_0 = 1.5$. b. Under slump block formulation HHC assuming $k_0 = 0.2U\tau_{form}^{-0.5}$ for $Rd_0 = 1.5$. c. Under slump block formulation EPS for $T_{ref} = 2.0$.

For both EPS and HHC, the rate of vegetation encroachment determines the pattern of channel width alteration, which in turn controls the deviation from the relation of channel migration to planform curvature described by the retreat of the outer bank in isolation (**Figure 25**). The impact of riparian vegetation removal from the outer riverbank on patterns of channel migration are therefore dependent upon the relative dominance of either bar push or bank pull, which is strongly controlled by the vegetation along the inner bank. Where deforestation occurs along outer and inner banks simultaneously, alterations to both the dynamics of slump block armouring and rates of sediment deposition may produce relations of channel migration to planform curvature that are strongly non-linear.

5.3.6 Slump block dimensions

Lastly, we need examine the effect of slump-block size on the relationship between rates of channel migration and planform curvature. To this end I vary the characteristic width of slump-blocks ($D_c = 0.25, 0.5, 1.0, 2.0$) (**Figure 37**), and the height of the cohesive layer ($H_c = 0.5, 1.0, 2.0, 4.0$) (**Figure 38**), whilst maintaining consistent initial channel geometry and curvature (**Table 13**, C = 0.01), and slump-block parameter values ($Rd_0 = 2.5, T_{ref} = 3.0$).

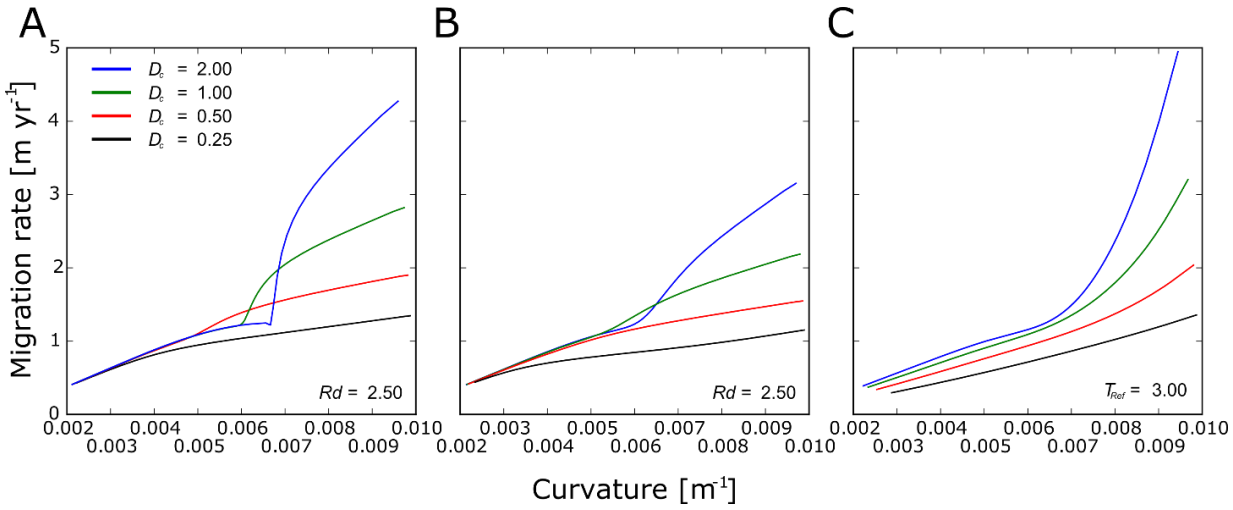

Figure 37: Rates of channel migration relative to planform curvature across a range of characteristic slump block widths. a. Under slump block formulation HHC assuming $k_0 = k_{d,non}$ for $Rd_0 = 2.5$. b. Under slump block formulation HHC assuming $k_0 = 0.2U{\tau_{form}}^{-0.5}$ for $Rd_0 = 2.5$. c. Under slump block formulation EPS for $T_{ref} = 3.0$.

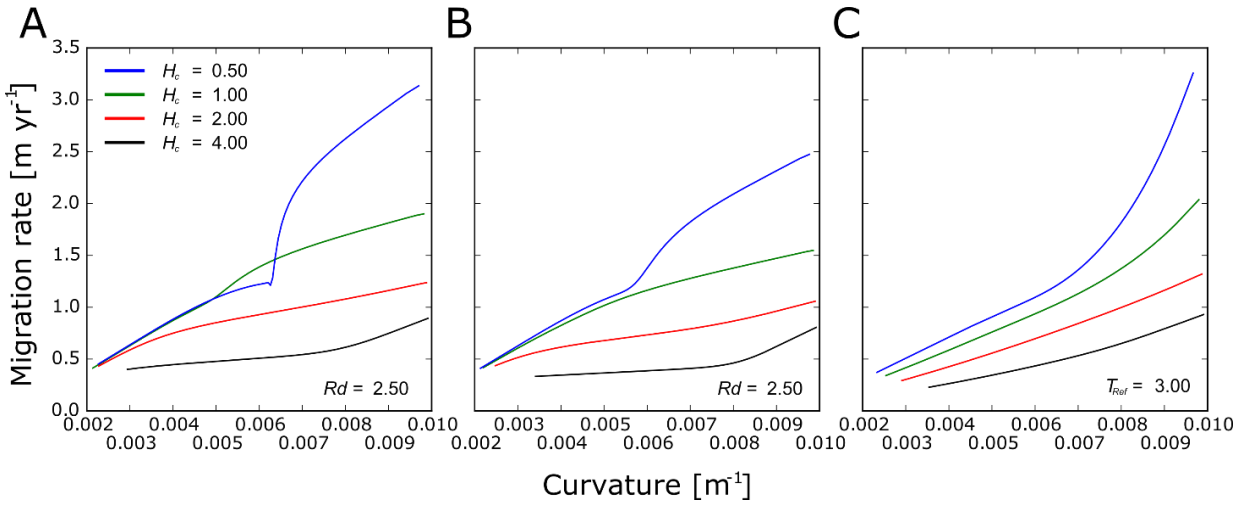

Figure 38: Rates of channel migration relative to planform curvature across a range of slump block heights. a. Under slump block formulation HHC assuming $k_0 = k_{d,non}$ for $Rd_0 = 2.5$. b. Under slump block formulation HHC assuming $k_0 = 0.2U{\tau_{form}}^{-0.5}$ for $Rd_0 = 2.5$. c. Under slump block formulation EPS for $T_{ref} = 3.0$.

For EPS, the consequences of altering Dc and Hc are predictable, as Eq. 34b describes how each variable relates to bank erosion by sediment transport. The ratio Hc:Dc equates to the length of non-cohesive bank face protected by each slump-block. Altering either variable to increase this ratio strengthens the effectiveness of slump-block armouring, and reduces rates of channel migration. For HHC, in addition to allocating bank protection, Dc also defines the integral relating slump block erosion rates to residency times (Eq. 42). Increasing Dc in Eq. 42 will extend the limits of integration necessary to satisfy the solution, and so increase Tc, which reduces rates of outer bank migration. Though this counteracts the reduction of Hc:Dc, the overall effect of altering Dc remains the same for both HHC and EPS (**Figure 37**).

5.3.7 Comparison with field data

Selecting parameter values that best describe slump-block characteristics along both forested and cleared sections of the Kinabatangan, I attempt to replicate observed rates of meander migration using both HHC and EPS.

Rather than calibrate each model, I have chosen values that are representative of the vegetation present along the banks of both forested and cleared sections of river, either from direct observation, literature, or appropriate values from the range defined in the analysis of the previous section. The previous analysis suggests that defining the Kd_0 parameter within HHC based on the critical shear stress of slump-blocks is a more stable formulation, and this method is adopted for the subsequent comparison. Parameter values used to define each vegetation type are listed in **Table 14**.

Table 14: Parameter values used to define forested and cleared vegetation types

Parameter					Origin
	Forested	Cleared	Forested	Cleared	
Initial Curvature	0.012	0.012	0.012	0.012	Appropriate from analysis
Rd_0	5.0	1.5			[Klinge and Herrera, 1978; Jackson et al., 1996]
T_{ref}			5.5	2.0	Approximated from the equivalent Rd values
E_{veg}	4	5	4	5	%5 of bankfull width. Reduced vegetation colonisation in forest [*Allmendinger et al.*, 2005b].
Exponent a in eq (19)	0.023	0.023			[*O'Loughlin and Watson*, 1979]
Exponent b in eq (20)	5.7	5.7			[*Flanagan and Nearing*, 1995]
Exponent n in eq (17)	1	1			
D_c	1	0.5	1	0.5	Represent field observations
H_c	1.5	1.0	1.5	1.0	Approximate rooting depth

Figure 39 shows the model outputs run for both forested (Blue) and cleared vegetation (Red) parameter sets (**Table 14**) against measured values for comparison [*Horton et al.,* 2017].

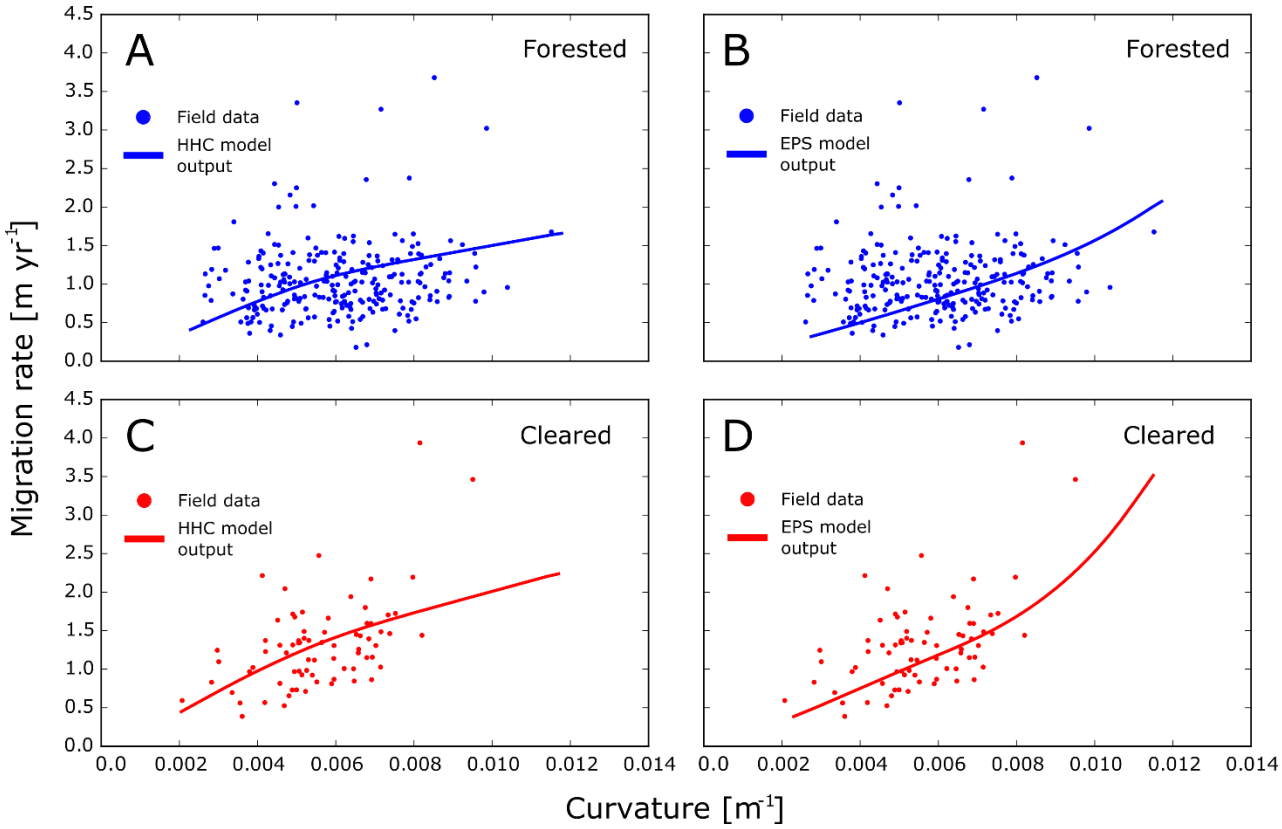

Figure 39: Comparison between observed ratres ofchannel migration relating to planform curvature along the Kinabatangan River (points) and model outputs (line) for forested sections of river (blue) and cleared sections of river (red): a. Under slump block formulation HHC for forested parameter set as described in Table 14. b. Under slump block formulation HHC for cleared parameter set as described in Table 14. c. Under slump block formulation EPS for forested parameter set. Under slump block formulation EPS for cleared parameter set.

Along forested sections of the Kinabatangan, the relationship between migration and curvature is ill defined - rates of riverbank migration appear to be largely independent of curvature. This is not likely to be the case where curvature is small, as the formation and development of meander patterns requires that migration ceases as curvature approaches zero. We can, therefore, expect that observations of channel migration along meanders with curvature values below 0.002, which are absent from this data set, would tend towards zero. The general pattern of migration relating to curvature for forested reaches can then be described as a rapid increase in riverbank migration reaching ~ 1.0 m a^{-1} where C = 0.002, which then remains consistent as curvature increases. Although HHC doesn't faithfully recreate the observed pattern, it does replicate some of the salient features. There is a rapid

increase in rates of meander migration at lower curvature values, levelling off to a more consistent rate of migration at around 1.0 – 1.5 m a^{-1}. Although I haven't implemented a model calibration as part of this investigation, patterns of meander migration for HHC depicted in **Figure 39** indicate that reproducing the observed pattern for forested sections of the Kinabatangan would require relatively few parameter adjustments. By way of an example, **Figure 40** shows model outputs of meander migration for HHC with the same parameter set as **Figure 39**, but with initial root density increased to 10 kg m^{-2}, which better represents the observed data.

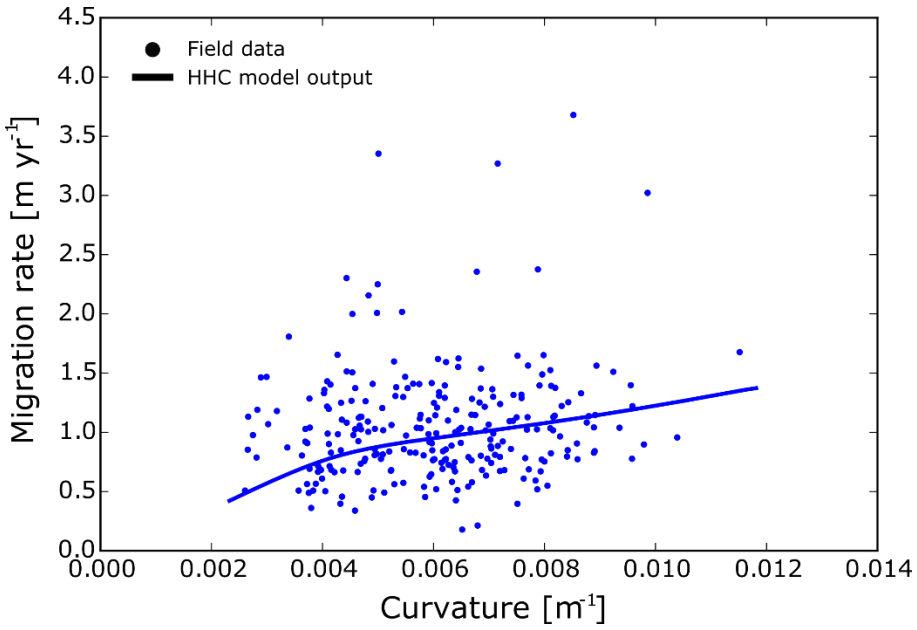

Figure 40: Comparison between observed ratres ofchannel migration relating to planform curvature along forested sections of the Kinabatangan River (points) and model outputs under slump block formulation HHC for forested parameter set as described in Table 14 with initial root density altered to 10 kg m^{-2} (line).

The pattern of meander migration produced by EPS depicts a consistently gradual increase in rates of channel migration with curvature until C = 0.01, at which point the rate of increase increases as curvature extends beyond the range of observations.

The relation between curvature and migration rates along cleared sections of the Kinabatangan are better defined (**Figure 40C** and **D**), displaying a linear increase with curvature for the range of observations up to ~0.007. For this range of curvatures, both

formulations do a good job of reproducing the expected migration rates. As curvature values exceed 0.007 the two models diverge, with HHC predicting a decline in the rate of migration increase, whereas EPS displays an acceleration. Without extending the range of observations, it is difficult to say which of the two is the more faithful representation.

5.4 Discussion

Our initial hypothesis stated that altering the composition of failed riverbank material delivered to the bank toe by mass wasting has the potential to affect rates of channel migration, and alter the dominant control on riverbank retreat. Furthermore, the influence of root decomposition on the residency time of failed material introduces a constraint that alters the relationship between planform curvature and channel migration. To test these hypotheses I adapted an existing formulation of channel migration that represents slump block armament [*Parker et al.,* 2011] to account for the presence of a root network within failed riverbank material, and compared model outputs across a range of root densities.

These results suggest that adding densely rooted material to failed slump blocks can profoundly alter the relationship between slump block residency times and the boundary shear stress along the outer bank. This in turn reduces the dominance of planform curvature in controlling rates of riverbank retreat along the outer bank. Reducing the root density within slump blocks had the effect of restoring the relative control of planform curvature on rates of outer bank retreat. When accounting for the progression of both outer and inner banks as the river channel dynamically adjusts, the influence of dense root networks within failed slump blocks on channel migration is apparent only at higher values of planform curvature. After an initial period of high migration rates propagated by the large boundary shear stresses that accompany higher planform curvatures, rates of channel migration

converge across the range of root densities as the inner bank dominates and the channel gradually narrows. This convergence of channel migration rates irrespective of slump block characteristics was not evident in the EPS formulation, suggesting that the composition of failed bank material along the outer bank can influence the balance between bank pull and bar push. The relative dominance of the inner bank in controlling rates of channel migration is determined by the rate of sediment deposition, which in this model framework is controlled by the type of vegetation. Therefore, deforestation along the inner bank may also contribute to the non-linearity observed in patterns of migration relating to planform curvature. The results from both HHC and EPS support my initial hypothesis that the composition of failed riverbank material can alter rates of channel migration, and that introducing a constraint on residency times that is independent of the flow field can reduce the relative dominance of planform curvature as a first order control.

Applying HHC and EPS model formulations to the case of the Kinabatangan River in Northern Borneo, I attempted to emulate the observed differences between sections of the river that are forested compared to sections of the river cleared of forest by altering slump block properties alone. Both formulations simulated rates of channel migration that were comparable to those observed between vegetation types, though HHC was better able to replicate the diminished dominance of planform curvature along forested sections. These results support the assertion that the observed increase in rates of channel migration along the Kinabatangan following forest removal are due to the changing nature of failed material delivered to the channel margins by mass wasting. That HHC is able to replicate the non-linearity between channel migration and planform curvature where EPS could not suggests that the presence of riparian forest alters the mechanisms that control the removal of failed material, introducing a constraint that is independent of the flow field around a meander

bend. Within HHC that constraint is plant mortality, though there may be other ways in which riparian forest might change the properties of failed bank material to alter the relation of its removal to planform curvature.

In addition to affecting the erodibility of slump-blocks, vegetation might moderate riverbank retreat along large rivers in ways that are not currently represented within the model framework. The presence of large woody debris has the potential to profoundly alter the three-dimensional flow structure around a meander bend, re-directing the high-velocity core away from the outer bank, and disrupting the helical secondary flow that is crucial for the transverse transportation of sediment [*Konsoer et al.*, 2016b]. Clearing riparian forest removes the source of large woody debris, and with it the associated form drag that would otherwise alter the near-bank flow field [*Kean and Smith*, 2006]. By altering the size and shape of failed slump-blocks, vegetation may again be of central importance, as the presence of a riparian root network has been shown to alter the geotechnical properties of riverbanks both mechanically and hydrologically [*Simon et al.*, 2000; *Simon and Collison*, 2001; *Darby et al.*, 2007; *Pollen-Bankhead and Simon*, 2010]. Contrary to my initial hypothesis, smaller more frequent mass wasting events resulting from forest removal would, under the assumptions of the modelling framework set out here, reduce mender migration by affording more bank protection per unit volume of failed material. However, the model does not account for alterations to the flow field due to the size of slump blocks which can significantly alter the structure of a near bank flow field [*Hackney et al.*, 2015], and assumes that all failed material remains in the channel margin to be gradually removed piecemeal by fluvial scour. Where failure events result in volumes of material small enough to be removed by the flow field intact, the protection afforded by a cohesive layer is circumvented, and channel migration would take place at rates controlled by to the removal

of non-cohesive sediment alone. This holds true at the larger scale, as the model framework presupposes that slump-block residency times are controlled by the rate of disaggregation by fluvial scour. In river systems with peak discharges large enough to remove vegetated slump-blocks, residency times have an upper limit of the return period corresponding to the discharge intensity required for slump-block removal. Although dense vegetation may increase the size of slump-blocks, thereby prolonging the armament of a non-cohesive bank face, rivers of a size that can transport failed material without the need for disaggregation render plant mortality irrelevant. As slump-block size does not scale relative to river discharge, explicitly representing the effect of vegetation as a control on residency times by altering the erodibility of slump blocks may not be valid for rivers much larger than the Kinabatangan.

5.5 Conclusion

In adapting an existing model of meander migration to include an explicit representation of riparian vegetation, I have demonstrated that floodplain forest can play a first order role in controlling rates and patterns of channel migration by altering the composition of failed material alone. Introducing a constraint on the residency time of slump-blocks that is independent of the flow field around a meander bend has the potential to reduce the relative dominance of planform curvature in controlling rates of channel migration. By consolidating failed material armouring the outer bank, a dense root network may affect the long term rates and patterns of meander migration along large rivers, even where bank heights exceed rooting depth.

Chapter 6:

Discussion and Conclusions

6.1 Key Findings

The first major finding from this investigation is that the removal of riparian vegetation accelerates rates of riverbank retreat despite bank heights being far in excess of root penetration. The distribution of observed migration rates along cleared sections of the Kinabatangan River has an average value more than 23% higher than along sections that retained forest cover (**Figure 8**).

The second is that the presence of riparian vegetation has the potential to alter the relationship between riverbank retreat and curvature driven forcing of river flows around a meander bend. I found that the correlation between planform curvature and rates of riverbank retreat only became strongly positive and significant after the removal of natural riparian cover (**Figure 10**).

The third major finding is that a dense root network within failed riverbank material can introduce a constraint on riverbank retreat that is independent of the flow field around a meander bend, and so reduce the dominance of planform curvature in controlling rates of meander migration.

The last major finding is that retaining riparian forest along tropical river boundaries can enhance the profitability of floodplain plantations by reducing the area of land lost to the river as it migrates, with the potential to increase returns within one plantation cycle.

6.2 Overview and Significance

The main aim of this research was to examine the role that tropical floodplain forest plays in controlling rates of channel migration along a large river. The results presented in chapters 3 and 5 broaden discourse on the spatial scaling of riparian vegetation as a control on channel migration. By way of mechanically strengthening riverbanks [*Abernethy and Rutherfurd*,

2000; *Pollen and Simon*, 2005], altering soil moisture content [*Simon and Collison*, 2001, 2002], disrupting near-bank flow fields [*Daniels and Rhoads*, 2003], and increasing channel roughness [*Konsoer et al.*, 2016b], vegetation has long been understood to influence riverbank retreat. However, as the scale of fluvial systems increase, the relative importance of these influences is assumed to diminish [*Lawler*, 1992; *Abernethy and Rutherfurd*, 1998; *Constantine et al.*, 2009; *Pizzuto et al.*, 2010]. In quantifying the geomorphic response of the Kinabatangan River to the removal of its floodplain forest, I have demonstrated that riparian vegetation continues to exert a significant influence within larger fluvial systems. Utilising Landsat satellite imagery spanning 1989–2014, I measured rates of channel migration and documented instances of deforestation through four meandering reaches of the lower Kinabatangan River. Average rates of channel migration are more than 23% higher through cleared sections of river than through forested sections (**Figure 8**), displaying a temporal structure to the proportional increase that implicates forest removal as the direct cause (**Figure 9**). This adds to an increasing body of work that highlights the importance of floodplain forest at larger spatial scales [*Latrubesse et al.*, 2009; *Schwendel et al.*, 2015; *Konsoer et al.*, 2016a].

What is presently lacking from this existing body of work is a clear demonstration of the mechanistic processes by which riparian vegetation affects riverbank retreat when bank heights far exceed rooting depths. In an attempt to identify a shift in the mechanistic driver of riverbank retreat following deforestation, I examined the relationship between average rates of channel migration and the velocity perturbations along the eroding bank face for forested sections of river and compared them to cleared sections. The results show that the correlation only becomes strongly positive and significant following deforestation (**Figure**

10), which implies that the removal of floodplain forest does indeed initiate a shift in the dominant control of riverbank retreat. This assertion holds true for the relationship between the magnitude of planform curvature and rates of channel migration, suggesting that forests play an important role in the evolution of meandering rivers, even when riverbank heights exceed the depth of root penetration.

In an attempt to account for the non-linearity displayed in these observations of migration rate against curvature induced forcing of river flows, I developed a conceptual model of riverbank retreat that replicates the observed shift in relationship by altering the representation of riparian vegetation alone. By modifying the model framework of channel migration outlined by *Eke et al.* [2014] to explicitly represent the decay of cohesive slump blocks with the inclusion of a dense root network, I tested the hypothesis that riparian vegetation can affect rates of channel migration by altering the properties of failed bank material. The results suggest that, despite bank heights far exceeding rooting depths, long term rates of channel migration can be reduced by a dense root network prolonging the protection afforded to a bank face by slump block armament. Furthermore, representing the effect of plant mortality introduces a constraint on the residency time of failed material that is independent of the flow field around a meander bend, reducing the dominance of curvature induced forcing of river flows in controlling riverbank retreat, and can plausibly explain the non-linearity displayed in my observations of the Kinabatangan River. Whilst this doesn't constitute a thorough testing of process representation, it does illustrate that the composition and fate of failed material can plausibly account for the apparent non-curvature dependant bank erosion along forested sections.

The results presented in Chapter 2 are intended to constitute a case study for the formal mapping of an ecosystem service provided by tropical forest to adjacent plantations that might inform a more holistic management of forest conversion in the future. Building on the results from chapter 3, I illustrate the potential ecosystem service that might be afforded by the retention of tropical forest buffers derived from the provision of the geomorphic ecosystem function of reducing riverbank retreat. Using a simplified numerical model of channel migration, I estimated the mean area of land lost per unit length of river under different scenarios of future forest conversion along unprotected sections. I then evaluated the economic worth of retaining forest buffers by comparing yield losses in the absence of a forest buffer to those when a buffer is maintained, with results suggesting that riparian forest can significantly enhance the profitability of floodplain plantations – particularly over longer time scales (on the order of decades). Along the margins of the Kinabatangan, large scale industrial plantations co-exist alongside independent small holdings, local communities, and conservation research trusts all with a vested interest in the future of unprotected forests. Linking measurements of riverbank retreat to projections of expected yields assigns an economic valuation to the preservation of riparian buffer zones, and demonstrates that floodplain forest provides a geomorphic ecosystem service to adjacent plantation. Though not a substitute for regulatory protection, quantitative assessments of the benefits tropical forests can provide to stakeholders along the Kinabatangan are crucial to the long term efforts of environmental sustainability. By accounting for the effects of landscape dynamics and projecting returns over long-term economic horizons, palm-oil industry goals may be brought into closer alignment with environmental conservation.

6.3 Wider implications

Land use conversion is the second largest anthropogenic source of carbon emissions after the burning of fossil fuels, with tropical deforestation accounting for more than 80% of the total carbon emissions resulting from global land-cover change [Van der Werf et al., 2009; Houghton et al., 2012]. Each year the conversion and degradation of an estimated 5.5 M ha of tropical forests contribute more than 1 billion tons (Pg) of carbon to the atmosphere as the need for food production continues to drive agricultural expansion [*Rudel et al.*, 2009; *Baccini et al.*, 2012; *Hosonuma et al.*, 2012; *Houghton*, 2012]. In addition to generating carbon emissions, deforestation threatens biodiversity and ecosystem function. At regional and local scales, agricultural expansion reduces biodiversity directly by supporting fewer species [Fitzherbert et al., 2008; Edwards et al., 2010] and indirectly by fragmenting the landscape and restricting animal movements, thus inhibiting genetic mixing [Goossens et al., 2006; Yaap et al., 2010].

Establishing forest reserves within agriculture-dominated landscapes can help limit carbon emissions, by preventing total deforestation, and preserve biodiversity, by acting as sanctuaries for species that otherwise cannot survive in an agricultural monoculture [Balen, 1996; Lucey et al., 2014]. However, such reserves lose species richness over time if they become isolated fragments [Turner, 1996]: sanctuaries can only safeguard tropical biodiversity if animals are able to move between forest reserves through dedicated habitat corridors [Bruford et al., 2010; Gregory et al., 2014]. Riparian corridors represent a space where the practicalities of land conversion and habitat preservation overlap [Naiman et al., 1993], but have historically been eschewed in pursuit of larger crop yields.

As the world's population is expected to exceed 9.5 billion by 2050 [*United Nations, Department of Economic and Social Affairs*, 2013], there is a growing need for holistic management of land conversion that makes best use of our natural resources across all spatial scales and for all social groups. Originating in response to the 2008 global food and economic crisis, the water-energy-food nexus has been promoted as an emerging global development paradigm and research agenda [*Allouche et al.*, 2014]. The decision 'NEXUS' is a system of socioecological thinking that promotes the understanding of trade-offs and synergies to increase efficiency and improve governance between food, water, energy, and natural systems [*Hoff*, 2011; *Davis*, 2014]. As such, the work presented in this thesis contributes to a larger dialogue that describes the complex interactions within shifting landscape dynamics, and could be incorporated within ongoing efforts to promote the sustainable development of Southeast Asia's forests through the application of holistic management practices [*Brown*, 1998; *Middleton et al.*, 2015; *Abram et al.*, 2016; *Zafirah et al.*, 2017]. At present. the biophysical modelling component of a decision NEXUS concerning the conversion of floodplain forests primarily focuses on quantifying alterations to water quality, groundwater reserves, river flow regimes, and/or storm hydrographs due to shifting water pathways and projections of water extraction for irrigation under different forest conversion scenarios [*Endo et al.*, 2015]. Yet each of these consequences of forest conversion will in turn affect rates of channel migration, thus accounting for the geomorphic response of large rivers may play an important role in shaping future forest management practices.

Our projection for the geomorphic response of the Kinabatangan River to the total removal of its floodplain forest over the next century only constitutes a small fraction of the total land converted. However, the geomorphic ecosystem service afforded by riparian

forests bordering more dynamic fluvial systems is likely to be much greater, as rates of channel migration along the Kinabatangan are relatively low. Assuming riparian forests provide proportionally equivalent protection along most fluvial systems, accounting for the shifting dynamics of meandering rivers could promote the preservation of large tracts of riparian forests worldwide. Though it remains to be established whether the effects of retaining riparian vegetation scale to fluvial systems much larger than the Kinabatangan.

6.4 Opportunities for Future Research

6.4.1 Slump block residency times

Within the context of the Kinabatangan I have demonstrated that the composition and fate of failed riverbank material can control rates of channel migration, and shift the relation between riverbank retreat and planform curvature. I have done this by describing the residency times of slump blocks in such a way as to reduce the dependency upon the boundary shear stress acting along the bank face for their removal. The formulation of slump block residency times presented here includes an expression that describes the decomposition rate of rooted material within the slump block, which introduces a parameter that is independent of the flow field around the meander bend, reducing the role of planform curvature as a first order control. However, the perceived relationship between slump block residency times and planform curvature may be altered in ways that are not accounted for within the analysis.

The removal of riparian vegetation has the potential to alter both the style and size of mas wasting events [*Milledge et al.*, 2014; *Wang et al.*, 2016], which in turn has the potential to alter the near bank flow field around a meander bend [*Kean and Smith*, 2006; *Hackney et al.*, 2015]. Were slump blocks in the presence of riparian vegetation large

enough to redirect the high momentum core of a flow field away from the outer bank and towards the channel centre, then despite being a function of boundary shear stress alone, slump block residency times might not display a direct correlation to planform curvature. In reducing the size of slump blocks, the removal of riparian vegetation might restore the positioning of high momentum flow to along the outer bank, thus displaying an apparent correlation between riverbank retreat and planform curvature.

In addition to altering the flow structure around a meander bend, removal of riparian vegetation might reduce the size of mass failure events sufficiently that slump blocks are removed whole, as opposed to gradually by fluvial scour as is assumed in the model formulation. Residency times would then correspond to return periods of flows around individual meander bends sufficiently large to remove slump blocks. As return periods are merely descriptions of flow fields, residency times would again display a direct correlation to planform curvature.

Lastly, the analysis assumes a constant friction factor around meander bends. The addition of large woody debris along the bank face, and dense vegetation to slump blocks, may add roughness to bank surfaces, and has the potential to alter boundary shear stresses in non-linear ways [*Thorne and Furbish*, 1995b; *Hopkinson and Wynn*, 2009; *Konsoer et al.*, 2016b].

Future work in this area should seek to quantify the impact riparian forest removal has on each of these considerations, examine the role they play in controlling the residency time of slump blocks, and assess the relative dominance of each in describing the relation of riverbank retreat to planform curvature.

6.4.2 River scaling

Whilst my quantification of the historic geomorphic response of the Kinabatangan River to wide spread land conversion is a significant contribution to the study of large tropical rivers, the inferences that can be drawn are limited by questions of scale and environment. Quantifying the geomorphic response of larger tropical rivers to the conversion of floodplain forest is necessary to discern if the results presented here are limited to rivers of a similar size to the Kinabatangan. Instances where the removal of natural riparian cover have been recorded in high quality imagery spanning timeframes long enough to capture geomorphic change are rare, but an ever expanding legacy of satellite imagery and continued deforestation across the tropics will bring future opportunities to examine the role of floodplain forest in controlling rates of meander migration.

6.4.3 Additional ecosystem function

Our assessment of the geomorphic ecosystem service provided by riparian forest to adjacent oil palm plantations along the Kinabatangan only account for alterations to riverbank erodibility. The secondary effects of forest removal aren't considered, such as increased sediment loading, increased mean average discharge, magnitude and frequency of peak flows, or the duration of high flows that can affect bank erosion, migration rates, and otherwise alter the river's internal flow regime [*Costa et al.*, 2003; *Liu et al.*, 2015]. Future work that looks to assign an economic valuation to riparian reserves should account for these secondary effects when comparing between scenarios of forest clearing to better represent the protection afforded by floodplain forests.

References

Abad, J. D., C. E. Frias, G. C. Buscaglia, and M. H. Garcia (2013), Modulation of the flow structure by progressive bedforms in the Kinoshita meandering channel, *Earth Surf. Process. Landforms*, *38*(13), 1612–1622, doi:10.1002/esp.3460.

Abernethy, B., and I. D. Rutherfurd (1998), Where along a river's length will vegetation most effectively stabilise stream banks?, *Geomorphology*, *23*(1), 55–75, doi:10.1016/S0169-555X(97)00089-5.

Abernethy, B., and I. D. Rutherfurd (2000), The effect of riparian tree roots on the mass-stability of riverbanks, *Earth Surf. Process. Landforms*, *25*(9), 921–937, doi:10.1002/1096-9837(200008)25:9<921::AID-ESP93>3.0.CO;2-7.

Abernethy, B., and I. D. Rutherfurd (2001), The distribution and strength of riparian tree roots in relation to riverbank reinforcement, *Hydrol. Process.*, *15*, 63–79.

Abram, N. K. et al. (2014), Synergies for improving oil palm production and forest conservation in floodplain landscapes, *PLoS One*, *9*(6), doi:10.1371/journal.pone.0095388.

Abram, N. K., C. Eriksson, and A. Amanprit (2016), *Trade-offs between ecosystem protection and oil palm development*.

Allmendinger, N. E., J. E. Pizzuto, N. Potter, T. E. Johnson, and W. C. Hession (2005a), The influence of riparian vegetation on stream width, eastern Pennsylvania, USA, *Bull. Geol. Soc. Am.*, *117*(1–2), 229–243, doi:10.1130/B25447.1.

Allmendinger, N. E., J. E. Pizzuto, N. Potter, T. E. Johnson, and W. C. Hession (2005b), The influence of riparian vegetation on stream width, eastern Pennsylvania, USA, *Geol. Soc. Am. Bull.*, *117*(1), 229, doi:10.1130/B25447.1.

Allouche, J., C. Middleton, and D. Gyawali (2014), Nexus Nirvana or Nexus Nullity? A dynamic approach to security and sustainability in the water-energy-food nexus, in *STEPS Working Paper 63*, Brighton: STEPS Centre.

Amiri-tokaldany, E., S. E. Darby, and P. Tosswell (2004), BANK STABILITY ANALYSIS FOR PREDICTING REACH SCALE LAND LOSS AND SEDIMENT YIELD, *J. Am. WATER Resour. Assoc.*, 897–909.

Annammala, K. V, R. Walsh, K. Bidin, and A. Nainar (2012), Higher erosion rate and enhanced sedimentation from disturbed landforms in eastern Sabah, Borneo., in *2nd International Conference on Water Resources in conjunction with 20th UNESCO-IHP Regional Steering Committee Meeting for Southeast Asia and the Pacific*, pp. 1–13.

Armenteras, D., G. Rudas, N. Rodriguez, S. Sua, and M. Romero (2006), Patterns and causes of deforestation in the Colombian Amazon, *Ecol. Indic.*, *6*(2), 353–368, doi:10.1016/j.ecolind.2005.03.014.

Arulanandan, K., E. Gillogley, and R. Tully (1980), Development of a Quantitative Method to Predict Critical Shear Stress and Rate of Erosion of Natural Undisturbed Cohesive Soils.,

Asahi, K., Y. Shimizu, J. Nelson, and G. Parker (2013), Numerical simulation of river meandering with self-evolving banks, *J. Geophys. Res. Earth Surf.*, *118*(4), 2208–2229, doi:10.1002/jgrf.20150.

ASCE Task Committee (1998), River width adjustment. I: Processes and mechanisms, *J. Hydraul. Eng.*, (September).

Baatz, M., a Schäpe, J. Strobl, T. Blaschke, and G. Griesebner (2000), Multiresolution Segmentation-an optimization approach for high quality multi-scale image segmentation, *Angew. Geogr. Informationsverarbeitung*, *12*, 12–23.

Baccini, a. et al. (2012), Estimated carbon dioxide emissions from tropical deforestation improved by carbon-density maps, *Nat. Clim. Chang.*, *2*(3), 182–185, doi:10.1038/nclimate1354.

De Baets, S., and J. Poesen (2010), Empirical models for predicting the erosion-reducing effects of plant roots during concentrated flow erosion, *Geomorphology*, *118*(3–4), 425–432, doi:10.1016/j.geomorph.2010.02.011.

De Baets, S., J. Poesen, G. Gyssels, and A. Knapen (2006), Effects of grass roots on the erodibility of topsoils during concentrated flow, *Geomorphology*, *76*(1–2), 54–67, doi:10.1016/j.geomorph.2005.10.002.

Bagnold, R. (1966), An approach to the sediment transport problem from general physics, *US Geol. Surv. Prof. Pap.*

Di Baldassarre, G., A. Viglione, G. Carr, L. Kuil, J. L. Salinas, and G. Blöschl (2013), Socio-hydrology: Conceptualising human-flood interactions, *Hydrol. Earth Syst. Sci.*, *17*(8), 3295–3303, doi:10.5194/hess-17-3295-2013.

Balen, V. (1996), The conservation value of small, isolated fragments of lowland tropical rain forest, , *5347*(8), 38–41.

Basiron, Y., M. Palm, O. Council, J. Perbandaran, and K. Jaya (2007), Palm oil production through sustainable plantations, , *109*, 289–295, doi:10.1002/ejlt.200600223.

Beeson, C. E., and P. F. Doyle (1995), Comparison of bank erosion at vegetated and non-vegetated channel bends, *J. Am. Water Resour. Assoc.*, *31*(6), 983–990.

Bennett, S., T. Pirim, and B. Barkdoll (2002), Using simulated emergent vegetation to alter stream flow direction within a straight experimental channel, *Geomorphology*, *44*, 115–126.

Bishop, A. W. (1955), The use of the Slip Circle in the Stability Analysis of Slopes, *Géotechnique*, *5*(1), 7–17, doi:10.1680/geot.1955.5.1.7.

Boucher, D. H., P. Elias, K. Lininger, C. May-Tobin, S. Roquemore, and E. Saxon (2011), The root of the problem: What is driving deforestation today?, in *Union of Concerned Scientists*, USC Publications, Cambridge, MA.

Brice, J. C. (1977), Lateral migration of the middle Sacramento River, California, *USGS Water-Resources Investig.*, *77*(43), 1–51.

Brown, M. (1998), Forest Plunder in Southeast Asia : An Environmental Security Nexus in, *Environ. Change Secur. Proj. Rep.*, *4*(4), 53–60.

Bruford, M., M. Ancrenaz, L. Chikhi, I. Lackmann-Ancrenaz, M. Andau, L. Ambu, and B.

Goossens (2010), Projecting genetic diversity and population viability for the fragmented orang-utan population in the Kinabatangan floodplain, Sabah, Malaysia, *Endanger. Species Res.*, *12*(3), 249–261, doi:10.3354/esr00295.

Butler, R. a, L. P. Koh, and J. Ghazoul (2009), REDD in the red: palm oil could undermine carbon payment schemes, *Conserv. Lett.*, *2*(2), 67–73, doi:10.1111/j.1755-263X.2009.00047.x.

Camporeale, C., and E. Perucca (2013), Modeling the interactions between river morphodynamics and riparian vegetation, *Rev. Geophys.*, *51*(1), doi:10.1002/rog.20014.1.INTRODUCTION.

Camporeale, C., P. Perona, A. Porporato, and L. Ridolfi (2005), On the long-term behavior of meandering rivers, *Water Resour. Res.*, *41*(12), n/a-n/a, doi:10.1029/2005WR004109.

Camporeale, C., P. Perona, A. Porporato, L. Ridolfi, P. Perona, and A. Porporato (2007), Hierarchy of Models for Meandering Rivers and Related Morphodynamic, , (2005), 1–28, doi:10.1029/2005RG000185.1.INTRODUCTION.

Cancienne, R., G. Fox, and A. Simon (2008), Influence of seepage undercutting on the stability of root-reinforced streambanks, *Earth Surf. Process. Landforms*, *1786*(1991), 1769–1786, doi:10.1002/esp.

Carlson, K. M., L. M. Curran, G. P. Asner, A. M. Pittman, S. N. Trigg, and J. Marion Adeney (2012), Carbon emissions from forest conversion by Kalimantan oil palm plantations, *Nat. Clim. Chang.*, *3*(3), 283–287, doi:10.1038/nclimate1702.

Casagli, N., M. Rinaldi, A. Gargini, and A. Curini (1999), Pore water pressure and streambank stability: results from a monitoring site on the Sieve River, Italy, *Earth Surf. Process. Landforms*, *24*(12), 1095–1114, doi:10.1002/(SICI)1096-9837(199911)24:12<1095::AID-ESP37>3.0.CO;2-F.

Castro, J. M., and P. L. Jackson (2001), BANKFULL DISCHARGE RECURRENCE INTERVALS AND REGIONAL HYDRAULIC GEOMETRY RELATIONSHIPS: PATTERNS IN THE PACIFIC NORTHWEST, USA1, *JAWRA J. Am. Water Resour. Assoc.*, *37*(5), 1249–1262.

Chavez, P. S. (1996), Image-based atmospheric corrections-revisited and improved, *Photogramm. Eng. Remote Sensing*, *62*(9), 1025–1035.

Cheong, S.-M., B. Silliman, P. P. Wong, B. van Wesenbeeck, C.-K. Kim, and G. Guannel (2013), Coastal adaptation with ecological engineering, *Nat. Clim. Chang.*, *3*(9), 787–791, doi:10.1038/nclimate1854.

Clark, L., and T. Wynn (2007), Methods for determining streambank critical shear stress and soil erodibility: Implications for erosion rate predictions, *Trans. ASABE*, *50*(1), 95–106.

Constantine, C. R., T. Dunne, and G. J. Hanson (2009), Examining the physical meaning of the bank erosion coefficient used in meander migration modeling, *Geomorphology*, *106*(3–4), 242–252, doi:10.1016/j.geomorph.2008.11.002.

Constantine, J. A., T. Dunne, J. Ahmed, C. Legleiter, and D. Eli (2014), Sediment supply as a driver of river evolution in the Amazon Basin, *Nat. Geosci.*, *7*(December), 899–903, doi:10.1038/NGEO2282.

Coon, W. F. (1997), Estimation of roughness coefficients for natural stream channels with vegetated banks, *U.S. Geol. Surv. water-supply Pap.*, (2441), 1–133.

Coppin, N. J., I. G. Richards, and C. I. R. and I. Association (1990), *Use of vegetation in civil engineering*, Butterworths.

Corley, R., and P. Tinker (2003), Growth, flowering and yield, *Oil Palm*, 89–131.

Corley, R. H. V, and P. B. H. Tinker (2015), *The Oil Palm*, World Agriculture Series, Wiley.

Costa, M. H., A. Botta, and J. A. Cardille (2003), Effects of large-scale changes in land cover on the discharge of the Tocantins River, Southeastern Amazonia, *J. Hydrol.*, *283*(1–4), 206–217, doi:10.1016/S0022-1694(03)00267-1.

Costanza, R., R. d'Arge, R. De Groot, S. Farber, M. Grasso, B. Hannon, K. Limburg, S. Naeem, R. V O'neill, and J. Paruelo (1997), The value of the world's ecosystem services and natural capital, *Nature*, *387*(6630), 253–260.

Czarnomski, N., and D. Tullos (2012), Effects of vegetation canopy density and bank angle on near-bank patterns of turbulence and Reynolds stresses, *J. Hydraul. Eng.*

Daniels, H. E. (1945), The Statistical Theory of the Strength of Bundles of Threads. I, *Proc. R. Soc. London A Math. Phys. Eng. Sci.*, *183*(995), 405–435, doi:10.1098/rspa.1945.0011.

Daniels, M. D., and B. L. Rhoads (2003), Influence of a large woody debris obstruction on three-dimensional flow structure in a meander bend, *Geomorphology*, *51*(1–3), 159–173, doi:10.1016/S0169-555X(02)00334-3.

Darby, S., and D. Sear (2008), *River restoration: managing the uncertainty in restoring physical habitat*, John Wiley & Sons.

Darby, S. E., and C. R. Thorne (1996), Development and Testing of Riverbank-Stability Analysis, *J. Hydraul. Eng.*, *122*(August), 443–454.

Darby, S. E., A. M. Alabyan, and M. J. Van de Wiel (2002), Numerical simulation of bank erosion and channel migration in meandering rivers, *Water Resour. Res.*, *38*(9), 2-1-2–21, doi:10.1029/2001WR000602.

Darby, S. E., M. Rinaldi, and S. Dapporto (2007), Coupled simulations of fluvial erosion and mass wasting for cohesive river banks, *J. Geophys. Res.*, *112*(F3), F03022, doi:10.1029/2006JF000722.

Davis, M. (2014), Managing environmental systems: The water-energy-food nexus, *Res. Synth. Brief. Stock. Sweden Stock. Environ. Inst.*

Docker, B. B., and T. C. T. Hubble (2009), Modelling the distribution of enhanced soil shear strength beneath riparian trees of south-eastern Australia, *Ecol. Eng.*, *35*(5), 921–934, doi:10.1016/j.ecoleng.2008.12.018.

Downs, P. W., and A. Simon (2001), Fluvial geomorphological analysis of the recruitment of large woody debris in the Yalobusha River network , Central Mississippi , USA,

Dunaway, D., S. R. Swanson, J. Wendel, and W. Clary (1994), The effect of herbaceous plant communities and soil textures on particle erosion of alluvial streambanks,

Geomorphology, *9*(1), 47–56, doi:10.1016/0169-555X(94)90030-2.

Dunne, T., J. A. Constantine, and M. B. Singer (2010), The role of sediment transport and sediment supply in the evolution of river channel and floodplain complexity, *Chikei/Transactions, Japanese Geomorphol. Union*, *31*(2), 155–170.

Durocher, M. G. (1990), Monitoring spatial variability of forest interception, *Hydrol. Process.*, *4*(3), 215–229, doi:10.1002/hyp.3360040303.

Dury, G. H. (1976), Discharge prediction, present and former, from channel dimensions, *J. Hydrol.*, *30*(3), 219–245.

Edwards, D. P., J. a. Hodgson, K. C. Hamer, S. L. Mitchell, A. H. Ahmad, S. J. Cornell, and D. S. Wilcove (2010), Wildlife-friendly oil palm plantations fail to protect biodiversity effectively, *Conserv. Lett.*, *3*(4), 236–242, doi:10.1111/j.1755-263X.2010.00107.x.

Einstein, H. A. (1950), The Bed-Load Function for Sediment Transportation in Open Channel Flows, *Soil Conserv. Serv.*, (1026), 1–31.

Eke, E., G. Parker, and Y. Shimizu (2014), Numerical modeling of erosional and depositional bank processes in migrating river bends with self-formed width: Morphodynamics of bar push and bank pull, *J. Geophys. Res. Earth Surf*, *119*(2), 1455–1483, doi:10.1002/2013JF003020.Received.

Eke, E. C., M. Czapiga, E. Viparelli, Y. Shimizu, J. Imran, T. Sun, and G. Parker (2013), Coevolution of width and sinuosity in meandering rivers, *J. Fluid Mech.*, *760*, 1–43, doi:10.1017/jfm.2014.556.

Ellis, E. C. (2011), Anthropogenic transformation of the terrestrial biosphere, *Phil. Trans. R. Soc. A*, *369*, 1010–1035, doi:10.1098/rsta.2010.0331.

Endo, A., K. Burnett, P. M. Orencio, T. Kumazawa, C. A. Wada, A. Ishii, I. Tsurita, M. Taniguchi, S. Jalilov, and O. Varis (2015), Methods of the Water-Energy-Food Nexus, *Water*, 5806–5830, doi:10.3390/w7105806.

Endo, T. (1980), Effect of tree roots upon the shear strength of soil., *JARQ (Japan Agric. Res. Quarterly)*, *14*(2), 112–115.

Engelund, F. (1974), Flow and bed topography in channel bends, *J. Hydraul. Div.*, *100*(11), 1631–1648.

Estes, J. G., N. Othman, S. Ismail, M. Ancrenaz, B. Goossens, L. N. Ambu, A. B. Estes, and P. A. Palmiotto (2012), Quantity and Configuration of Available Elephant Habitat and Related Conservation Concerns in the Lower Kinabatangan Floodplain of Sabah , Malaysia, , *7*(10), doi:10.1371/journal.pone.0044601.

Everard, M., and N. Quinn (2017), Realizing the value of fluvial geomorphology, , *5124*(August), doi:10.1080/15715124.2015.1048457.

Fatahi, B., B. Indraratna, and H. Khabbaz (2006), Numerical analysis of matric suction effects of tree roots, *Proc. ICE - Geotech. Eng.*, *159*(2), 77–90, doi:10.1680/geng.2006.159.2.77.

Fernandez Luque, R., and R. Van Beek (1976), Erosion And Transport Of Bed-Load Sediment,

J. Hydraul. Res., *14*(2), 127–144, doi:10.1080/00221687609499677.

Fitzherbert, E., M. Struebig, a Morel, F. Danielsen, C. Bruhl, P. Donald, and B. Phalan (2008), How will oil palm expansion affect biodiversity?, *Trends Ecol. Evol.*, *23*(10), 538–545, doi:10.1016/j.tree.2008.06.012.

Flanagan, D., and M. Nearing (1995), *USDA-Water Erosion Prediction Project (WEPP), hillslope profile and watershed model documentation*.

Fox, G., and G. Wilson (2006), Sediment transport model for seepage erosion of streambank sediment, *J. Hydrol. Eng.*, *11*(6), 603–611.

Fredlund, D. G., and H. Rahardjo (1993), Shear Strength Theory, in *Soil Mechanics for Unsaturated Soils*, pp. 217–259, John Wiley & Sons, Inc.

Furbish, D. J. (1991), Spatial autoregressive structure in meander evolution, *Geol. Soc. Am. Bull.*, *103*(12), 1576–1589, doi:10.1130/0016-7606(1991)103<1576:SASIME>2.3.CO;2.

Gilbert, G. K. (1877), *Report on the Geology of the Henry Mountains*, US Government Printing Office.

Gomi, T., R. C. Sidle, S. Noguchi, J. N. Negishi, A. R. Nik, and S. Sasaki (2006), Sediment and wood accumulations in humid tropical headwater streams: Effects of logging and riparian buffers, *For. Ecol. Manage.*, *224*(1–2), 166–175, doi:10.1016/j.foreco.2005.12.016.

Goossens, B., L. Chikhi, M. F. Jalil, M. Ancrenaz, I. LACKMAN-ANCRENAZ, M. Mohamed, P. Andau, and M. W. Bruford (2005), Patterns of genetic diversity and migration in increasingly fragmented and declining orang-utan (Pongo pygmaeus) populations from Sabah, Malaysia, *Mol. Ecol.*, *14*(2), 441–456.

Goossens, B., L. Chikhi, M. Ancrenaz, I. Lackman-Ancrenaz, P. Andau, and M. W. Bruford (2006), Genetic Signature of Anthropogenic Population Collapse in Orang-utans, *PLoS Biol.*, *4*(2), e25, doi:10.1371/journal.pbio.0040025.

Gordon, J. E., and H. F. Barron (2013), The role of geodiversity in delivering ecosystem services and benefits in Scotland, *Scottish J. Geol.*, *49*(1), 41–58.

Gran, K., and C. Paola (2001), Riparian vegetation controls on braided stream dynamics, *Water Resour. Res.*

Gray, C. L., and O. T. Lewis (2014), Do riparian forest fragments provide ecosystem services or disservices in surrounding oil palm plantations?, *Basic Appl. Ecol.*, *15*(8), 693–700, doi:10.1016/j.baae.2014.09.009.

Gray, D. H., and H. Ohashi (1983), Mechanics of fiber reinforcement in sand, *J. Geotech. Eng.*, *109*(3), 335–353.

Gregory, S. D., M. Ancrenaz, B. W. Brook, B. Goossens, R. Alfred, L. N. Ambu, and D. a. Fordham (2014), Forecasts of habitat suitability improve habitat corridor efficacy in rapidly changing environments, *Divers. Distrib.*, *20*(9), 1044–1057, doi:10.1111/ddi.12208.

Gurnell, A. (2014), Plants as river system engineers, *Earth Surf. Process. Landforms*, *39*(1), 4–25, doi:10.1002/esp.3397.

Gyssels, G., J. Poesen, E. Bochet, and Y. Li (2005), Impact of plant roots on the resistance of soils to erosion by water: a review, *Prog. Phys. Geogr.*, *29*, 189–217, doi:10.1191/0309133305pp443ra.

Gyssels, G., J. Poesen, G. Liu, W. Van Dessel, A. Knapen, and S. De Baets (2006), Effects of cereal roots on detachment rates of single- and double-drilled topsoils during concentrated flow, *Eur. J. Soil Sci.*, *57*(3), 381–391, doi:10.1111/j.1365-2389.2005.00749.x.

Hackney, C., J. Best, J. Leyland, S. E. Darby, D. Parsons, R. E. Aalto, and A. Nicholas (2015), Modulation of outer bank erosion by slump blocks: Disentangling the protective and destructive role of failed material on the three-dimensional flow structure, *Geophys. Res. Lett.*, (42), 10,663–10,670, doi:10.1002/2015GL066481.Received.

Hanson, G. J., and A. Simon (2001), Erodibility of cohesive streambeds in the loess area of the midwestern USA, *Hydrol. Process.*, *15*(1), 23–38, doi:10.1002/hyp.149.

Hasegawa, K. (1977), Computer simulation of the gradual migration of meandering channels, *Proc. Hokkaido Branch*, *2*(Jpn. Soc. of Civ), 197–2.

Hasegawa, K. (1989), Universal Bank Erosion Coefficient for Meandering Rivers, *J. Hydraul. Eng.*, *115*(6), 744–765, doi:10.1061/(ASCE)0733-9429(1989)115:6(744).

Hickin, E. J. (1974), The development of meanders in natural river-channels, *Am. J. Sci.*, *274*(4), 414–442, doi:10.2475/ajs.274.4.414.

Hickin, E. J. (1984), Vegetation and River Channel Dynamics, *Can. Geogr. Géographe Can.*, *28*(2), 111–126, doi:10.1111/j.1541-0064.1984.tb00779.x.

Hoff, H. (2011), Understanding the nexus. background paper for the Bonn2011 Conference: the water, energy and food security nexus, *Stock. Environ. Institute, Stock.*

Hooke, J. M. (1980), Magnitude and distribution of rates of river bank erosion, *Earth Surf. Process.*, *5*(2), 143–157, doi:10.1002/esp.3760050205.

Hopkinson, L., and T. Wynn (2009), Vegetation impacts on near bank flow, *Ecohydrology*, *418*(October), 404–418, doi:10.1002/eco.

Horton, A. J., J. A. Constantine, T. C. Hales, B. Gossens, M. W. Bruford, and E. D. Lazarus (2017), Modification of river meandering by tropical deforestation, *Geology*, doi:doi:10.1130/G38740.1.

Hosonuma, N., M. Herold, V. De Sy, R. S. De Fries, M. Brockhaus, L. Verchot, A. Angelsen, and E. Romijn (2012), An assessment of deforestation and forest degradation drivers in developing countries, *Environ. Res. Lett.*, *7*(4), 44009, doi:10.1088/1748-9326/7/4/044009.

Houghton, R. a. (2012), Carbon emissions and the drivers of deforestation and forest degradation in the tropics, *Curr. Opin. Environ. Sustain.*, *4*(6), 597–603, doi:10.1016/j.cosust.2012.06.006.

Houghton, R. a., J. I. House, J. Pongratz, G. R. Van Der Werf, R. S. Defries, M. C. Hansen, C. Le Quéré, and N. Ramankutty (2012), Carbon emissions from land use and land-cover change, *Biogeosciences*, *9*(12), 5125–5142, doi:10.5194/bg-9-5125-2012.

Hupp, C. R., and W. R. Osterkamp (1996), Riparian vegetation and fluvial geomorphic processes, *Geomorphology*, *14*(4), 277–295, doi:10.1016/0169-555X(95)00042-4.

Ikeda, S., G. Parker, and K. Sawai (1981), Bend theory of river meanders. Part 1. Linear development, *J. Fluid Mech.*, *112*(1), 363, doi:10.1017/S0022112081000451.

Jackson, R. B., J. Canadell, J. R. Ehleringer, H. a. Mooney, O. E. Sala, and E. D. Schulze (1996), A global analysis of root distributions for terrestrial biomes, *Oecologia*, *108*(3), 389–411, doi:10.1007/BF00333714.

Johannesson, H., and G. Parker (1989), Linear theory of river meanders, in *River Meandering*, vol. 12, pp. 181–214.

Julian, J. P., and R. Torres (2006), Hydraulic erosion of cohesive riverbanks, *Geomorphology*, *76*(1–2), 193–206, doi:10.1016/j.geomorph.2005.11.003.

Kamphuis, J. W., and K. R. Hall (1983), Cohesive Material Erosion by Unidirectional Current, *J. Hydraul. Eng.*, *109*(1), 49–61, doi:10.1061/(ASCE)0733-9429(1983)109:1(49).

Kandiah, A. (1974), Fundamental aspects of surface erosion of cohesive soils,

Kean, J. W., and J. D. Smith (2006), Form drag in rivers due to small-scale natural topographic features: 1. Regular sequences, *J. Geophys. Res. Earth Surf.*, *111*(4), 1–13, doi:10.1029/2006JF000490.

Keenan, R. J., G. a Reams, F. Achard, J. V. De Freitas, A. Grainger, and E. Lindquist (2015), Forest Ecology and Management Dynamics of global forest area : Results from the FAO Global Forest Resources Assessment 2015 q, *For. Ecol. Manage.*, *352*, 9–20, doi:10.1016/j.foreco.2015.06.014.

Klinge, H., and R. Herrera (1978), Biomass studies in Amazon caatinga forest in southern Venezuela. 1. Standing crop of composite root mass in selected stands, *Trop. Ecol.*

Knighton, A. D. (1973), Riverbank erosion in relation to streamflow conditions, River Bollin-Dean, Cheshire, *East Midl. Geogr.*, *5*(8), 416–426.

Koh, L. P., and D. S. Wilcove (2008), Is oil palm agriculture really destroying tropical biodiversity?, *Conserv. Lett.*, *1*(2), 60–64, doi:10.1111/j.1755-263X.2008.00011.x.

Konsoer, K. M., B. L. Rhoads, E. J. Langendoen, J. L. Best, M. E. Ursic, J. D. Abad, and M. H. Garcia (2016a), Spatial variability in bank resistance to erosion on a large meandering, mixed bedrock-alluvial river, *Geomorphology*, *252*, 80–97, doi:http://dx.doi.org/10.1016/j.geomorph.2015.08.002.

Konsoer, K. M., B. L. Rhoads, J. L. Best, E. J. Langendoen, J. D. Abad, D. R. Parsons, and M. H. Garcia (2016b), Three-dimensional flow structure and bed morphology in large elongate meander loops with different outer bank roughness characteristics, *Water Resour. Res.*, *52*(12), 9621–9641, doi:10.1002/2016WR019040.

Kouwen, N. N., and R.-M. Li (1980), Biomechanics of vegetative channel linings, *J. Hydraul. Div.*, *106*(ASCE 15464).

Kraft, D. (1988), *A software package for sequential quadratic programming*, DFVLR Obersfaffeuhofen, Germany.

Krone, R. B. (1999), Effects of bed structure on erosion of cohesive sediments, *J. Hydraul. Eng.*, *125*(December), 1297–1301, doi:10.1061/(ASCE)0733-9429(1999)125:12(1297).

Kun, F., and F. Raischel (2006), Extensions of fibre bundle models, *Model. Crit.*

Lane, E. (1955), Design of stable channels, *Trans. Am. Soc. Civ. Eng.*, (120), 1234–1260.

Langendoen, E. J., and A. Simon (2008), Modeling the Evolution of Incised Streams. II: Streambank Erosion, *J. Hydraul. Eng.*, *134*(7), 1094–1100, doi:10.1061/(ASCE)0733-9429(2008)134.

Langendoen, E. J., R. R. Lowrance, and A. Simon (2009), Assessing the impact of riparian processes on streambank stability, *Ecohydrology*, *2*(3), 360–369.

Latrubesse, E. M., M. L. Amsler, R. P. de Morais, and S. Aquino (2009), The geomorphologic response of a large pristine alluvial river to tremendous deforestation in the South American tropics: The case of the Araguaia River, *Geomorphology*, *113*(3–4), 239–252, doi:10.1016/j.geomorph.2009.03.014.

Lauer, J. W., and G. Parker (2008a), Modeling framework for sediment deposition, storage, and evacuation in the floodplain of a meandering river: Theory, *Water Resour. Res.*, *44*(4), n/a-n/a, doi:10.1029/2006WR005528.

Lauer, J. W., and G. Parker (2008b), Net local removal of floodplain sediment by river meander migration, *Geomorphology*, *96*(1–2), 123–149, doi:10.1016/j.geomorph.2007.08.003.

Lawler, D. (1992), Process dominance in bank erosion systems, *Lowl. floodplain rivers Geomorphol. …*.

Lawler, D. (1995), The impact of scale on the processes of channel-side sediment supply: a conceptual model, *IAHS Publ. Proc. …*, (226).

Lawler, D. M., J. Couperthwaite, L. J. Bull, N. M. Harris, D. M. Lawler, J. Couperthwaite, L. J. Bull, and N. M. H. Bank (1997), Bank erosion events and processes in the Upper Severn basin,

Lazarus, E. D. (2014), Land grabbing as a driver of environmental change, *Area*, *46*(1), 74–82, doi:10.1111/area.12072.

Leopold, B. L., and M. G. Wolman (1957), River Chanel Patterns: Braided, Meandering and Straight, *US Geol. Surv. Proffesional Pap.*, *282B*, 85.

Leopold, L. B., and M. G. Wolman (1960), River Meanders, *Bull. Geol. Soc. Am.*, *71*(3), 769–794, doi:10.1130/0016-7606(1960)71[769:RM]2.0.CO;2.

Leopold, L. B., M. G. Wolman, and J. P. Miller (1964), *Fluvial processes in geomorphology*, H. Freeman, London.

Liu, W., X. Wei, H. Fan, X. Guo, Y. Liu, M. Zhang, and Q. Li (2015), Response of flow regimes to deforestation and reforestation in a rain-dominated large watershed of subtropical China, *Hydrol. Process.*, *29*(24), 5003–5015, doi:10.1002/hyp.10459.

Loades, K. W., a. G. Bengough, M. F. Bransby, and P. D. Hallett (2010), Planting density influence on fibrous root reinforcement of soils, *Ecol. Eng.*, *36*(3), 276–284, doi:10.1016/j.ecoleng.2009.02.005.

Lucey, J. M., N. Tawatao, M. J. M. Senior, V. K. Chey, S. Benedick, K. C. Hamer, P. Woodcock, R. J. Newton, S. H. Bottrell, and J. K. Hill (2014), Tropical forest fragments contribute to species richness in adjacent oil palm plantations, *Biol. Conserv.*, *169*, 268–276, doi:10.1016/j.biocon.2013.11.014.

Mamo, M., and G. D. Bubenzer (2001), Detachment rate, soil erodibility, and soil strength as influenced by living plant roots. Part II: Field study, *Trans. ASAE*, *44*(5), 1175–1181.

Micheli, E. R., J. W. Kirchner, and E. W. Larsen (2004), Quantifying the effect of riparian forest versus agricultural vegetation on river meander migration rates, central Sacramento River, California, USA, *River Res. Appl.*, *20*(5), 537–548, doi:10.1002/rra.756.

Middleton, C., J. Allouche, and S. Allen (2015), The Rise and Implications of the Water-Energy-Food Nexus in Southeast Asia through an Environmental Justice Lens, *Water Altern.*, *8*(1), 627–654.

Milledge, D. G., D. Bellugi, J. A. McKean, A. Densmore, and W. Dietrich (2014), A multidimensional stability model for predicting shallow landslide size and shape across landscapes, *J. Geophys. Res. Earth Surf.*, *119*, 2481–2504, doi:10.1002/2014JF003135.Received.

Motta, D., J. D. Abad, E. J. Langendoen, and M. H. Garcia (2012), A simplified 2D model for meander migration with physically-based bank evolution, *Geomorphology*, *163–164*, 10–25, doi:10.1016/j.geomorph.2011.06.036.

Motta, D., E. J. Langendoen, J. D. Abad, and M. H. García (2014), Modification of meander migration by bank failures, *J. Geophys. Res. Earth Surf.*, *119*(5), 1026–1042, doi:10.1002/2013JF002952.

Murphy, D. J. (2014), The future of oil palm as a major global crop: Opportunities and challenges, *J. Oil Palm Res.*, *26*(MAR), 1–24.

Murray, a. B. et al. (2009), Geomorphology, complexity, and the emerging science of the Earth's surface, *Geomorphology*, *103*(3), 496–505, doi:10.1016/j.geomorph.2008.08.013.

Naiman, R. J., J. J. Latterell, N. E. Pettit, and J. D. Olden (1993), Flow variability and the biophysical vitality of river systems, *Comptes Rendus - Geosci.*, *340*(9–10), 629–643, doi:10.1016/j.crte.2008.01.002.

Naiman, R. J., H. Decamps, and M. E. McClain (2010), *Riparia: ecology, conservation, and management of streamside communities*, Academic Press.

Nanson, G. C., and E. J. Hickin (1986), A statistical analysis of bank erosion and channel

migration in western Canada., *Geol. Soc. Am. Bull.*, *97*(4), 497–504, doi:10.1130/0016-7606(1986)97<497:ASAOBE>2.0.CO;2.

Nardi, L., L. Campo, and M. Rinaldi (2013), Quantification of riverbank erosion and application in risk analysis, *Nat. Hazards*, *69*(1), 869–887, doi:10.1007/s11069-013-0741-8.

Nepf, H., and E. Vivoni (2000), Flow structure in depth-limited, vegetated flow, *J. Geophys. Res. …*.

O'Loughlin, C., and A. Watson (1979), Root-wood strength deterioration in radiata pine after clearfelling, *New Zeal. J. For. Sci.*, *9*(3), 284–293.

Obidzinski, K., a Andrianto, and C. Wijaya (2007), Cross-border timber trade in Indonesia: critical or overstated problem? Forest governance lessons from Kalimantan, *Int. For. Rev.*, *9*(1), 526–535, doi:10.1505/ifor.9.1.526.

Odgaard, A. (1987), Streambank erosion along two rivers in Iowa, *Water Resour. Res.*, *23*(7), 1225–1236.

Odgaard, a. J. (1986), Meander Flow Model. I: Development, *J. Hydraul. Eng.*, *112*(12), 1117–1135, doi:10.1061/(ASCE)0733-9429(1986)112:12(1117).

Osman, A., and C. Thorne (1988), Riverbank stability analysis I: Theory, *J. Hydraul. Eng.*, *114*(2), 134–150.

Paola, C., R. R. Twilley, D. A. Edmonds, W. Kim, D. Mohrig, G. Parker, E. Viparelli, and V. R. Voller (2011), Natural processes in delta restoration: application to the Mississippi Delta, *Ann Rev Mar Sci*, *3*, 67–91, doi:10.1146/annurev-marine-120709-142856.

Parker, D. C. (2007), Revealing "space" in spatial externalities: Edge-effect externalities and spatial incentives, *J. Environ. Econ. Manage.*, *54*(1), 84–99, doi:10.1016/j.jeem.2006.12.004.

Parker, G. (1979), Hydraulic geometry of active gravel rivers, *J. Hydraul. Div.*, *105*(9), 1185–1201.

Parker, G., Y. Shimizu, G. V. Wilkerson, E. C. Eke, J. D. Abad, J. W. Lauer, C. Paola, W. E. Dietrich, and V. R. Voller (2011), A new framework for modeling the migration of meandering rivers, *Earth Surf. Process. Landforms*, *36*(1), 70–86, doi:10.1002/esp.2113.

Partheniades, E. (1965), Erosion and deposition of cohesive soils, *J. Hydraul. Div.*, *91*(1), 105–139.

Perona, P., C. Camporeale, E. Perucca, M. Savina, P. Molnar, P. Burlando, and L. Ridolfi (2009), Modelling river and riparian vegetation interactions and related importance for sustainable ecosystem management, *Aquat. Sci.*, *71*(3), 266–278, doi:10.1007/s00027-009-9215-1.

Perucca, E., C. Camporeale, and L. Ridolfi (2006), Influence of river meandering dynamics on riparian vegetation pattern formation, *J. Geophys. Res.*, *111*(G1), G01001, doi:10.1029/2005JG000073.

Perucca, E., C. Camporeale, and L. Ridolfi (2007), Significance of the riparian vegetation dynamics on meandering river morphodynamics, *Water Resour. Res.*, *43*(3), n/a-n/a, doi:10.1029/2006WR005234.

Piegay, H., M. Cuaz, E. Javelle, and P. Mandier (1997), BANK EROSION MANAGEMENT BASED ON GEOMORPHOLOGICAL , ECOLOGICAL AND ECONOMIC CRITERIA ON THE GALAURE RIVER , FRANCE, , *13*(March), 433–448.

Pirker, J., A. Mosnier, F. Kraxner, P. Havlík, and M. Obersteiner (2016), What are the limits to oil palm expansion?, *Glob. Environ. Chang.*, *40*, 73–81, doi:10.1016/j.gloenvcha.2016.06.007.

Pittaluga, M. B., and G. Seminara (2011), Nonlinearity and unsteadiness in river meandering: a review of progress in theory and modelling, *Earth Surf. Process. Landforms*, *36*(1), 20–38, doi:10.1002/esp.2089.

Pizzuto, J., and T. Meckelnburg (1989), Evaluation of a linear bank erosion equation, *Water Resour. Res.*, *25*(5), 1005–1013.

Pizzuto, J., M. O'Neal, and S. Stotts (2010), On the retreat of forested, cohesive riverbanks, *Geomorphology*, *116*(3–4), 341–352, doi:10.1016/j.geomorph.2009.11.008.

Pizzuto, J. E. (1984), Bank erodibility of shallow sandbed streams, *Earth Surf. Process. Landforms*, *9*(2), 113–124, doi:10.1002/esp.3290090203.

Pojasok, T., and B. Kay (1990), Effect of root exudates from corn and bromegrass on soil structural stability, *Can. J. soil Sci.*, *362*, 351–362.

Pollen-Bankhead, N., and A. Simon (2010), Hydrologic and hydraulic effects of riparian root networks on streambank stability: Is mechanical root-reinforcement the whole story?, *Geomorphology*, *116*(3–4), 353–362, doi:10.1016/j.geomorph.2009.11.013.

Pollen, N., and A. Simon (2005), Estimating the mechanical effects of riparian vegetation on stream bank stability using a fiber bundle model, *Water Resour. Res.*, *41*(7), doi:10.1029/2004WR003801.

Pollen, N., A. Simon, and A. Collison (2004), Advances in assessing the mechanical and hydrologic effects of riparian vegetation on streambank stability, *Riparian Veg. Fluv. …*.

Renó, V. F., E. M. L. M. Novo, C. Suemitsu, C. D. Rennó, and T. S. F. Silva (2011), Assessment of deforestation in the Lower Amazon floodplain using historical Landsat MSS/TM imagery, *Remote Sens. Environ.*, *115*(12), 3446–3456, doi:10.1016/j.rse.2011.08.008.

Righetti, M. (2008), Flow analysis in a channel with flexible vegetation using double-averaging method, *Acta Geophys.*, *56*(3), 801, doi:10.2478/s11600-008-0032-z.

van Rijn, L. C. (1984), Sediment pick-up functions, *J. Hydraul. Eng.*, *110*(10), 1494–1502.

Rinaldi, M., and N. Casagli (1999), Stability of streambanks formed in partially saturated soils and effects of negative pore water pressures: the Sieve River (Italy), *Geomorphology*, 253–277.

Rinaldi, M., N. Casagli, S. Dapporto, and A. Gargini (2004), Monitoring and modelling of pore

water pressure changes and riverbank stability during flow events, *Earth Surf. Process. Landforms*, *29*(2), 237–254, doi:10.1002/esp.1042.

Rudel, T. K., R. Defries, G. P. Asner, and W. F. Laurance (2009), Changing drivers of deforestation and new opportunities for conservation, *Conserv. Biol.*, *23*(6), 1396–1405, doi:10.1111/j.1523-1739.2009.01332.x.

Schiller, M., and S. Wynne (2009), The effect of declining water levels on the stability of riverbank slopes, , 1–6.

Schumm, S. (1960), The Shape of Alluvial Channels in Relation To Sediment Type, *Office*, 24.

Schwarz, M., F. Preti, F. Giadrossich, P. Lehmann, and D. Or (2010), Quantifying the role of vegetation in slope stability: A case study in Tuscany (Italy), *Ecol. Eng.*, *36*(3), 285–291, doi:10.1016/j.ecoleng.2009.06.014.

Schwendel, A. C., A. P. Nicholas, R. E. Aalto, G. H. Sambrook Smith, and S. Buckley (2015), Interaction between meander dynamics and floodplain heterogeneity in a large tropical sand-bed river: The Rio Beni, Bolivian Amazon, *Earth Surf. Process. Landforms*, *40*(15), 2026–2040, doi:10.1002/esp.3777.

Shields, A. (1936), Application of Similarity Principles and Turbulence Research to Bed-Load Movement, *Mitt. Preuss. Versuchsanst. Wasserbau Schiffbau*, *26*(5–24), 47.

Sidle, R. C., A. D. Ziegler, J. N. Negishi, A. R. Nik, R. Siew, and F. Turkelboom (2006), Erosion processes in steep terrain—truths, myths, and uncertainties related to forest management in Southeast Asia, *For. Ecol. Manage.*, *224*(1), 199–225.

Simon, A. (1989), A model of channel response in disturbed alluvial channels, *Earth Surf. Process. Landforms*, *14*(1), 11–26, doi:10.1002/esp.3290140103.

Simon, A., and A. J. C. Collison (2001), Pore-water pressure effects on the detachment of cohesive streambeds: seepage forces and matric suction, *Earth Surf. Process. Landforms*, *26*(13), 1421–1442, doi:10.1002/esp.287.

Simon, A., and A. J. C. Collison (2002), Quantifying the mechanical and hydrologic effects of riparian vegetation on streambank stability, *Earth Surf. Process. Landforms*, *27*(5), 527–546, doi:10.1002/esp.325.

Simon, A., A. Curini, S. E. Darby, and E. J. Langendoen (2000), Bank and near-bank processes in an incised channel, *Geomorphology*, *35*(3–4), 193–217, doi:10.1016/S0169-555X(00)00036-2.

van Slobbe, E., H. J. de Vriend, S. Aarninkhof, K. Lulofs, M. de Vries, and P. Dircke (2013), Building with Nature: In search of resilient storm surge protection strategies, *Nat. Hazards*, *66*(3), 1461–1480, doi:10.1007/s11069-013-0612-3.

Smith, D. (1976), Effect of vegetation on lateral migration of anastomosed channels of a glacier meltwater river, *Geol. Soc. Am. Bull.*, doi:10.1130/0016-7606(1976)87<857.

Stibig, H.-J., F. Achard, S. Carboni, R. Raši, and J. Miettinen (2014), Change in tropical forest cover of Southeast Asia from 1990 to 2010, *Biogeosciences*, *11*(2), 247–258, doi:10.5194/bg-11-247-2014.

Sun, T., P. Meakin, T. Jøssang, and K. Schwarz (1996), A simulation model for meandering rivers, *Water Resour. Res.*, *32*(9), 2937–2954, doi:10.1029/96WR00998.

Tal, M., and C. Paola (2010), Effects of vegetation on channel morphodynamics: results and insights from laboratory experiments, *Earth Surf. Process. Landforms*, *35*(9), 1014–1028, doi:10.1002/esp.1908.

Temmerman, S., P. Meire, T. J. Bouma, P. M. J. Herman, T. Ysebaert, and H. J. De Vriend (2013), Ecosystem-based coastal defence in the face of global change, *Nature*, *504*(7478), 79–83, doi:10.1038/nature12859.

Thorne, C. (1990), Effects of vegetation on riverbank erosion and stability, *Veg. Eros.*

Thorne, C. (1991), Bank erosion and meander migration of the Red and Mississippi Rivers, USA, *IAHS PUBL, IAHS, WALLINGFORD,(ENGL), 1991,*, (201).

Thorne, C. R., N. K. Tovey, E. Sciences, and N. Nr (1981), Stability of composite river banks, *Earth Surf. Process. Landforms*, *6*(5), 469–484, doi:10.1002/esp.3290060507.

Thorne, S. D., and D. J. Furbish (1995a), Influences of coarse bank roughness on flow within a sharply curved river bend, *Geomorphology*, *12*(3), 241–257, doi:10.1016/0169-555X(95)00007-R.

Thorne, S. D., and D. J. Furbish (1995b), Influences of coarse bank roughness on flow within a sharply curved river bend, *Geomorphology*, *12*(3), 241–257, doi:10.1016/0169-555X(95)00007-R.

Turner, I. M. (1996), Species Loss in Fragments of Tropical Rain Forest: A Review of the Evidence, *J. Appl. Ecol.*, *33*(2), 200–209, doi:10.2307/2404743.

United Nations, Department of Economic and Social Affairs, P. D. (2013), *World Population Prospects The 2012 Revision*.

United States Department of Agriculture (2015), *Oilseeds: World Markets and Trade*.

Vannoppen, W., M. Vanmaercke, S. De Baets, and J. Poesen (2015), A review of the mechanical effects of plant roots on concentrated flow erosion rates, *Earth-Science Rev.*, *150*(September), 666–678, doi:10.1016/j.earscirev.2015.08.011.

Varnes, D. J. (1978), Slope Movement Types and Processes, *Transp. Res. Board Spec. Rep.*, (176), 11–33, doi:In Special report 176: Landslides: Analysis and Control, Transportation Research Board, Washington, D.C.

Waldron, L. J. (1977), The Shear Resistance of Root-Permeated Homogeneous and Stratified Soil1, *Soil Sci. Soc. Am. J.*, *41*, 843–849, doi:10.2136/sssaj1977.03615995004100050005x.

Waldron, L. J., and S. Dakessian (1981), Soil reinforcement by roots: calculation of increased soil shear resistance from root properties., *Soil Sci.*, *132*(6).

Wang, Z., Z. Li, M. Xu, and G. Yu (2016), Physical characters of slump blocks, in *River Morphodynamics and Stream Ecology of the Qinghai-Tibet Plateau*, pp. 99–104.

Van der Werf, G. R., D. C. Morton, R. S. DeFries, J. G. J. Olivier, P. S. Kasibhatla, R. B. Jackson,

G. J. Collatz, and J. T. Randerson (2009), CO2 emissions from forest loss, *Nat. Geosci.*, *2*, 737–738.

Werner, B. T., and D. E. McNamara (2007), Dynamics of coupled human-landscape systems, *Geomorphology*, *91*(3–4), 393–407, doi:10.1016/j.geomorph.2007.04.020.

Wicke, B., R. Sikkema, V. Dornburg, and A. Faaij (2011), Exploring land use changes and the role of palm oil production in Indonesia and Malaysia, *Land use policy*, *28*(1), 193–206, doi:10.1016/j.landusepol.2010.06.001.

Wickert, A. D., J. M. Martin, M. Tal, W. Kim, B. Sheets, and C. Paola (2013), River channel lateral mobility: Metrics, time scales, and controls, *J. Geophys. Res. Earth Surf.*, *118*(2), 396–412, doi:10.1029/2012JF002386.

Wiel, M. Van De, and S. Darby (2004), Numerical modeling of bed topography and bank erosion along tree-lined meandering rivers, *Water Sci. Appl.*, 267–282.

Van der Wiel, M., and S. E. Darby (2009), A new model to analyse the imapct of woody riparain vegetation on the geotechnical stability of riverbanks, *Earth Surf. Process. Landforms*, *34*, 16–25, doi:10.1002/esp.

Wilson, G., and R. Periketi (2007), Soil properties controlling seepage erosion contributions to streambank failure, *Earth Surf. Process. Landforms*, *459*(1), 447–459, doi:10.1002/esp.

Wolman, G. M. (1959), Factors influencing erosion of a cohesive rier bank, *Am. J. Sci.*, *257*(March), 204–216.

Wu, T. H., W. P. McKinnell III, and D. N. Swanston (1979), Strength of tree roots and landslides on Prince of Wales Island, Alaska, *Can. Geotech. J.*, *16*(1), 19–33, doi:10.1139/t79-003.

Wynn, T., and S. Mostaghimi (2006), The effects of vegetation and soil type on streambank erosion, southwetern Virginia, USA, *JAWRA J. Am. Water*, *42*(1), 69–82.

Wynn, T. M. (2004), Effects of Vegetation on Stream Bank Erodibility and Critical Shear Stress.

Xu, D., Y. Bai, J. Ma, and Y. Tan (2011), Numerical investigation of long-term planform dynamics and stability of river meandering on fluvial floodplains, *Geomorphology*, *132*(3–4), 195–207, doi:10.1016/j.geomorph.2011.05.009.

Yaap, B., M. J. M. J. Struebig, G. Paoli, L. P. L. P. Koh, and L. Pin Koh (2010), Mitigating the biodiversity impacts of oil palm development, *CAB Rev. Perspect. Agric. Vet. Sci. Nutr. Nat. Resour.*, *5*(19), 1–11, doi:10.1079/PAVSNNR20105019.

Zafirah, N., N. A. Nurin, M. S. Samsurijan, M. H. Zuknik, and M. Rafatullah (2017), Sustainable Ecosystem Services Framework for Tropical Catchment Management : A Review, *Sustainability*, *9*(4), 1–25, doi:10.3390/su9040546.

Zhang, G., K. Tang, and Z. Ren (2013), Impact of Grass Root Mass Density on Soil Detachment Capacity by Concentrated Flow on Steep Slopes, *Trans. ASABE*, *56*(3), 927–934, doi:10.13031/trans.56.9566.

Zolezzi, G., and G. Seminara (2001), Downstream and upstream influence in river meandering. Part 1. General theory and application to overdeepening, *J. Fluid Mech.*, *438*, 183–211, doi:10.1017/S0022112001004281.

Appendix

Table A1: Reach measurements of river area, centreline length and corresponding average widths for each Landsat image

	Reach A			Reach B			Reach C + D			Total		
Year	Area	Length	Width	Area	Length	Width	Area	Length	Width	Area	Length	Width
1989	4784320	54400	87.95	4889936	43300	112.93	6680857	49600	134.69	16355113	147300	111.03
1996	4774540	54400	87.78	4969936	43400	114.49	6666429	49800	133.86	16410905	147600	111.19
2001	5003576	54400	91.98	4919638	43400	113.38	7013878	49900	140.56	16937093	147700	114.68
2005	4834398	54500	88.70	4854038	43500	111.59	7027178	50100	140.27	16715614	148100	112.87
2009	5042701	54500	92.53	5037636	43500	115.82	6772678	50300	134.64	16853015	148300	113.64
2014	4759049	54500	87.32	5020536	43600	115.14	6990878	50500	138.43	16770463	148600	112.85
Average Width			89.38			113.89			137.08			112.71